AN ABSTRACT OF THE THESIS OF

Jonathan R. Ellinger for the degree of Master of Science in Geography presented on July 9, 2010

Title: The Changing Glaciers of Mt. Hood, Oregon and Mt. Rainier, Washington: Implications for Periglacial Debris Flows

Abstract approved: _____

Anne W. Nolin

Mountain glaciers are receding worldwide with numerous consequences including changing hydrology and geomorphology. This study focuses on changes in glacier area on Mt. Hood, Oregon and Mt. Rainier, Washington where damaging debris flows have occurred in glaciated basins. Landsat imagery is used to map debris-free ice on a decadal time scale from 1987 to 2005. Debris-free glacier ice is clearly delineated using a ratio of Landsat spectral bands in the near-infrared part of the spectrum (bands 4 & 5). Landsat scenes were chosen during the months of September and October to minimize snow cover left over from the accumulation season and maximize exposure of debris-free glacial ice. SNOTEL data were also used to find the lowest snow year for each decade to minimize the potential of misclassifying remnant snow as glacial ice. Changes in debris-free ice are mapped to produce the most up-to-date rates of glacier retreat. Average glacial slopes, derived from airborne LiDAR data are used to compute slope corrected debris-free ice areas

for all glaciers. A threshold value for the Landsat NDGI scenes was selected based on threshold testing on the Eliot and Reid glaciers on Mt. Hood. Contradicting earlier studies that say the glaciers on Mt. Hood are receding faster than the glaciers on Mt. Rainier, results show that from 1987 to 2005 Mt. Rainier and Mt. Hood lost similar amounts of debris-free ice extent at 14.0% and 13.9%, respectively. For both Mt. Hood and Mt. Rainier the change in slope corrected debris-free ice area was greater than that of the projected area change due to the steep slopes of both mountains. For Mt. Rainier an increase in recession rate was shown from 1992-2005 compared to 1987-1992 while on Mt. Hood the opposite is seen. On Mt. Rainier it was found that highly fragmented glaciers at lower elevations such as the Inter, Pyramid, and the Van Trump Glaciers lost the highest percent of their original 1987 ice extent and were also shown to be associated with new debris flows in 2006. On Mt. Hood none of the 2006 debris flows initiated within zones of recent glacial recession, however, all debris flows from 2006 originated from streams with a direct connection to glaciers. The Newton Clark Glacier, having lost the most coverage of debris-free ice from 1987 to 2005, is also associated with the highest number of debris-flows in its drainage since 1980. Precipitation data for both mountains show no trend but there was a statistically significant increase in summer air temperature at Mt. Hood over the period 1984-2009. This study suggests that glaciers may play a role in the location of initiation sites, of debris flows, but there is not enough evidence to argue that glacier recession is responsible for producing debris flows.

The Changing Glaciers of Mt. Hood, Oregon and Mt. Rainier, Washington: Implications for Periglacial Debris Flows

by
Jonathan R. Ellinger

A THESIS

Submitted to

Oregon State University

in partial fulfillment of
the requirements for the
degree of

Master of Science

Presented July 9, 2010
Commencement June 2011

Master of Science thesis of Jonathan R. Ellinger presented on July 9, 2010

APPROVED:

Major Professor, representing Geography

Chair of the Department of Geosciences

Dean of the Graduate School

I understand that my thesis will become part of the permanent collection of Oregon State University Libraries. My signature below authorizes release of my thesis to any reader upon request.

Jonathan R. Ellinger, Author

ACKNOWLEDGEMENTS

This study was guided by Anne Nolin. Despite being halfway around the world on sabbatical for my final year of research she was always in touch, expertly guiding me in my research and providing timely responses to any questions I had. I feel lucky to have had her as my advisor. This study would not have been possible without the assistance of Beth Copeland at Oregon State University, Tom DeRoo of the Mount Hood National Forest, and Rachel Pirot and the Glacier Research group at Portland State University. I would also like to acknowledge my committee members Stephen Lancaster, Jon Kimerling, and Kipp Shearman for their valuable insight and constructive feedback during the completion of this research and the revisions of the manuscript. Review, helpful insight, and support were provided by Gordon Grant, Julia Jones, Aaron Wolf, Roy Haggerty, Alexa Ramirez, Chris Holm, Lauren Parker, Kristina Thorneycroft, Tracy Kugler, Quin Ourada, Layne Bennett, and Colin Cooper. I would also like to thank my co-workers at Watershed Sciences for their patience and understanding while I finished my studies. Funding for this project was provided by the National Science Foundation, grant (Award 0844017, Geomorphology and Land Use Dynamics) “Climate and Geomorphic Triggering Mechanisms of Cascadian Periglacial Debris Flows”. I thank my family and friends who have provided endless love and support throughout my graduate studies. A special thanks to Emily Riggott for her never-ending support and always knowing the right thing to say to cheer me up when times got rough.

TABLE OF CONTENTS

Page

TABLE OF CONTENTS (Continued)

Page

TABLE OF CONTENTS (Continued)

Page

LIST OF FIGURES

LIST OF FIGURES (continued)

LIST OF FIGURES (continued)

LIST OF FIGURES (continued)

LIST OF FIGURES (continued)

LIST OF TABLES

LIST OF TABLES (Continued)

LIST OF APPENDICES

Chapter 1: Introduction and Statement of Goals

With alpine glaciers disappearing at record rates due to climate change there needs to be a better understanding of the natural hazards associated with glacier recession in mountainous regions (IPCC, 2007). Monitoring changes in alpine glaciers over time with free satellite data will provide a cost effective method of risk assessment of glacier-associated hazards, such as debris flows. Periglacial debris flows, rapid mixtures of unconsolidated sediment and water that originate near the termini of glaciers, have the power to destroy vital infrastructure such as roads, buildings and trails in the Pacific Northwest. Antecedent climate conditions such as temperature and precipitation are often what trigger debris flows in mountain environments, but debris supply and transport capacity of streams are also important and are found to be directly linked to historical and recent recession of glaciers (Walder, 1994; Roberts, 2005; Fischer, 2006). There have been many studies in the Pacific Northwest using historical maps to assess glacier extents, but very few studies have used satellite measurements of glacial ice to determine glacier recession rates (Oerlemans, 2005; Lillquist, 2006).

To better understand glacier recession in the Pacific Northwest and how that recession may lead to potential natural hazards in alpine environments such as periglacial debris flows, this study will:

1) document glacier recession over the past three decades on two prominent volcanoes in the Cascade range: Mt. Rainier, Washington, and Mt. Hood, Oregon;

2) examine how glacial recession on these two volcanoes relates to known debris flow initiation sites.

This study uses remote sensing and in situ data, to assess recession rates of individual glaciers at a decadal scale. Using mapped locations of debris flow initiation sites, this research examines possible spatial relationships between debris flows and glacier recession. The results of this study will serve to enhance our understanding of how climate change may be affecting Pacific Northwest glaciers and debris flows.

1.1 Global Impacts of Climate Change on Mountain Glaciers & Environs

In 2007 the Intergovernmental Panel on Climate Change, organized by the World Meteorological Organization and the United Nations Environmental Program, affirmed that climate change is "very likely" due to anthropogenic activities (>90% probability) and would "continue for centuries" (IPCC, 2007). Rising levels of greenhouse gases are recognized as the primary cause of global climate change (Kargel, 2005). With populous third world countries now experiencing their own industrial revolutions, the emissions of these gases are continually increasing, guaranteeing climate change will continue well into the future. Carbon dioxide, currently at 390 ppm in the atmosphere, could increase to between 540 ppm to 970 ppm by 2100 (Watson, 2004). In the past 100 years the global average temperature has risen about 1°C but climate projections indicate a similar magnitude of temperature increase will take place in the next 50 years (Watson, 2004).

Rising temperatures around the world due to climate change are responsible for the rise of the glacial equilibrium-line altitude (ELA) by approximately 125 vertical meters (Kargel, 2005). The ELA is where annual snow accumulation above balances ablation below. With the ELA at a higher elevation, glaciers will receive more liquid precipitation, which could result in greater downstream flooding and lower glacier mass accumulation at high altitudes thereby leading to further glacier retreat (WWF, 2005). In a study of 169 glaciers from around the world, Oerlemans

(2005) found a rapid rate of glacier length retreat beginning at the turn of the 20th century.

Glaciers store 69.9% of the world's freshwater (Coudrain, 2005). According to the IPCC, sea level will likely rise by 0.5 m during the 21st century, with approximately 27% of the rise from glacier meltwater (IPCC, 2007). This rise in sea level could prove disastrous to the nearly 100 million people worldwide that live at an elevation within 1 m of sea level (Khalsa, 2004).

Alpine glaciers can serve as indicators of regional climate change due to their sensitivity to changes in both temperature and precipitation. As such, they have been identified as essential climate variables (ECV's) in the Global Climate Observing System (GCOS) (Granshaw & Fountain, 2006; Andreassan, 2008; Ohmura, 2006). Since the mid 1970s the average air temperature measured at 49 stations in the Himalaya rose by 1°C, much higher than the 0.74°C global average, expressing this sensitivity of mountain regions to climate change (IPCC, 2007). The recession of alpine glaciers, composing up to 4% of the total land ice in the world, already accounts for 20-50% of the 10-15 cm rise in sea level observed during the last century (Oerlemans, 1992; Dyurgerov, 2000). If global warming continues at the current pace, energy-balance models indicate that 30-50% of existing alpine glacier mass could disappear by 2100 (Beniston, 2003). Orographic effects of mountainous regions result in climate conditions varying more sharply with elevation over short distances than with latitudinal changes (Beniston, 2003).

1.11 Climate Change in the Pacific Northwest

Since the Little Ice Age Maximum in the mid-19th century, climate in the Pacific Northwest has been influenced by the Pacific Decadal Oscillation (PDO;

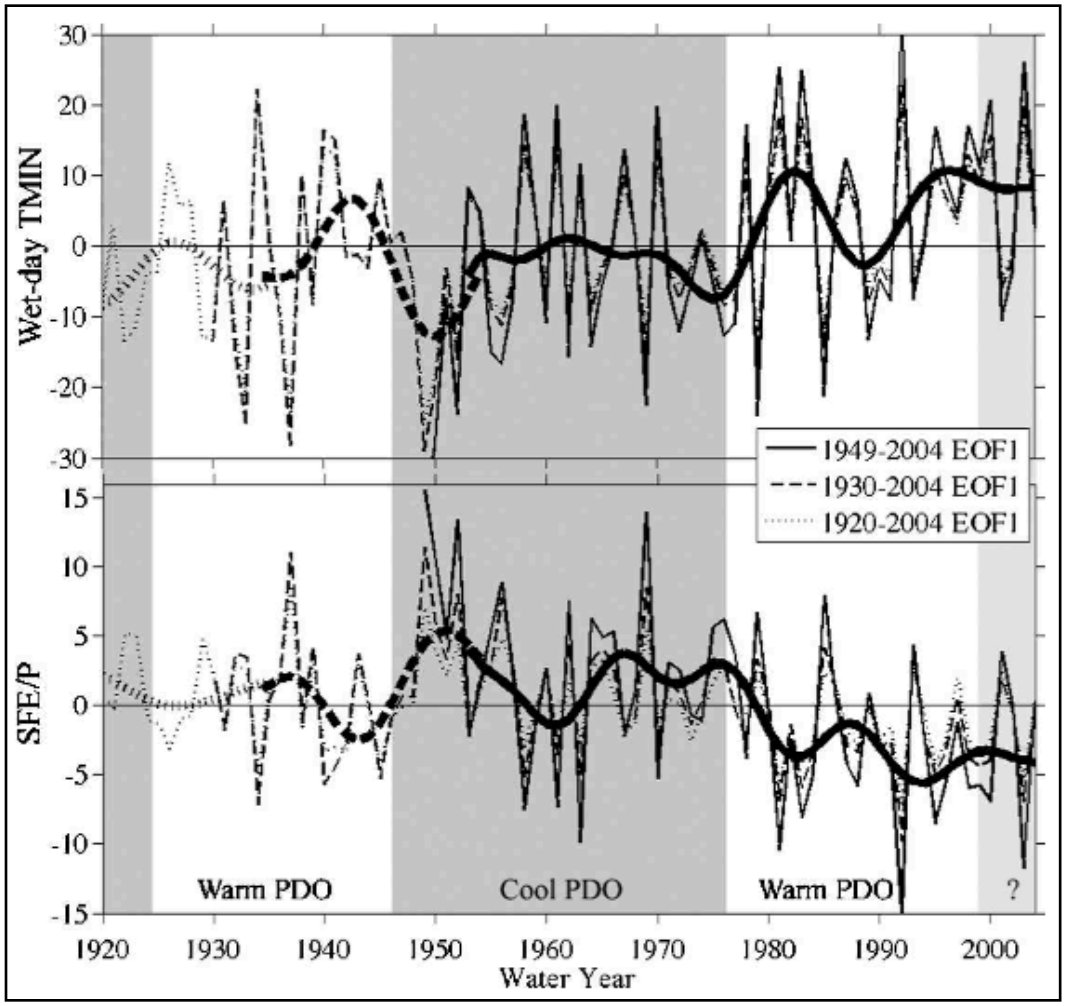

Figure 1.1. Pacific Decadal Oscillation showing climate trends since 1920. Knowles, 2006

Mantua, 2002). The PDO is characterized by decadal scale warm/dry and cool/wet phases (Josberger, 2007). During cool PDO phases, winter storms are directed towards Washington and Oregon, while in warm phases winter storms are driven

further north towards Alaska (Josberger, 2007). During the 19th century the Pacific Northwest saw three distinct PDO phases (Fig 1.1). From 1925 to 1946 and again from 1977 to 2003 the region experienced a warm PDO phase characterized by warmer temperatures and overall negative net glacier mass balances (Knowles, 2006). Between these two warm PDO phases was a cool phase, lasting from 1947 to 1977, where cooler temperatures and increased winter precipitation led to small glacial advances or slower retreats in the Pacific Northwest (Walder & Driedger, 1994). Knowles (2006) believes the PDO may be entering into a cool phase, but with the warmest winter on record in 2010 this is unclear.

Despite the predicted cool phase of the PDO, a general trend towards warmer temperatures in the Pacific Northwest has been observed. In Figure 1.1 Knowles (2006) shows that the warm PDO cycle of 1977 to 2003 is warmer than any other one previously on record. A substantial decrease in Snow Water Equivalent (the amount of water stored in the snowpack, SWE) has also been observed throughout the Pacific Northwest with snowmelt coming earlier in the spring and more precipitation falling as rain in the mountains during the winter (Mote, 2003; Nolin & Daly, 2006; Mote, 2010). Since 1916 the date of peak SWE now occurs 15-45 days earlier and the date of 90% melt out now occurs 15-40 days earlier in the Pacific Northwest (Hamlet, 2005). In general, there has been a regional trend in the Western U.S. towards smaller ratios of winter-total snowfall water equivalent (SFE) to winter-total precipitation (P) during the last 60 years (Knowles, 2006). In 2000, the Accelerated Climate

Prediction Initiative (ACPI) was launched to investigate the impacts of greenhouse warming on water supplies in the western United States (Barnett, 2005). Simulations generated by the project indicated a potential warming of 0.8-1.7°C by the middle of the 21st century accompanied by little or no change in precipitation (Barnett, 2005; Mote, 2010). A recent 2007 IPCC Report predicts temperatures in the Northwest to rise as much as 3°C by 2099 (Christensen, 2007). This would result in reduced depth and duration of winter snowpack, the only insulation the glaciers have against short wave solar radiation from the sun.

1.2 Periglacial Debris Flows

As mountain glaciers are retreating at increasingly faster rates, the frequency of periglacial debris flows worldwide also has the potential to increase (IPCC, 2007). A debris flow is defined as, "a rapid, gravity-induced mass movement consisting of sediment mixed with water and air"(Varnes, 1978). They typically contain as much as 65-70% rock and soil by volume and have the consistency of wet concrete (Walder, 1993). Periglacial debris flows are flows that originate near the terminus of a glacier where large quantities of loose rock are left behind as glaciers recede up the mountain (Figure 1.2). This debutressing and uncovering of steep valley flanks by retreating glaciers and melting permafrost significantly destabilizes the unvegetated slopes of

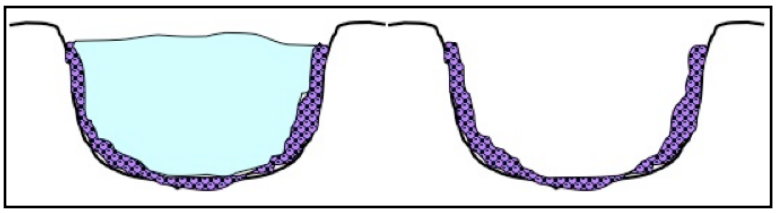

Figure 1.2. Loose debris on lateral moraines left by glacier recession.

glacial terminal and lateral moraines (Zimmerman, 1992; Huggel, 2009). In a study of the Monte Rosa face in the Italian Alps it was shown that the majority of debris flow events originated in recently deglaciated parts of the mountain's east face (Fischer, 2006; Huggel, 2009).

Although debris flows can be triggered by earthquakes, hydrothermal activity or glacial lake outburst floods, they are most often associated with intense rain events that result in jökulhlaups (glacial outburst floods) or landslides of supersaturated debris on the moraines left by retreating glaciers (Walder, 1994; Iverson, 2000). Intense rain events rapidly input water to the bed of the glacier, causing an increased englacial water pressure, which destabilizes the system of ice cavities underneath the glacier (Walder, 1994; Roberts, 2005). This pressure, in combination with decreased shear strength in rocks from melting permafrost, results in an outburst flood that entrains loose debris left on the moraines by the retreating glacier (Fischer, 2006; Roberts, 2005). Smaller outburst floods or increased stream discharge from melting can also undercut the toe slopes of glacier lateral moraines, leading to slope failure

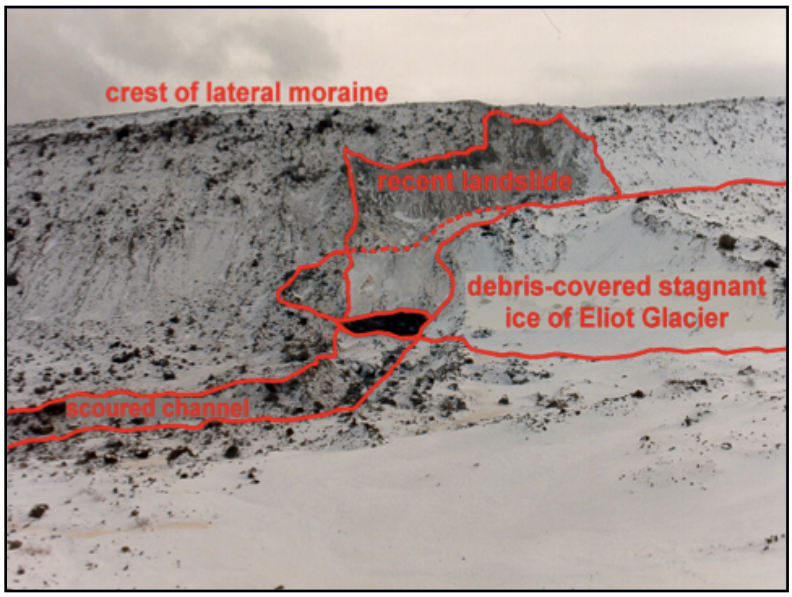

Figure 1.3. A landslide on the lateral moraine of Eliot Glacier, Mt. Hood. Courtesy Amit Armstrong

and landslide initiation (Figure 1.3 and 1.4). The collapse of steeply angled sediment due to increased stream discharge, coupled with outburst floods from glaciers during intense rain events, may be one of the leading triggers of debris flow initiation (Copeland, 2009; Iverson,

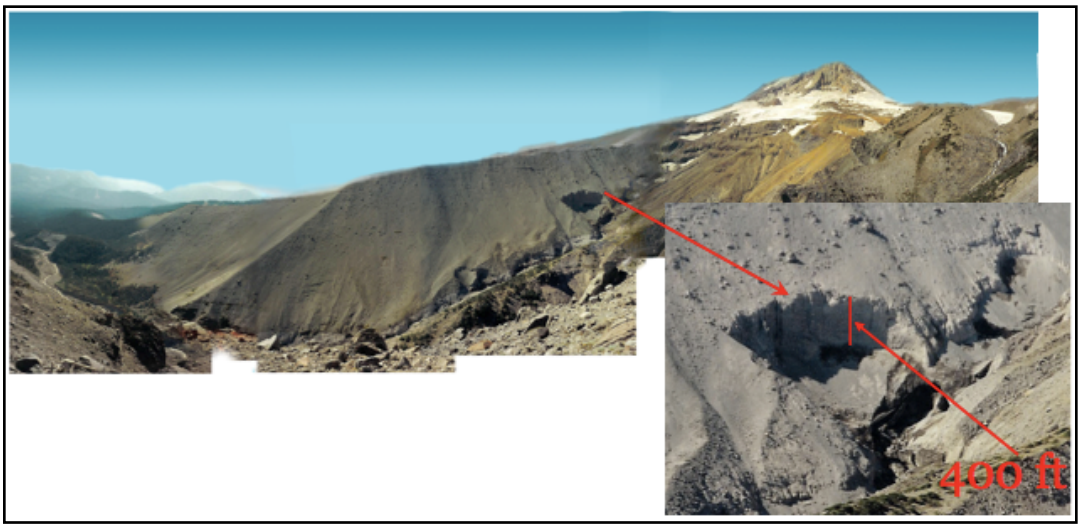

Figure 1.4. A large landslide on the lateral moraine of the Newton Clark Glacier on Mt. Hood due to Newton Creek undercutting the toe of the slope. Courtesy Tom DeRoo.

2000). Several studies in the Alps have also shown a correlation between increased

frequency and the rate of intense rainfall in glacierized basins with the triggering of debris flows (Bacchini & Zannoní, 2003; Haeberli, 1990; Zimmerman, 1992; Rebetez, 1997; Steijn, 1996; Stoffel, 2005; Huggel, 2005). Chiarle (2007) found that most debris flows in the Alps were initiated by slope failures of supersaturated debris left by retreating glaciers during intense rain events. He also found that most debris flows initiated after the ablation season, asserting that snow-free ice enhances the impact of intense rain events as the ice responds quickly to rainfall, creating glacial drainages and faster infiltration and transmission of water to stream channels below (Chiarle, 2007).

Debris flows have been observed in alpine areas for over a century but only in the past 25-30 years have they gained widespread attention due to their destructive nature (Berlepsch, 1861). Debris flows from glaciated basins are incredibly destructive to valuable infrastructure such as hydroelectric dams, roadways, farmland, bridges, buildings and recreational sites. They can travel at speeds of up to 85 km hr^{-1} and have discharge rates up to 3×10^5 m^3s^{-1} (Roberts, 2005). These flows destroy riparian vegetation and aquatic habitats and often drastically alter channel morphologies (Figure 1.5). The widening of channels by debris flows often leads to an increase in stream temperature from solar radiation thereby altering the ecosystem (Johnson, 2000). Increased stream temperatures have been linked to increased fish mortality, increased prevalence of disease, and changes in interspecific competition

Figure 1.5. Newton Creek before and after a massive debris flow on Mt. Hood. Courtesy Amit Armstrong.

(Fagre, 1997). At the present time, cryosphere-related disasters such as debris flows, outburst floods, and ice avalanches from retreating glaciers have the potential to kill hundreds or possibly thousands of people with damage costs estimated to be upwards of $100 million annually (Bishop, 2004; Figure 1.6).

Figure 1.6. Highway 35 repair after a debris flow washed out the bridge over the White River.

1.3 Previous Remote Sensing Studies of Glaciers Worldwide

Since the end of the Little Ice Age in the mid-19th century, glacial recession has been observed in nearly all the glaciated mountainous regions of the world. Initially, glacier analysis was completed through ground field surveys or through aerial photographs and historical maps. When access to glaciers is convenient, ground surveys are still the most accurate way to assess area and mass balance changes. However, the use of historical maps to assess glacial change often leads to questionable accuracy. For example, Phillippe (2008) found the 1956 USGS maps missed more than 60% of the debris-covered Eliot Glacier on Mt. Hood but overestimated other areas due to existence of seasonal snow when the survey was completed. If the glaciers being studied are located in remote regions, traditional glacier mapping methods prove difficult and prevent fine temporal resolution studies, which are necessary to analyze effects of regional climate change. Because of these early difficulties in glacier monitoring, only 10 continuous direct annual mass balance time series extend beyond 1960 (Haeberli, 1998). With the arrival of satellite technology in the late 1960s it became possible to monitor glaciers on a broader scale.

Satellites have provided optical imagery of glacier extents since 1972 but these observations were only in the visible spectrum at first, which prevented the classification of ice from snow. Glacier monitoring began in 1986 with the creation of the World Glacier Monitoring Service (WGMS), now a sub-part of the Global

Climate Observing System (GCOS) run by the World Meteorological Organization (WMO) (Raup, 2007). In 2005 the WGMS established the GLIMS (Glacial Land Ice Measurement System) to create a satellite imagery derived inventory of the world's estimated 160 thousand glaciers for the purpose of understanding glacial change in terms of climate change and other environmental forcings (Raup, 2007). GLIMS is composed of 60 institutions worldwide with researchers from 27 different countries. Several of the glacial outlines for Mt. Hood used in this study were obtained from the GLIMS glacier database online.

One of the most popular methods utilized by GLIMS researchers to investigate glacier change is the combination of spectral bands to delineate glacial ice from surrounding rock. Dozier (1984) used different combinations of Landsat spectral bands 1, 2, 4 and 5 (Figure 2.5) to distinguish between snow, non-snow, and clouds in mountain scenes. The spectral reflectance of snow is very high in the visible part of the electromagnetic spectrum but much lower in the near-infrared wavelengths. Thus, it can easily be distinguished from other land cover types. Based on the spectral reflectance work of Dozier, Hall (1987) found that the ratio between Landsat TM bands 4 and 5 provided clear outlines of ice extent in a study of alpine glaciers in Austria and southern Alaska. Hall's work was later verified by Paul (2001, 2002) who compared TM4/TM5 band ratio classifications of glaciers in the European Alps to those of the panchromatic bands of the French Satellite Pour l'Observation de

la Terre (SPOT), finding that the Landsat ratio was within 3% of the higher spatial resolution SPOT classification.

During the 1990's multiple studies used Landsat Thematic Mapper data to assess glacial change throughout the world. Debris-covered glacier ablation in the Khumbu Himal region of the Himalaya was studied by Nakawo (1993) using the Multi-Spectral Electronic Self-Scanning Radiometer (MESSR) but at a spatial resolution of only 50 m. A Landsat band 4/band 5 ratio was also used to study the eastern Alps of Austria based on Halls' methods (Bayr, 1994). Until the Advanced Space borne Thermal Emission and Reflection Radiometer (ASTER) was launched on board the TERRA satellite in 1999, studies of alpine glaciers with remote sensing were restricted to Landsat or SPOT data sets.

One of the first major studies using satellite imagery to determine glacier retreat on a large scale was the Swiss Glacier Inventory of 2000 (Kääb, 2002). In the Swiss Alps, glacier recession increased from -2.8% per decade for the period 1850 to 1973 to -14% for the years 1985 to 1999 (Paul, 2004, 2005, 2007). Since 1850, the total aerial extent of glacierized areas in the European Alps has decreased by 35%, with the volume of ice decreased by 50% (Hall, 2003). This decrease is particularly troubling for Switzerland which obtains most of its electricity through hydropower, 24% of which is produced through reservoirs that collect glacier meltwater (Chen, 1990). Initially Switzerland will see a surplus in hydropower but in the long term streamflow to hydroelectric dams will diminish and the country will lose one of its

primary sources of electricity. Berthier (2004) has also shown that the large "Mer de Glace" glacier descending from Europe's tallest mountain, Mont. Blanc, has undergone rapid retreat in the last 25 years.

Glaciers in other regions of the world have also been surveyed using remote sensing. The Austrian Alps have seen an area change of -17% between the years 1969 and 1998, a decrease of 6% per decade (Hall, 2003; Lambrecht, 2007). The Tien Shan region of China saw an area decrease of -17% from 1955 to 1999, a decrease of 9% per decade (Kääb, 2003; Khalsa, 2004; Bolch, 2007). In a study by Andreassen (2008) 164 glaciers in the Jotunheimen and Breheimen regions of Norway were found to have shrunk 12% since the 1960s. In Peru, Silverio (2005) found the glacier area in the Cordillera Blanca retreated by more than 15% in just 25 years. Glacier cover in the Canadian Rockies has decreased by 25% during the 20th century (Luckman, 2000). Satellite data have also been particularly useful in identifying glacial lakes with potential to cause outburst floods in the Himalaya (Bolch, 2008). Figure 1.7 from the IPCC report on climate change in 2007 shows the relative rate of global glacial retreat.

With the launch of very high spatial resolution satellite sensors such as IKONOS in 2000 with a 1-m spatial resolution and QuickBird with a sub-meter panchromatic resolution in 2001, it has recently become possible to study glacial

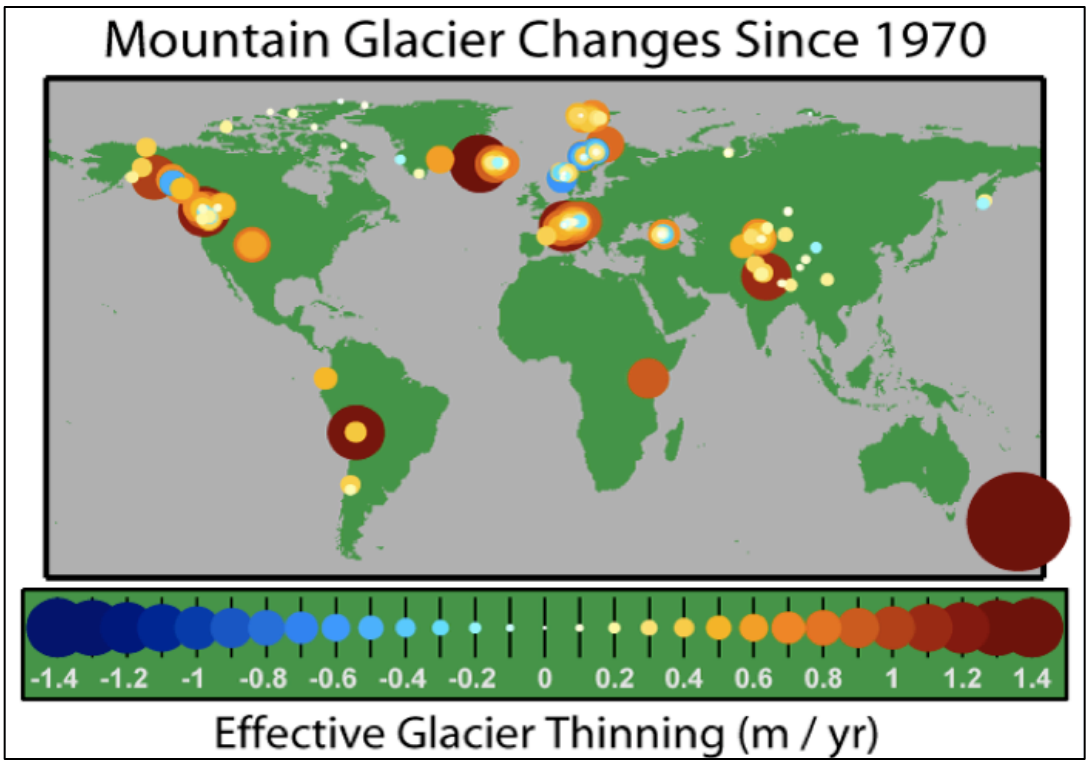

Figure 1.7. Mountain glacier change since 1970 worldwide. IPCC 2007.

geomorphology from space (Huggel, 2004; Kääb, 2003). High resolution panchromatic satellite bands have also been used to build digital elevation models (DEMs) to evaluate changes in glacier thickness in remote areas where high resolution DEMs do not exist (Berthier, 2004). ASTER data have also been used to measure glacier surface velocity in inaccessible mountainous regions such as the Himalaya (Bolch, 2009). However, many of these new high spatial resolution satellites lack the broad spectral resolution of Landsat's Thematic Mapper that remains, along with ASTER, the best tool for assessing the spectral reflectance of glacial ice in mountainous regions (Bishop, 2004; Quincy, 2005; Racoviteanu, 2008).

1.31 Previous studies of Glacier Change in the Pacific Northwest

With its isolated volcanic peaks situated on the Pacific "Ring of Fire" in a maritime environment, the Pacific Northwest provides a perfect study location for comparison of glacier retreat to other regions of the world. Scientific study of glaciers in the Western US did not begin until September 1871 when the King expedition discovered glaciers on Mt. Shasta in California, Mt. Hood and Mt. Rainier (Hague, 1871). Only six states in the lower 48 have significant glacier cover (Colorado, Wyoming, Montana, California, Oregon, and Washington) with 71% located in Washington (Bishop, 2004). The largest glacier in the lower 48 states, Emmons on Mt. Rainier, occupies an area of 11.2 km^2.

Previous studies have shown that glacier retreat in the Pacific Northwest is less than in other parts of the country and world, possibly due to very high accumulation zones on the stratovolcanoes (Bishop, 2004; Medley, 2008). Fountain (2010) found the total volume loss in the North Cascades National Park to be 7% compared to the average loss of 21% (1973-98) in Switzerland (Kääb, 2002) and 18.3% in Austria (1969-92) (Paul, 2002). Hall & Fagre (2003) found the Grinnell glacier in Glacier National Park shrank by 30% over the same period. Currently, detailed historical measurements of glacier mass balance are only available for the South Cascade Glacier (Dyurgerov, 2000). One unique exception in the region is the glacier growth in the crater of Mt. St. Helens which is attributable to the eruption in 1980 that created a deep north-facing crater, perfect conditions for snow collection

Figure 1.8. Location of the major volcanoes of the Pacific Northwest. Glacier distribution from 1:100k USGS topographic maps is overlaid on regional topography.

and solar radiation protection (Schilling, 2004). In a study of the glaciers on Mt. Hood from 1901 to 2001, Lillquist (2006) found that glacier termini fluctuated in response to climate forcings such as the PDO on multiple occasions but overall a dramatic retreat was observed. Kennard & Walder (1984) also observed large glacier area recession throughout the 20th century, based on historical USGS mapped glacier outlines dating back to 1913.

1.4 Study Site Description

Both Mt. Rainier and Mt. Hood are situated in a maritime climatic region where persistent seasonal pressure systems such as the Aleutian Low cause winters of heavy rain and snow while the North Pacific High produces hot and dry summers (Latif, 1994; Figure 1.9). The Cascade Range, with its north-south axis, intercepts

significant amounts of precipitation and the western side receives about 10 times more than the eastern side (Nolin, Personal Communication). Figure 1.8 shows the locations of Mt. Rainier and Mt. Hood in the Cascade Range of the Pacific Northwest. Whether the current climate is wet or dry is linked to the Pacific Decadal Oscillation Regime (PDO) (Armstrong, 2010). In the fall the subtropical jet stream shifts northward, allowing intense, warm rainstorms of tropical origin to hit the West Coast. These so-called "Pineapple Express" storms can sometimes reach as far north as the Pacific Northwest.

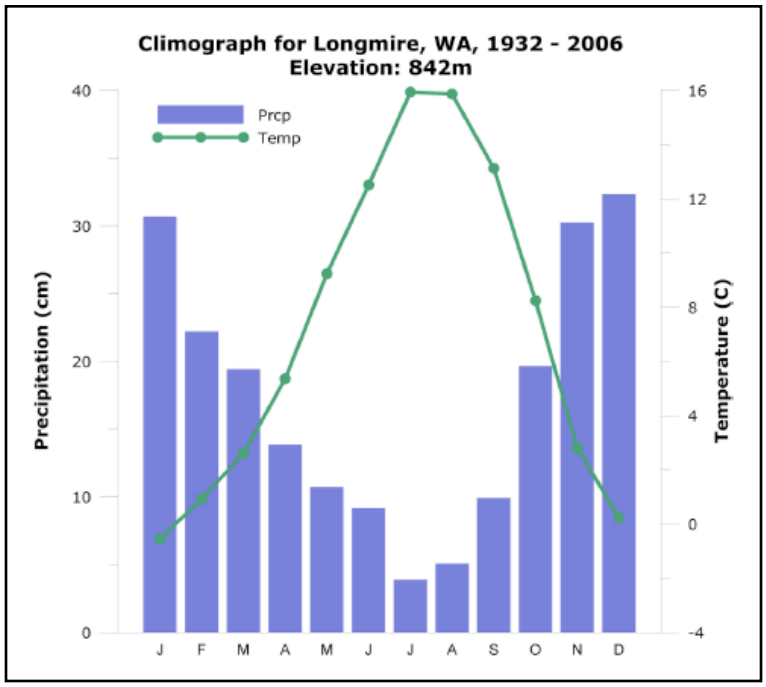

Figure 1.9. Climograph of mean monthly temperature and precipitation for Longmire, WA, 1932-2006. This is representative of typical Pacific Northwest Climate. Courtesy B. Medley.

In 1996 and again in 2006 the Pacific Northwest received heavy precipitation leading to heavy flooding and multiple debris flows (McCabe, 2007). Both of these events were the result of a Pineapple Express storm that made landfall in the Pacific Northwest. More recently, the moisture for these storms have been defined as

"Atmospheric Rivers", which are long (greater than 2000 km) and narrow (less than 1000 km wide) bands of enhanced water vapor flux and high tropospheric winds that diverge from the tropical circulation (Neiman, 2008; Figure 1.10). These Atmospheric Rivers are thought to be responsible for over 90% of the water vapor transported poleward and play a crucial role in the global water cycle. Historical

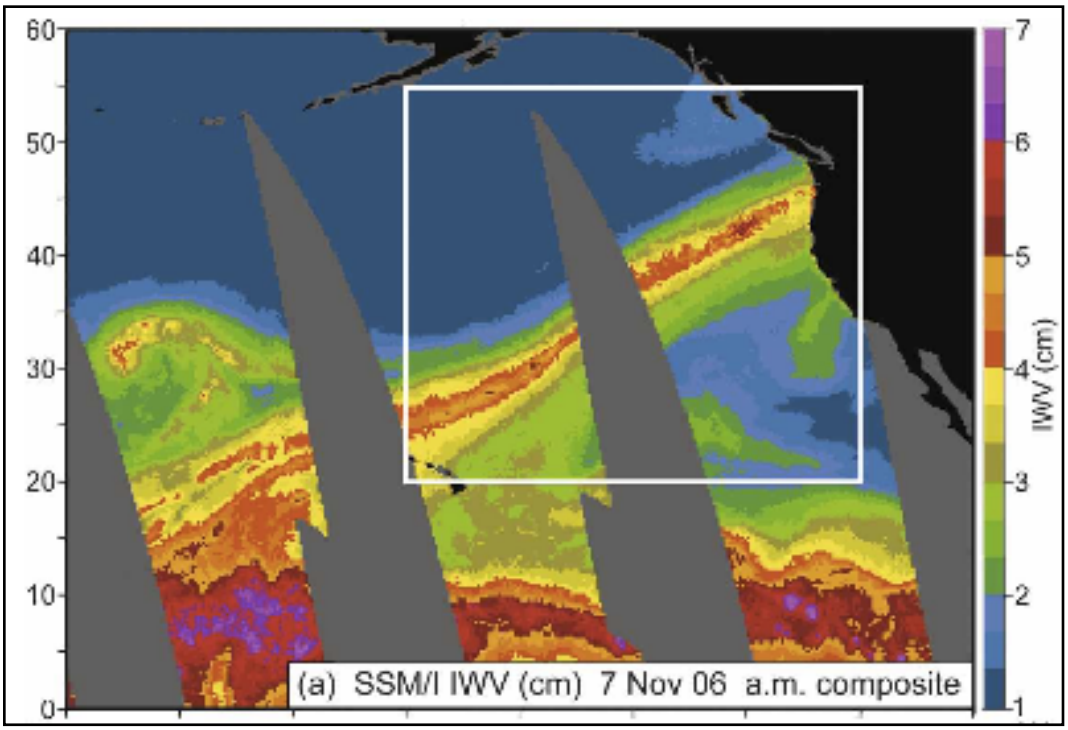

Figure 1.10. An Atmospheric River of moisture making landfall the same day as multiple debris flow initiations on both Mt. Rainier and Mt. Hood. 7 Nov 2006. Neiman, 2008.

records of these occurrences are sparse, but modern polar orbiting weather satellites and stationary satellites over North America and soundings from the Observing System for Meteorology, Ionosphere, and Climate (COSMIC) now allow identification of these events in the troposphere (Neiman, 2008).

1.4 Study Site Description

1.41 Mt. Hood Oregon

Mt. Hood, geographic location 45.374°N, 121.694°W, is a chiefly andesitic composite volcano of Quaternary age in the Cascade Range of the Pacific Northwest that rises to 3430 m in elevation. With a volume of 50 km^3 the active volcano is mid-sized in the Cascade Volcanic Range (Scott, 2003). The peak, named in 1792 after the British Naval Officer A.A. Hood, lies 70 km east of Portland, Oregon (Scott, 2003). On average the mountain receives about 12 to 13 m of snowfall annually (CVO, 2010). Four major rivers drain the volcano: the White, Hood, Zigzag and

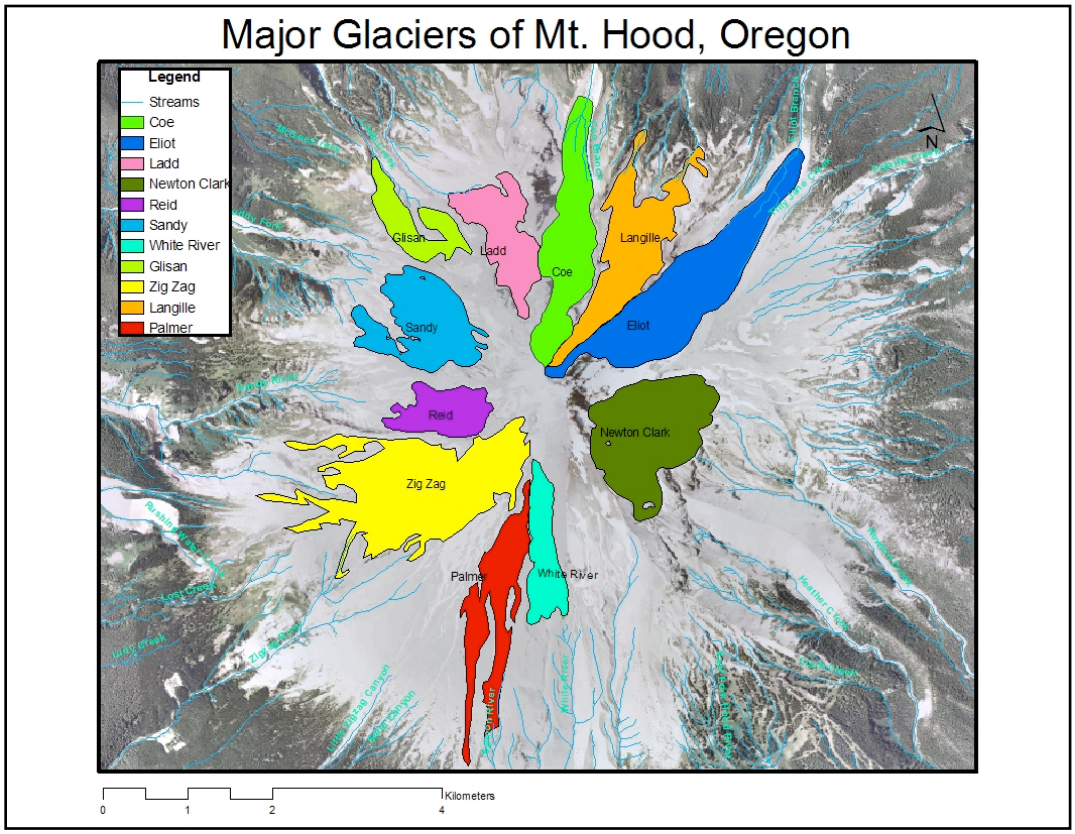

Figure 1.11. The glaciers on Mt. Hood overlaid on top of a 2005 orthorectified NAIP.

Sandy. All drainages from the mountain empty into the Columbia River to the North with the Hood watershed accounting for 60% of the total area covered by snow and ice (Driedger, 1984).

Of the 11 major glaciers on Mt. Hood (the 12th glacier, the small Coalman Glacier within Crater Rock, is not examined in this study), the Eliot Glacier has the largest volume and thickness of ice with the Coe-Ladd glacier system having the largest surface area (Driedger, 1984). The glaciers on Mt. Hood cover about 80% of the summit cone at 13.5 km^2 and contain an ice volume of about 400 km^3 (Driedger, 1984; Figure 1.11). Today the glaciers on Mt. Hood terminate around at 2100 m elevation but during the Frasier Ice Age, 29,000 to 10,000 years ago they reached down to 700-800 m and reached as far as 15 km from the summit (Crandell, 1971; Lillquist, 2006).

Figure 1.12. Polallie Creek on Mt. Hood before and after a debris flow. Courtesy Amit Armstrong.

Mt. Hood has seen many significant debris flows, with most triggered by intense rain events such as the November 2006 storm that resulted from a Pineapple

Express/Atmospheric River in November 2006 (Figure 1.13 and Table 2.10). Several drainages, the White River, Polallie Creek, and Newton Creek, have seen the most extensive change over the past 30 years (Figure 1.12). Other remote drainages such as the Sandy and the Muddy Fork have experienced debris flows in recent years. In 2002 a rockslide quickly transformed into a large debris flow in the upper reaches of the Muddy Fork and glacial outburst floods have been recorded on the Zigzag, Ladd, Coe, and White River Glaciers.

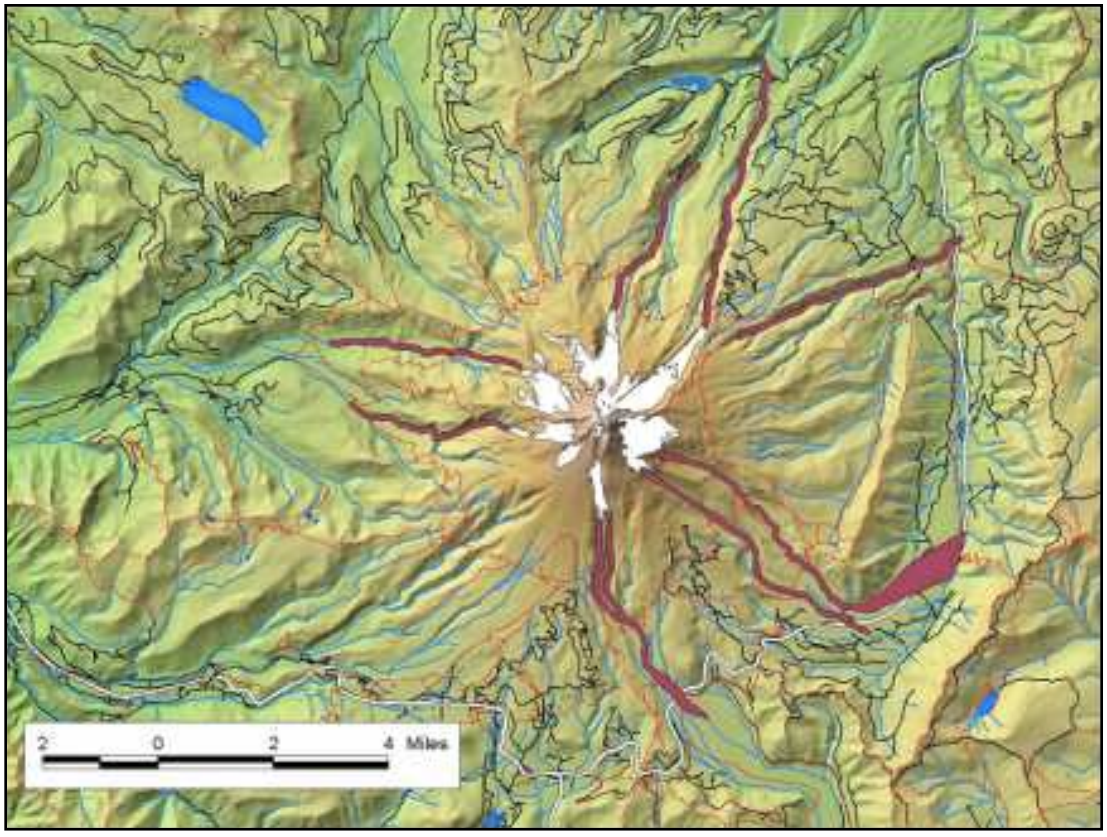

Figure 1.13. Historical debris flow paths and inundation areas for Mt. Hood. Courtesy Amit Armstrong.

One of the first recorded debris flows observed on the peak occurred in 1922 when a dark debris flow exited a crevasse high on the Zigzag glacier and moved 650

m over the ice before entering another crevasse (Scott, 2003). The event led to concern that the mountain was beginning to erupt. In 1961, the Ladd Glacier outburst flood destroyed sections of the road around the West side of the mountain and in 1963 the Coe Glacier outburst flood forced the re-routing of the "Round-the-Mountain" trail farther from the glacier (Swanson, 1989). On Christmas Day 1980, after an

Figure 1.14. The Highway 35 White River Bridge after the November 2006 storm. Photo by William J. Burns, DOGAMI.

intense rain, a landslide at the head of Polallie Creek Canyon transformed into a debris flow that deposited approximately 7.65×10^4 m^3 of debris up to 11 m thick at the confluence with the East Fork Hood River. This quickly formed a 34-hectare lake

behind the debris that subsequently broke, causing one fatality and over $13 million in property damage (Gallino, 1985).

The White River drainage on Mt. Hood has been the site of numerous devastating debris flows. Glacier outburst floods from 1926, 1931, 1946, 1949, 1959, and 1968 each destroyed the Highway 35 bridge over the White River, an important recreational access road for hiking trailheads, Mt. Hood Meadows Ski Area as well as

Figure 1.15. The Oregon Highway Department repairing the White River Bridge after a debris flow in 1998 tore it out.

a crucial link between I-84 and US 26 (Swanson, 1989). Recently, the White River drainage experienced debris flows during or shortly after intense rain events in 1998, 2000 and again in 2006 causing extensive damage each time to Oregon Highway 35 (Figure 1.14). Each event forced the Oregon Department of Transportation to close

the highway with repairs exceeding $1 million for each occurrence (CVO, 2010; Figure 1.15). The narrow, steep White River Glacier continues to slowly erode a trench leading up to Crater Rock which ensures the drainage will be a primary path for pyroclastic flows should another eruption occur (Scott, 2003; Figure 1.16). T. Deroo (personal communication) found that debris flows on Mt. Hood most frequently occur in the fall when three conditions are met: minimal snow cover, a freezing level greater than 2500 m and a rainfall intensity exceeding 5 cm in 24 hours.

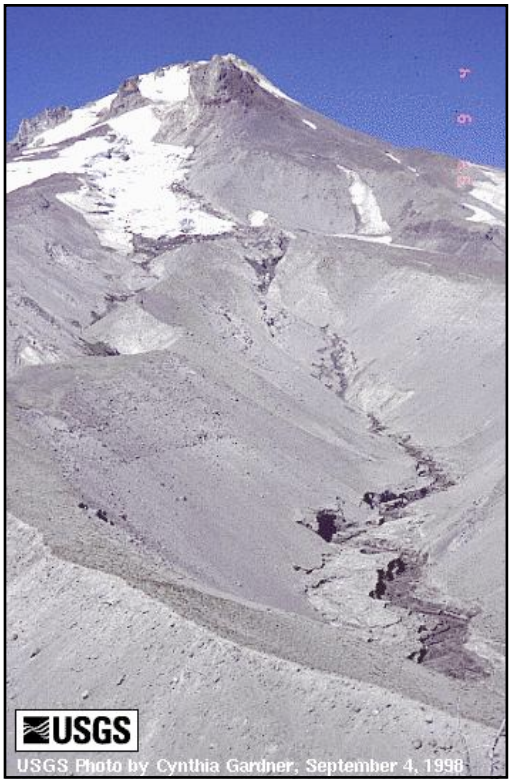

Figure 1.16. A debris flow initiation area with scour evidence below the White River Glacier, Mt. Hood. Photo by Cynthia Gardner 1998.

One of the most recent and best studied debris flow events on Mt. Hood occurred in November 2006 when an intense rainstorm deposited 34 cm of precipitation over six days on Mt. Hood. This storm triggered seven debris flows in the 11 drainages of the mountain with the most damaging torrents coming from the White River, Clark Creek, Newton Creek, Eliot Creek and Sandy River (Pirot, 2010). Two bridges on Eliot creek were ripped away, the White River Bridge was destroyed, and a new delta formed on the Columbia River from the sediment

transported downstream from the storm (Pirot, 2010). This study looks at the known locations of these debris flows in relation to glacier recession on the mountain.

1.4.2 Mt. Rainier, Washington

At 4329 m in elevation, Mt. Rainier, a large stratovolcano of andesitic rock composition, is the most glaciated peak in the lower 48 states. At geographic location 46.87°N, 121.758°W, Mt. Rainier appears to sit atop Tacoma's skyline just 40 miles away. By volume Rainier is the third largest in the Cascade volcano chain behind Mt. Shasta, California and Mt. Adams, Washington (Wood, 1990). Captain George Vancouver named the mountain on May 8, 1792 after his friend Admiral Peter Rainier and on March 2, 1899 Congress established the Mount Rainier National Park making it the fifth oldest National Park in the country (National Park Service). Mt. Rainier experiences an average of nearly 18 m of snow annually with the record breaking winter of 1971-72 bringing 28 m of snowfall to the peak (Driedger, 1986). Mt. Rainier is drained by five major rivers, the Carbon, White, Cowlitz, Nisqually and Puyallup, which empty into Puget Sound, and the Cowlitz, which enters the Columbia River. Each of the major rivers occupy deep canyons with Tahoma Creek, North and South Puyallup and Mowich Rivers having the steepest gradients in the park (Crandall, 1971).

Since the last ice age the volcano has undergone three major eruptions resulting in mudflows, the largest being the Osceola and Paradise Mudflows 5,600 years ago, one of the largest known in the world (Crandall 1969). At that time, a

catastrophic collapse, much greater than that of Mt. St. Helens in 1980, created the mudflows, which travelled down the White and Nisqually rivers pushing out the Puget Sound shoreline several miles (Sisson, 1995). Before this collapse the summit was estimated to reach a height of nearly 5000 m (Crandall, 1969).

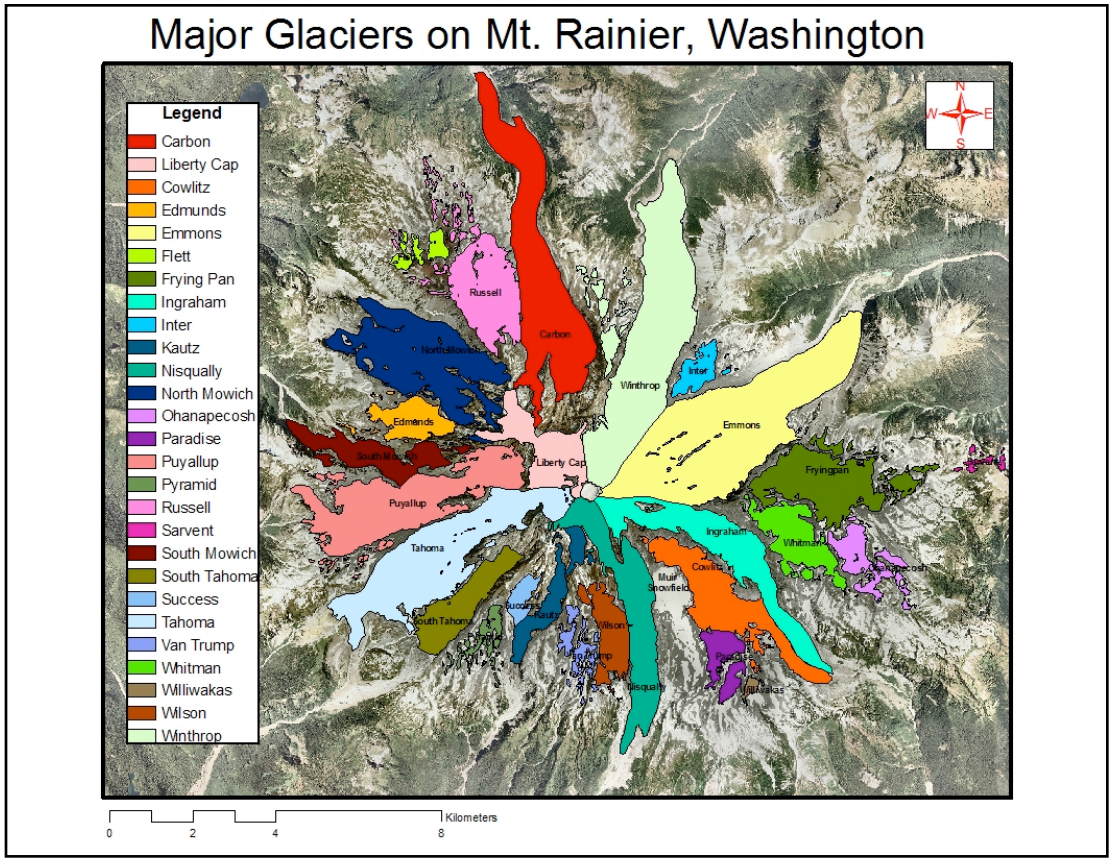

Figure 1.17. The glaciers of Mt. Rainier on top of a 2009 orthorectified NAIP.

The 27 glaciers of Mt. Rainier cover more area than all the other Cascade volcano glaciers combined at 92 km^2 with a volume of 4400 km^3 (Walder, 1986; Figure 1.17). The Emmons Glacier is the largest in the contiguous United States and the Carbon glacier has the lowest terminus at just over 1000 m (Driedger, 1992). During the last ice age about 15,000 years ago the glaciers on Mt. Rainier extended

well beyond the perimeter of the National Park to the Puget Sound Basin (Driedger, 1992) with their maximum extent during the last several centuries occurring around

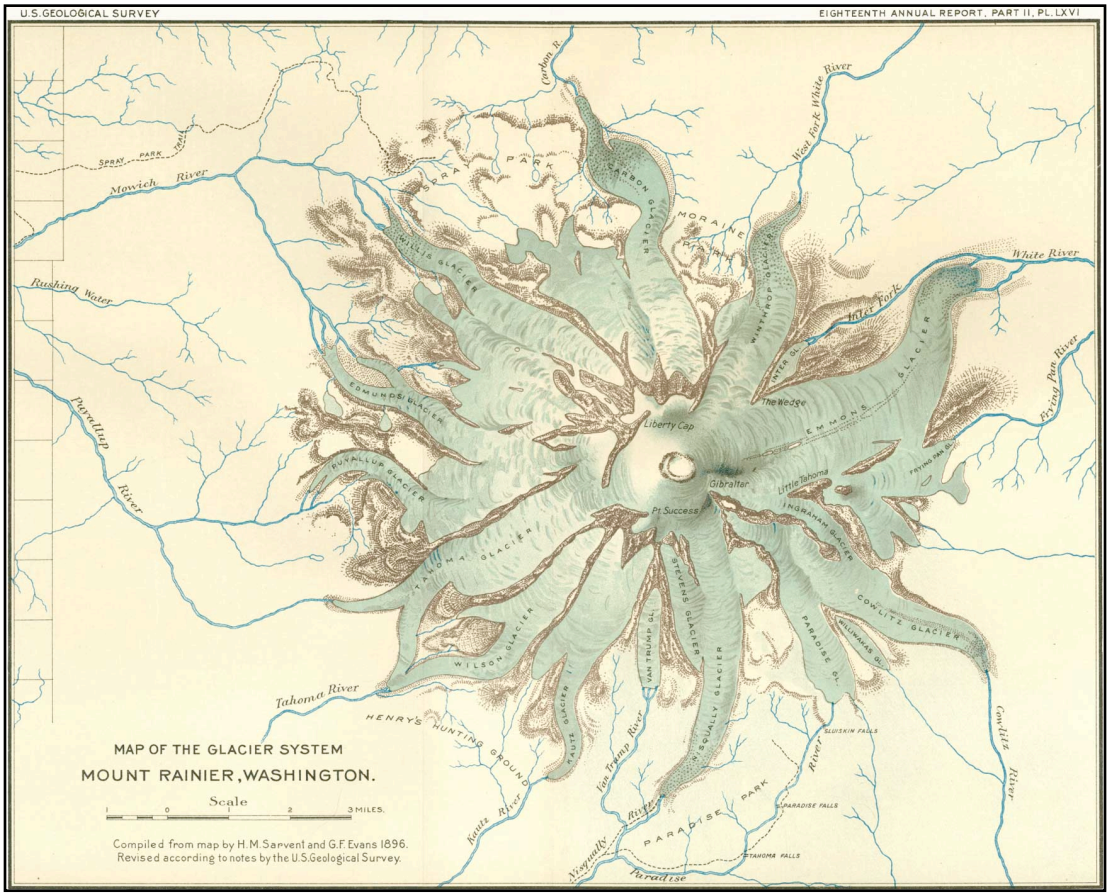

Figure 1.18. The first map of Mt. Rainier glaciers compiled by H.M. Sarvent and G.F. Evans of the USGS in 1896.

1750 (Burbank, 1981; Driedger, 1986). The first rudimentary map of glacier locations for Mt. Rainier was sketched by H.M.S. Sarvent and G.F. Evans in 1896 as part of the USGS Geological Survey 18th Annual Report (Sigafoos, 1972; Figure 1.18). The first research of glacier positions on Mt. Rainier was reported by geologist I.C. Russell in 1898 who noted that some glaciers had retreated more than 3 km up their valleys since 1750 (Russell, 1898; Reid, 1906).

Figure 1.19. Debris flow at Tahoma Creek, Mt. Rainier. 26 July 1998. Photograph by G.G. Parker of the USGS.

Over 40 debris flows have now been documented on Mt. Rainier since 1926, most during intense late summer or fall rainstorms with several during hot and dry weather (Vallance, 2003; Table 2.7). Flows have been recorded traveling 10 km or more from their sources (Vallance, 2003). Debris flows occurring primarily from glacial outburst floods have been recorded most from the Nisqually, Kautz, South Tahoma and Winthrop glaciers on Mt. Rainier (Copeland, 2009). Since 1967 there have been 26 debris flows in Tahoma Creek alone (Figure 1.19). These flows have transported approximately 1×10^7 m^3 of sediment down the mountain and over time have carved a gorge 40 m deep into the sediments and stagnant ice below the Tahoma Glacier from which the creek originates (Walder, 1994; Figures 1.19 and 1.20). From 1986 to 1992 the glacier experienced 15 outburst floods, at least one every year (Walder, 1995).

Figure 1.20. Debris flow descending Comet Falls on Mt. Rainier, 15 Aug 2001. Photo by J.W. Vallance.

Debris flows on Mt. Rainier travel downstream at speeds of up to 10 ms^{-1}, have steep boulder-filled snouts up to 20 m in height, and can continue down the mountain for up to an hour (Walder, 1993). The largest debris flow since the park was established occurred in 1947 in Kautz Creek when a rain-induced outburst flood mobilized 38×10^6 m^3 of debris, burying the Nisqually-Longmire Road under nine m of debris, including some boulders measured at over four m in diameter (Walder, 1993). Debris flows have occurred as seldom as once every eight years and as often as four times a year on Mt. Rainier (Walder, 1993; Richardson, 1968). Smaller debris

flows are common with as many as four occurring in one year, but larger debris flows such as the 1947 Kautz flow have an estimated recurrence of once every 100 to 200 years based off historical records (Vallance, 2003). Unfortunately, after Walder and Driedger completed their debris flow studies of Mt. Rainier from 1985 to 1993 there was a gap in the chronology of debris flows for the peak with the exception of a debris flow in 2001 observed by Vallance and other Cascade Volcano Observatory (CVO) scientists (Figure 1.20; Table 2.7). In the years since 2001, as Regional Geomorphologist for Mt. Rainier, Kennard has been informally studying debris flows in the park and field studies by B. Copeland in the summer of 2008 have done much to replenish the chronological record of debris flows.

The November 2006 rain event delivered over 45.7 cm of rainfall in 36 hours, triggering multiple periglacial debris flows on Mt. Rainier (Table 2.9). These flows traveled down the mountain destroying large sections of the Wonderland Hiking Trail as well as numerous man-made facilities within the National Park. The storm also resulted in several debris flows originating from glacial drainages not previously associated with historical debris flow initiation. This study looks at the locations of these debris flows in relation to glacier recession on the mountain.

Chapter 2: Methodology

This study uses a combination of remote sensing data obtained from Landsat 5 and Landsat 7 Thematic Mapper (TM) imagery, airborne LiDAR, climate data, and aerial photos in combination with Geographic Information System (GIS) software to

look at glacier change in relation to debris flows at both spatial and temporal scales. Previous studies have shown that multispectral Landsat imagery can effectively delineate glacial ice from surrounding rock (Paul 2002 & 2004; Andreassen, 2008). Therefore, the first step in this study was to apply a similar technique to our study areas in order to map glacier areas. The second step was to compare local glacier recession to the locations and dates of known debris flows for both Mt. Hood and Mt. Rainier.

2.1 Data Descriptions

2.11 Landsat Thematic Mapper

Landsat was chosen for this study because of its long life of operation, frequent scene capture and consistent sensors. The Landsat program, jointly managed by NASA and the USGS has been in operation since 1972 (Figure 2.1). Since 1982 the Landsat series of satellites have carried Thematic Mapper instruments capable of measuring multiple bands of electromagnetic radiation reflected from the earth at

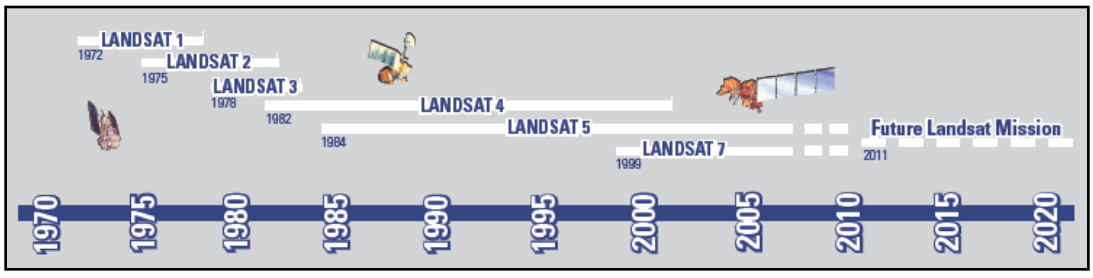

Figure 2.1. Historical Landsat Missions. USGS:Landsat.

high spectral resolutions (Figure 2.2). Landsat 5 and Landsat 7 imagery, used for this study, were launched from Vandenburg Air Force Base, California, on 1 March 1984

and 15 April 1999 respectively (NASA). Both satellites operate on a 16-day polar orbit at an altitude of 705 km above the earth's surface (NASA, 2009). The Landsat Thematic Mapper has a cross-track scanning angle of 5.78°, resulting in a 185 km swath width (Figure 2.3). The resulting scenes have a ground-projected instantaneous field of view of 30 m. Each Landsat image is 185 km wide and 170 km in the along-track dimension (Jensen, 2000). Each Landsat band is recorded in 8-bit radiometric resolution on a scale of 0-255 (Figure 2.4). The Landsat TM sensor acquires data in 7 distinct bands (Figure 2.5). Bands 1 through 3 are in the visible electromagnetic spectrum, 4 is in the near-infrared, and 5 and 6 are in the mid-infrared and all have a spatial resolution of 30 m. Band 7 is a thermal

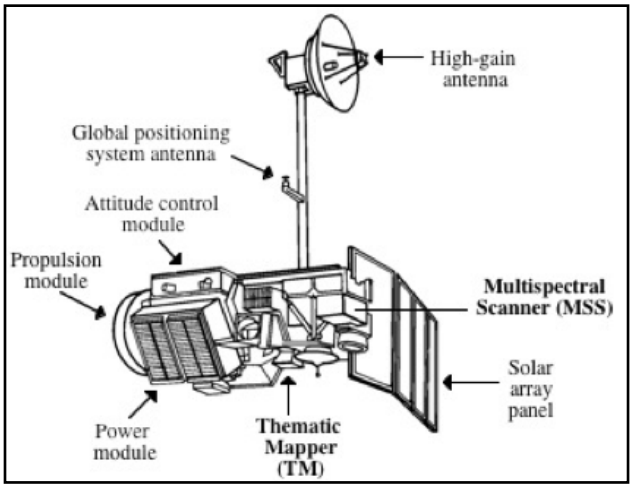

Figure 2.2. Landsat 5 and 7 satellite schematic. Jensen, 2000.

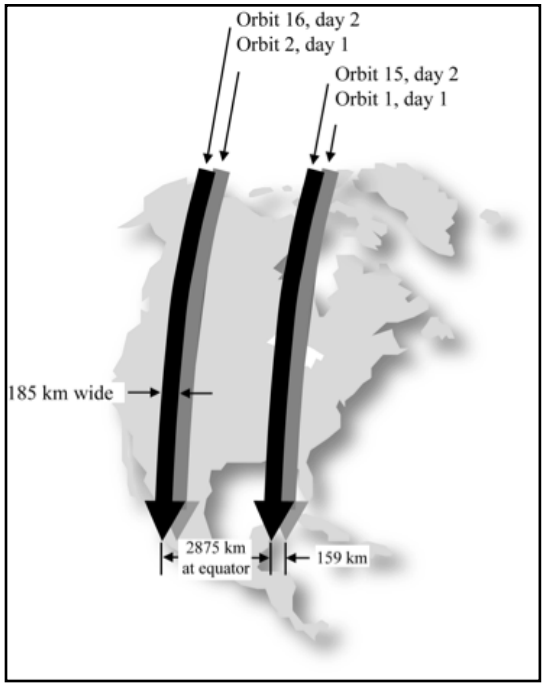

Figure 2.3. Landsat Scene acquisition. The scanner creates orbital paths 185 km wide which are then split into 170km long scenes. Jensen, 2000.

infrared band used to interpret surface temperatures with a reduced spatial resolution of 120 m. This study uses Thematic Mapper bands 4 and 5 which are known for their utility in the differentiation of clouds, snow and ice, water penetration, soil and plant moisture, and vegetation type and health, making them very appropriate for a study of temporal glacier recession. Band 4 (0.76-0.90μm) shows strong spectral variability in response to glacial ice while band 5 (1.55-1.75μm) can be used to distinguish between clouds, snow and ice as well as to determine water content in soil and vegetation (Dozier, 1989).

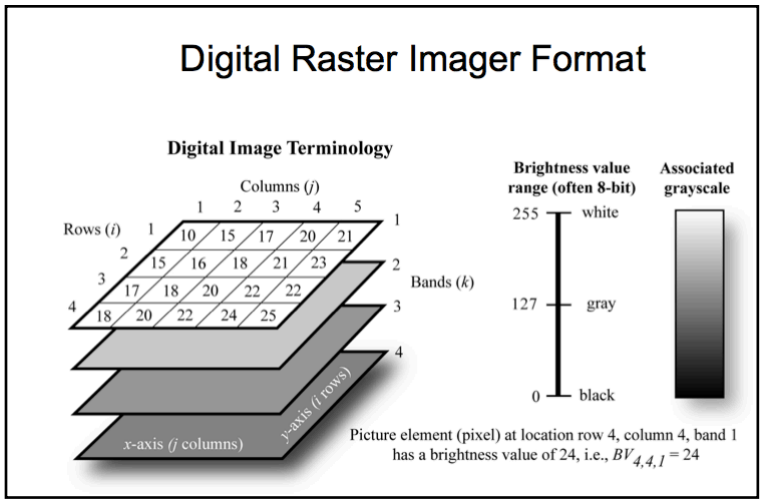

Figure 2.4. Conversion of radiance to a digital number (brightness value on a scale of 0-255 (8-bit radiometric resolution). Jensen, 2000.

As of January 2009, all imagery from the Landsat program has been made free to the public (USGS, 2010).

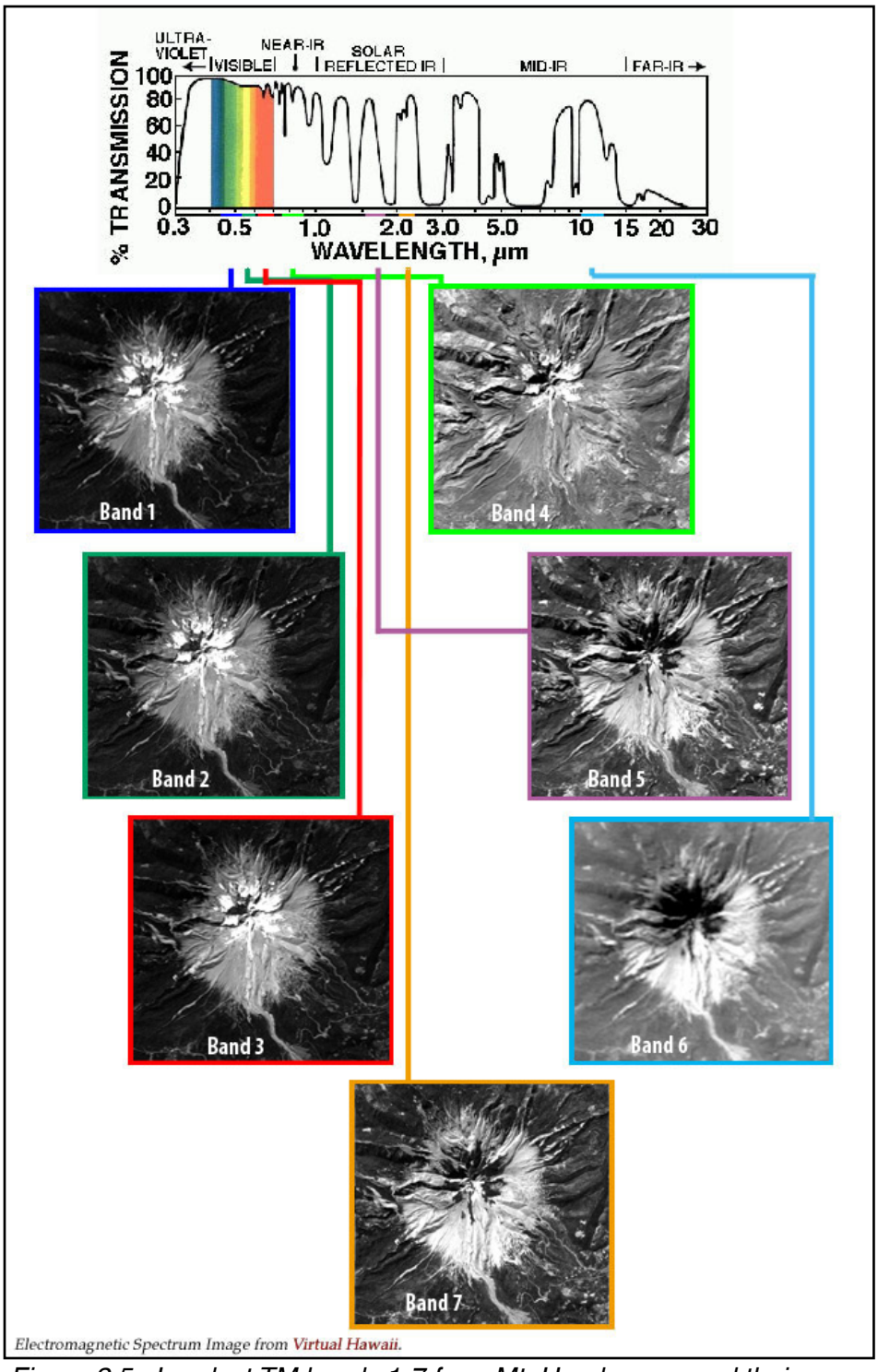

Figure 2.5. Landsat TM bands 1-7 for a Mt. Hood scene and their respective positions on the electromagnetic spectrum. Adapted from USGS "Virtual Hawaii" education site. Note bands 4 and 5.

2.12 Airborne LiDAR

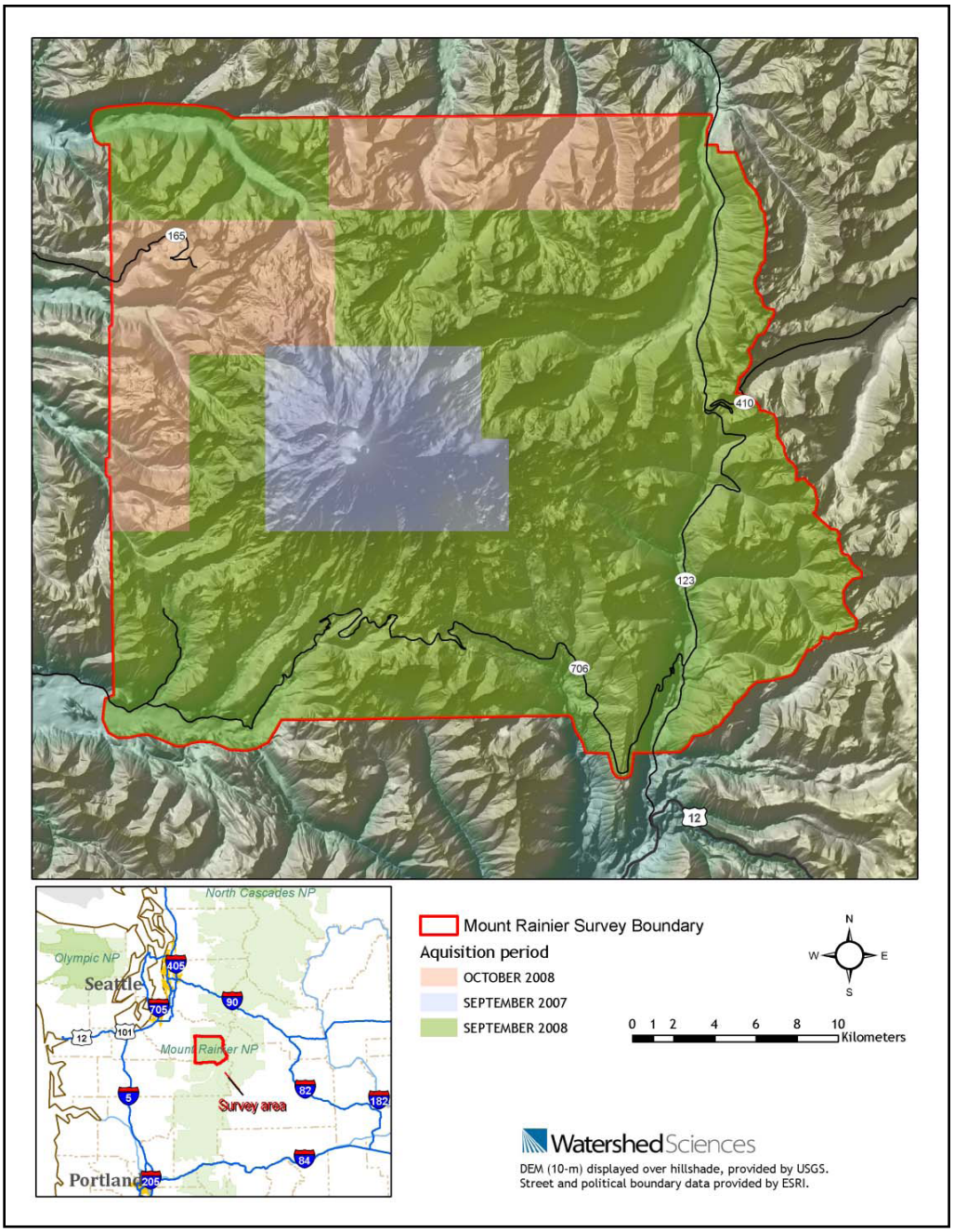

Figure 2.6. LiDAR acquisition areas and dates for Mt. Rainier. Courtesy Watershed Sciences Inc.

LiDAR (Light Detection and Ranging) data were obtained for both mountains from Watershed Sciences, Inc. of Corvallis, Oregon. The Mt. Rainier data were

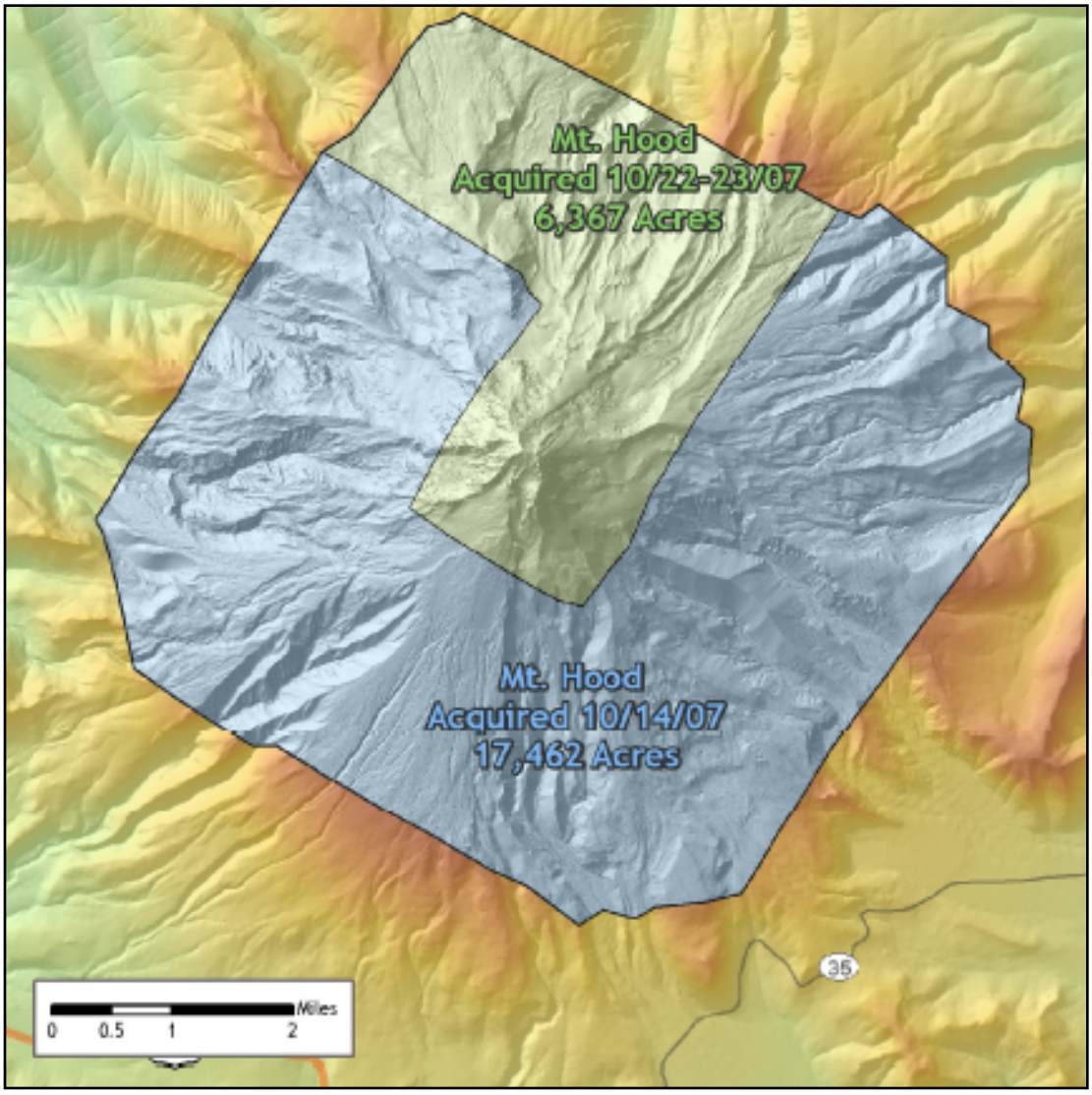

Figure 2.7. LiDAR acquisition areas and dates for Mt. Hood. Courtesy Watershed Sciences Inc.

collected between September 2007 and October 2008. Due to weather complications the LiDAR survey was not completed in one season and was continued in fall 2008. All the glaciers assessed in this study fall within the acquisition period of September

2007 which was a low snow year compared to 2008. This ensures that the measurements the laser picked up were from glacier ice and not remnant snow from the previous season (Figure 2.6). Mt. Hood LiDAR data were collected on 14 Oct 2007 and from 22-23 Oct 2007 (Figure 2.7).

For Mt. Rainier the mean relative accuracy (the internal consistency of the LiDAR-derived locations) was 0.11 m and the mean absolute accuracy (vertical

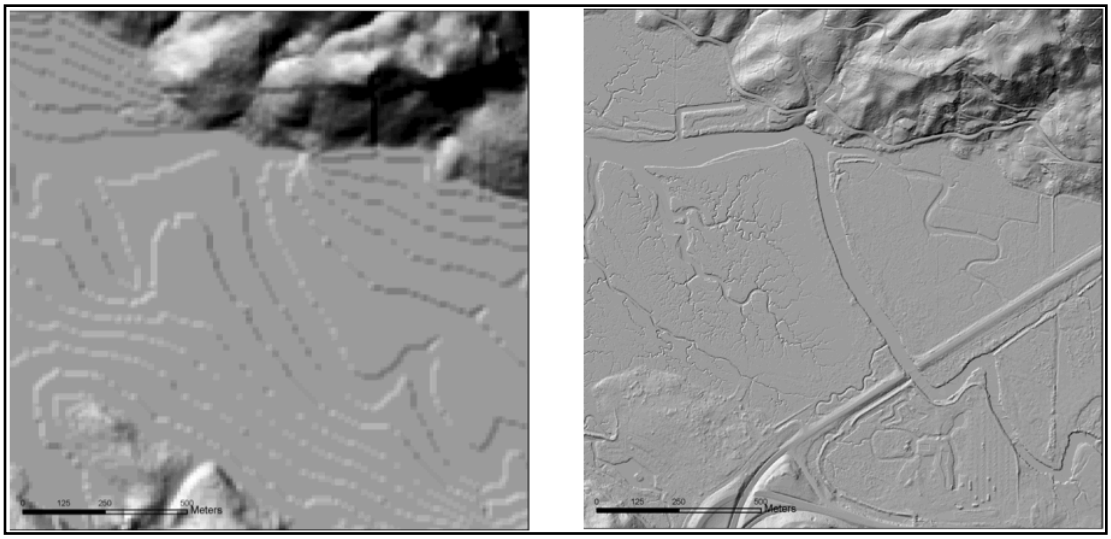

Figure 2.8. Comparison of detail between a 10 m DEM (left) and a 1-m LiDAR derived DEM (right). Courtesy R. Faux of Watershed Sciences Inc.

accuracy) was 3.7 cm with an average ground pulse density of 0.87 points per square meter. For Mt. Hood the mean relative accuracy was 0.08 m and the mean absolute accuracy was 3.96 cm with an average ground pulse density of 0.76 points per square meter. The data cloud of LiDAR points was used to create representative hillshade digital elevation models of both Mt. Hood and Mt. Rainier using ArcMap with a nominal resolution of around 1 m (Figure 2.8).

2.13 NAIP Aerial Photos

National Agriculture Imagery Program (NAIP) orthorectified aerial photographs were obtained for both Mt. Rainier and Mt. Hood. The "leaf-on" NAIP digital ortho quarter quad (DOQQ) geotiff imagery has a ground pixel resolution of 1 m with a horizontal accuracy that matches within 6 m of photo-identifiable ground control points which are used in image identification (FSA, 2010). The default spectral resolution is natural color (RGB) and cloud cover is specified to be less than 10%. All imagery is rectified into the UTM coordinate system (FSA, 2010). Quarter quads were joined in a mosaic for both peaks using raster processing tools within ArcMap. 2005 NAIP 1-m resolution photos were used for Mt. Hood and 2006 1-m resolution photos were used for Mt. Rainier.

2.15 Climate Data (SNOTEL)

Figure 2.9. The Mount Hood SNOTEL Site. NRCS.

SNOTEL (SNOwpack TELemetry) data are collected by the National Water and Climate Center (NWCC) as part of the Natural Resources Conservation Service (NRCS) under the United States Department of Agriculture (USDA).

There are now over 730

SNOTEL sites in thirteen Western states, which are designed to operate unattended powered by solar cells. All SNOTEL sites have a pressure sensing snow pillow to provide snowpack water content (Snow Water Equivalent, SWE), a sonic sensor for snow depth, storage precipitation gage to monitor accumulation, and air temperature sensor to provide daily maximums, minimums, and averages (NRCS 2010).

For Mt. Hood the Mt. Hood Test Site was used (site 651) located at 45° 19' N, 121° 43'W at an elevation of 1637 m. The site has been operating since 1 Oct 1979 (NRCS, 2010; Figure 2.9).

Figure 2.10. The Paradise SNOTEL Site on Mt Rainier. NRCS.

For Mt. Rainier the Paradise SNOTEL site was used (site 679) located at 46° 47' N, 121° 45' W at an elevation of 1563 m. This site has been operational since 1 Oct 1979 (NRCS, 2010; Figure 2.10).

2.15 Debris Flow Initiation Sites

The locations of debris flow initiation sites for Mt. Rainier were obtained from prior research by National Park Service personnel (Vallance, 2003; P. Kennard; E. Copeland personal communication). Debris flow locations for Mt. Hood were

obtained from the Mt. Hood National Forest, US Forest Service (T. DeRoo, personal communication). Precise locations of the debris flows originating from the November 2006 event were found in Pirot (2010). Debris flow locations can be seen in Tables 2.7, 2.8, 2.9 and 2.10.

2.16 Glacier Outlines

Outlines for Mt. Hood were obtained from A. Fountain and K. Thorneycroft (personal communication). Outlines for Mt. Rainier were obtained from A. Fountain (personal communication) and Nylen (2004). The first determination of glacial outlines for Mt. Rainier was produced by F. Matthes and the US Geological Survey in 1913 (Driedger, 1986). Nylen modified these original outlines based on historical photos to compile his 1913 outline. He later used over 70 years of aerial photography and data from field studies from Mt. Rainier National Park to revise the 1913 map, creating his 1994 glacier outlines (Nylen, 2004). For his outlines Nylen only considered the active glacier terminus in his analysis and divided glaciers with common boundaries based on ice flow directions derived from surface contours (Nylen, 2004). The 1913 outline has a much larger glacial area of coverage compared to the 1994 outline. Ultimately these outlines would be used to crop areas of individual glaciers from the band ratio images, so a comparison was needed between

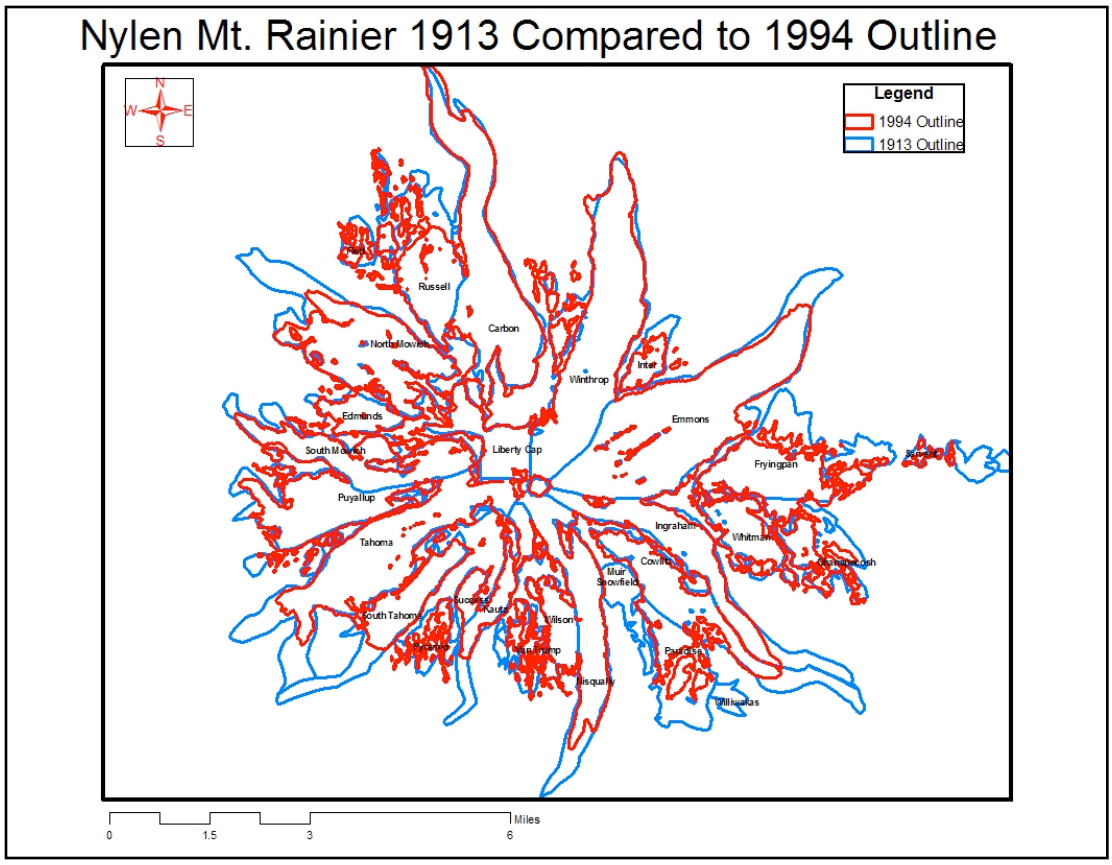

Figure 2.11. Mt. Rainier 1913 glacial outlines (blue) compared to the 1994 (red) outlines, obtained from A. Fountain and Nylen (2004).

the two outline sets to determine which one would be most appropriate for this study (Figure 2.11). To make an accurate comparison, several of the 1913 and 1994 individual glacier outlines needed to be slightly modified for a complete comparison of all 27 glaciers on Mt. Rainier. These modifications were performed by careful visual analysis of the 2009 NAIP, the LiDAR-derived hillshade model, and glacier outlines obtained from the GLIMS glacier database. Table 2.1 lists the small modifications made to both the 1913 and 1994 Nylen outlines.

Table 2.1. Glacier outline modifications made for Mt. Rainier.

Glaciers Affected	Modifications done
Carbon & Liberty Cap	Nylen's 1994 outline of the Carbon glacier was split into separate Liberty Cap and Carbon glaciers using the same split line as the 1913 outline at higher elevations. The 1994 resulting Liberty Cap outline was also slightly adjusted to better match the 1913 outline and to cover a section of glacial ice.
Ingraham and Cowlitz	The Nylen 1913 Ingraham outline was split into the Ingraham and Cowlitz glaciers using the same line as the 1994 outline. Both the 1913 and 1994 outlines were also slightly altered to better match GLIMS outlines as well as the LiDAR hillshade.
Wilson & Nisqually	The 1913 outline of the Nisqually glacier was split into the Wilson and Nisqually glaciers using the 1994 split line of the glaciers. The 1913 Wilson glacier outline was also slightly modified to better fit the 2005 hillshade of rock outlines, also using the 1994 outline as a reference.
S. Mowich & Puyallup	These glacier outlines are different for both the 1913 and 1994 outlines but were left unchanged due to lack of knowledge of which was more accurate.

With these small changes it became possible to compare the projected areas of each of the 27 glaciers using both the 1913 and 1994 outlines. Because both outlines were based on the extent of the full glaciers including the debris covered tongues, and not just the smaller debris-free ice extent of this study, both would have sufficient coverage for cropping the debris-free ice area out of the band ratio images. However, from visual inspection, the 1994 outline appeared to be better at eliminating snowfield coverage on the lower flanks of the mountain that may be misclassified as glacial ice.

The glacial outlines from Thorneycroft contained some glacier outlines dating back to 1901 for several glaciers but only the years 1972 and 1984 contained outlines for the majority of glaciers on Mt. Hood (Figure 2.12). Outlines for both years were constructed from USFS aerial photographs with source scales of 1:12000. To compare the areas for all 11 glaciers using the 1972 or 1984 outline, several

modifications of individual glacier outlines were performed. As at Mt. Rainier, these modifications on the Mt. Hood glacier outlines were completed through visual analysis of the 2005 NAIP photos, the LiDAR-derived hillshade model, and glacier

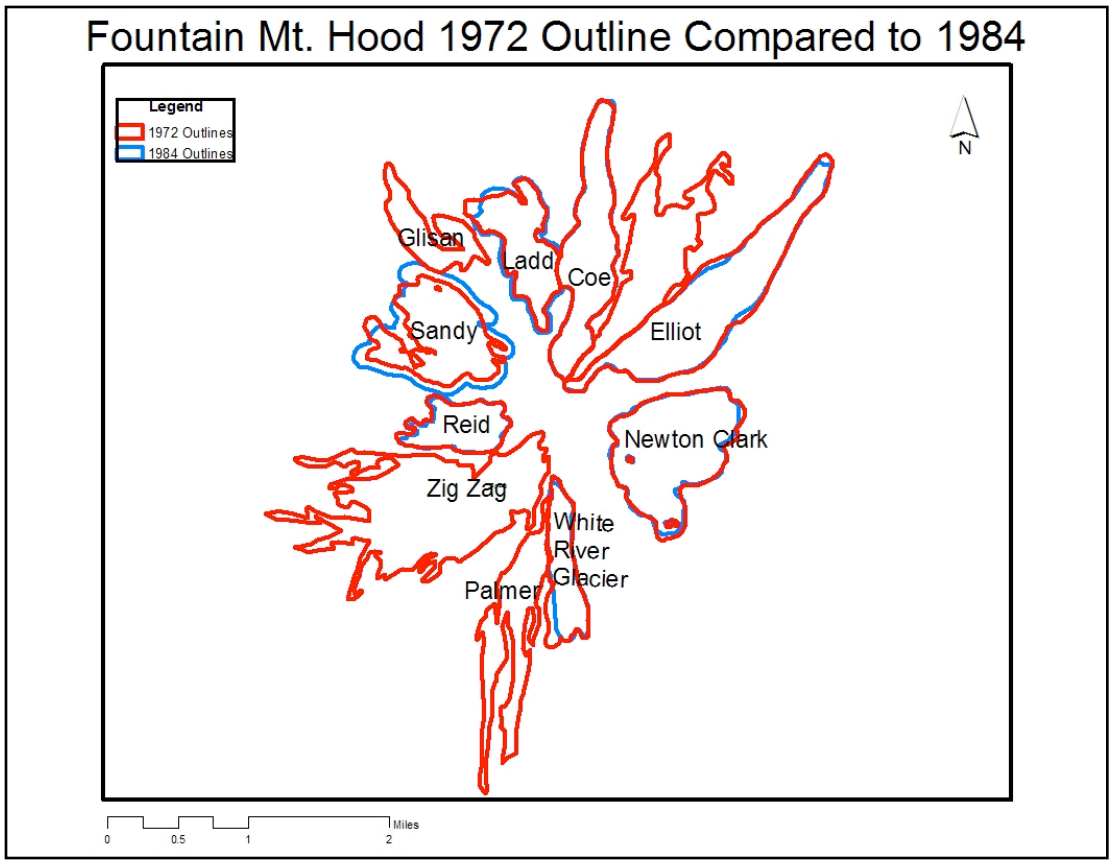

Figure 2.12. Mt. Hood 1972 outlines (red) compared to the 1984 outlines (blue). Obtained from K. Thorneycroft and A. Fountain of Portland State University.

outlines obtained from the GLIMS glacier database. The 1984 data set was missing outlines for the Glisan, Zigzag, Ladd, Langille, Palmer and Sandy glaciers while the 1972 data set was missing outlines for the Glisan, Zigzag, Palmer and Langille glaciers. GLIMS outlines created by A. Fountain from 1950 USGS maps were used

for the missing glaciers (GLIMS, 2010). A complete list of modifications and added glaciers can be seen in Table 2.2

Table 2.2. Glacier outline modifications made to Mt. Hood.

Glaciers Affected	Modifications done
Glisan, Zigzag, Palmer, Langille	1950 USGS-Derived GLIMS outline used for both 1972 and 1984 outlines. The Langille and Palmer glaciers were slightly modified so as not to overlap neighboring glaciers in both the 1972 and 1984 data sets.
Ladd	Created a new Ladd outline for the 1984 set based on a 1989 Ladd outline with a 30 m buffer to account for larger ice area in 1984 compared to 1989.
Sandy	Created a new Sandy outline for the 1984 set based on a 2000 Sandy outline with a 90 m buffer to account for a possible larger ice area in 1984 compared to 1989

Because the outlines from both 1972 and 1984 were based on the extent of the full glaciers including the debris-covered tongues and not just the smaller, debris-free ice extent of this study, both would have sufficient coverage for cropping the band ratio images. However, from visual inspection, the 1984 outline appeared to be better at eliminating snowfield coverage on the lower flanks of the mountain that may be misclassified as glacial ice.

2.2 Mapping Glacier Extent from Satellite Imagery

2.21 Scene Selection

For this study it was important to choose Landsat scenes in the early fall after the summer ablation season and before snow accumulation. This minimizes temporary snow cover and maximizes exposure of debris-free glacial ice (Paul, 2005; Keshri, 2009). Using images from the same time of year also ensures similar

illumination properties in each scene (Giles, 2001). For each Landsat scene used, SNOTEL data were checked to assure a zero SWE before the date as well as zero

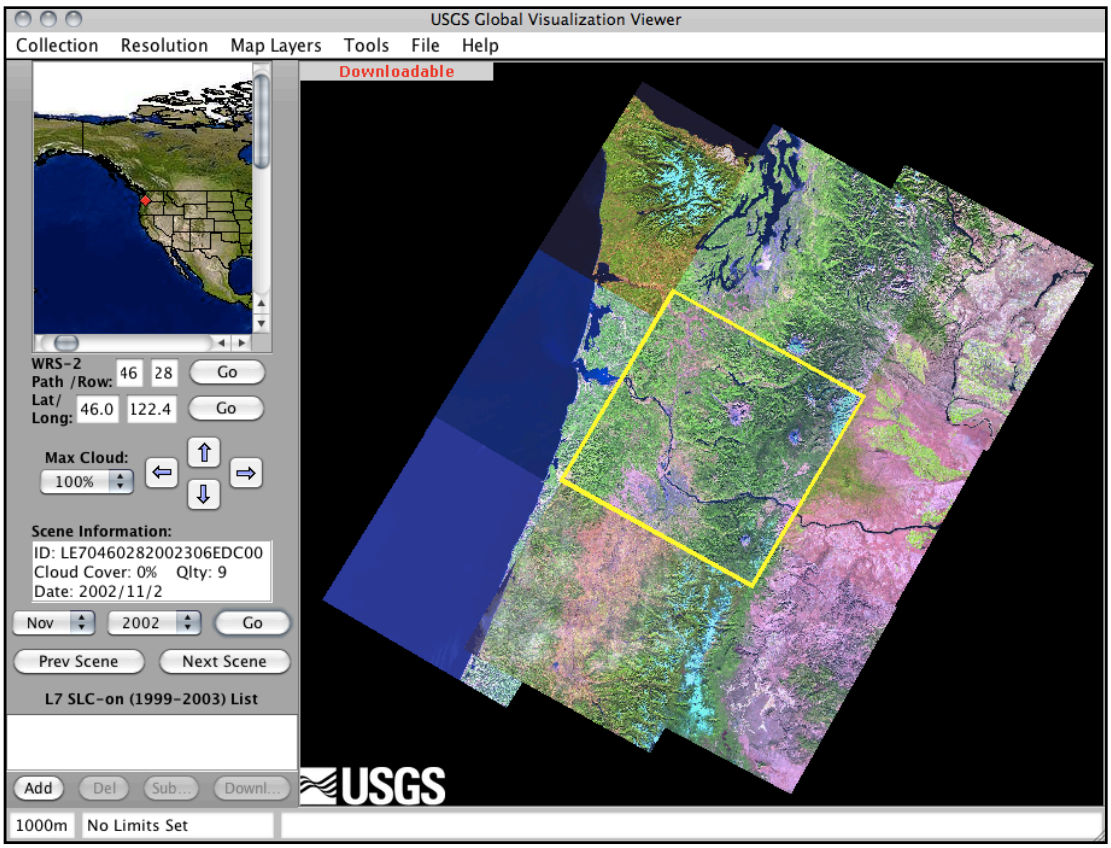

Figure 2.13. A screenshot of the USGS Global Visualization Viewer (GLOVIS) used to download Landsat scenes.

antecedent snowfall. Landsat scenes were also visually inspected for snow since the SNOTEL site may not account for precipitation at higher elevations. Scenes were downloaded via the USGS Global Visualization Viewer (GLOVIS) interactive tool on the USGS website (Figure 2.13). The objective was to obtain images that were free of atmospheric effects such as clouds or smoke from forest fires because band 4 and 5 cannot penetrate cloud cover (Figure 2.14).

The goal was to obtain clear images free of clouds but this proved difficult in the rainy Pacific Northwest. Figure 2.14 shows two scenes that contained too many clouds for accurate analysis. It was not possible to obtain a cloud-free image of Mt.

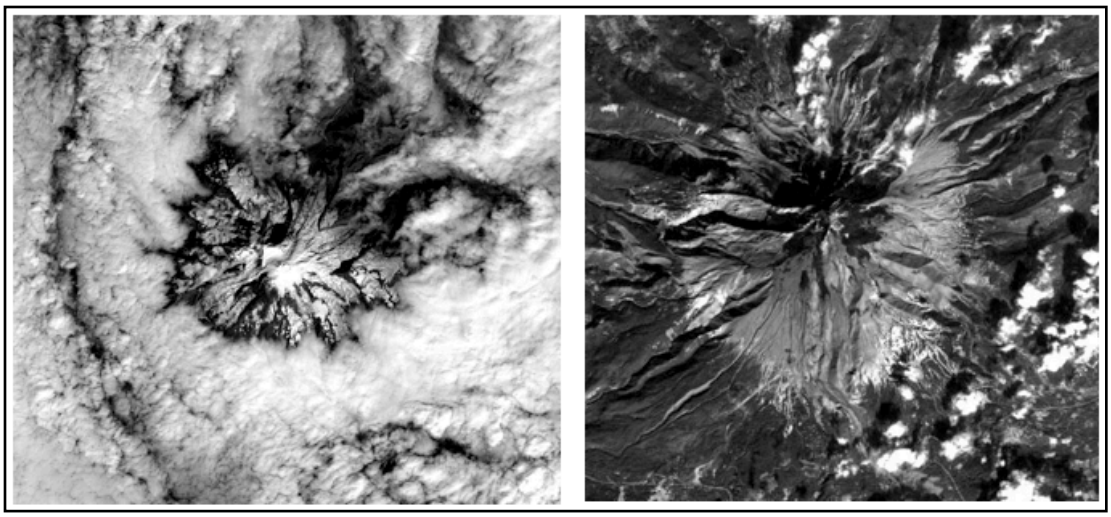

Figure 2.14. Examples of scenes with too much cloud cover. Band 4 on left and Band 5 on right.

Hood for the year 2004. The Landsat archive was also lacking images from several dates during the early years of this study, thus requiring the use of scenes from late July and early August for 1984 and 1985 for both mountains. It was also not possible to find a cloud-free image for Mt. Rainier for fall 1997 so an image from 8 Aug was used.

For 1984 through 1999 only Thematic Mapper scenes from Landsat 5 were available, but with the launch of Landsat 7 in 1999 more scene choices became available (Figure 2.15). This is because the two satellites operate on a slightly different 16-day scene acquisition cycle allowing more dates to be available in the fall

to avoid cloud cover. On 31 May 2003 the Scan Line Corrector malfunctioned in

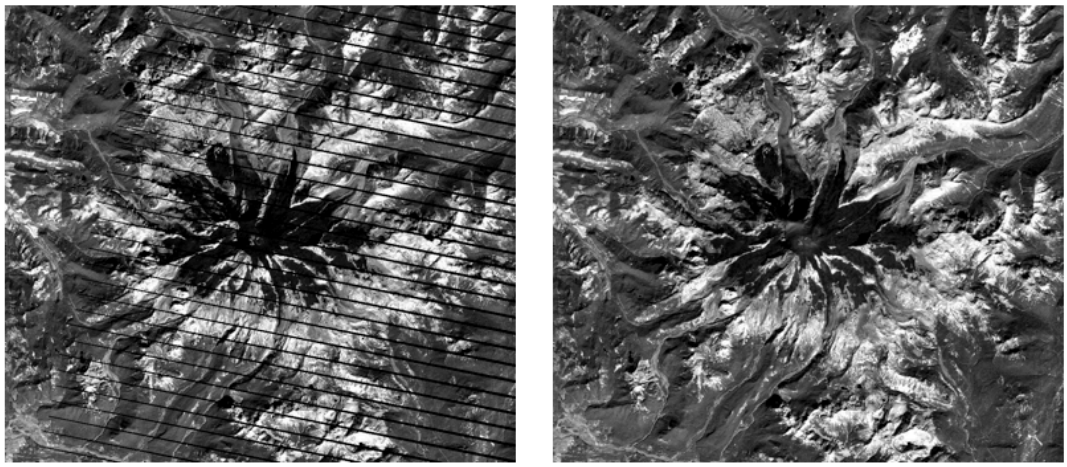

Figure 2.15. The result of the Scan Line Corrector malfunction seen in a Landsat 7 band 5 image from 13 Sept 2007 compared to a usable Landsat 5 image taken just 8 days later of Mt. Rainier.

Landsat 7 causing all subsequent scenes to have lines of no data within them (approximately 30% data loss in each image) (Figure 2.15). Because the Thematic Mapper in both Landsat 5 and Landsat 7 measure the same exact spectrums for both Band 4 and 5 it was easiest to simply continue using scenes from Landsat 5 instead of Landsat 7 after the SLC malfunctioned. A list of all dates used is given in Table 2.3. The dates shown in red are the ones chosen for final analysis.

Table 2.3. Landsat scenes chosen for each year 1984-2009. After assessing SNOTEL data, dates highlighted in red were chosen for decadal analysis.

Mt. Hood Dates	Mt. Rainier Dates
July 28, 1984	August 13, 1984
August 16, 1985	August 23, 1985
September 11, 1986	September 11, 1986
September 30, 1987	September 30, 1987
October 2, 1988	August 31, 1988
October 14, 1989	September 19, 1989
September 22, 1990	September 22, 1990
October 20, 1991	October 11, 1991
August 26, 1992	August 26, 1992
September 23, 1993	August 29, 1993
September 26, 1994	September 26, 1994
September 13, 1995	September 20, 1995
October 1, 1996	October 8, 1996
September 2, 1997	August 8, 1997
September 28, 1998	September 28, 1998
October 2, 1999	September 7, 1999
October 4, 2000	September 25, 2000
September 20, 2001	September 20, 2001
September 23, 2002	September 23, 2002
September 26, 2003	September 26, 2003
2004 - No clear date	September 28, 2004
September 24, 2005	September 8, 2005
September 27, 2006	September 2, 2006
September 21, 2007	September 21, 2007
September 16, 2008	September 16, 2008
September 26, 2009	September 23, 2009

2.22 Radiometric Correction

2.22.1 Conversion from Digital Number to Radiometric Value

Scenes were pre-processed using the minimum and maximum radiance values for each Landsat band as well as the sun elevation and the date of acquisition. This processing converts the Landsat scene Digital Numbers (DN) into top of the atmosphere (TOA) radiance.

2.22.2 Atmospheric Correction

Although Landsat scenes were chosen visually based on minimal cloud cover and quantitatively using SNOTEL data they needed to also be radiometrically corrected for atmospheric effects. Previous studies in the European Alps have shown the atmospheric correction model 6S (Second Simulation of a Satellite Signal in the Solar Spectrum) to be very effective at correcting Landsat ETM+ scenes for atmospheric effects (Paul, 2005).

As sunlight passes through the atmosphere, a portion of it is absorbed by gases such as water vapor, carbon dioxide, oxygen, ozone, and nitrous oxide and scattered by aerosols and particles such as dust and soot (Jensen, 2000; Figure 2.16). The collective effect of this absorption and scattering is to attenuate the amount of energy that is received by the sensor. Before being able to extract meaningful information

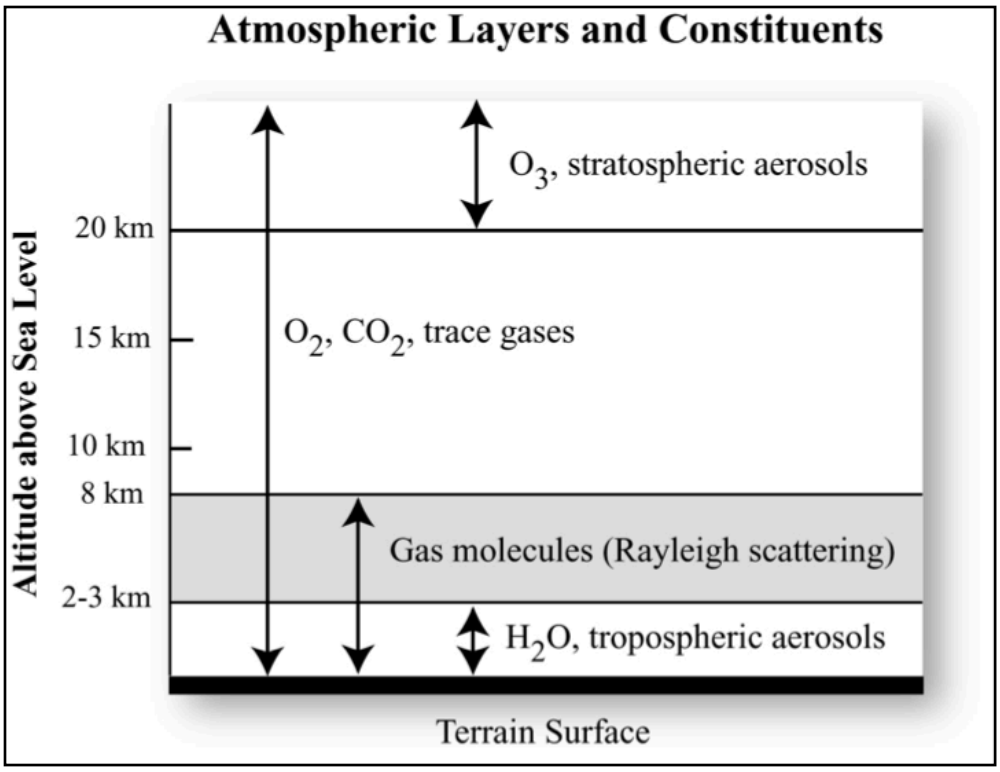

Figure 2.16. Gases and particles in the atmosphere scatter and absorb both incoming and reflected spectral energy. Jensen, 2000.

from the Landsat scenes chosen it was necessary to remove these effects using the atmospheric correction model, 6S. By providing an atmospheric model and information about the sensor and the location of interest within each scene 6S is able to invert the remote sensing radiance to a scaled surface reflectance based on the atmospheric conditions at the exact time of data acquisition by the satellite.

6S is able to account for multiple scattering contributions within the atmosphere at small wavelengths and at various simulated altitudes (Vermote, 1997). 6S, unlike previous iterations, uses the target altitude as a parameter to calculate the

quantity of gases and particles based off the selection of an atmospheric profile model. This process creates a new atmospheric profile based on the target altitude by stripping the effect of atmosphere under the target altitude (Vermote, 1997). By specifying both the altitude of the sensor as well as the altitude of the target, 6S is able to account for the interaction of photons with the atmosphere both on the way to the target as well as on the path from the target to the sensor (Figure 2.17).

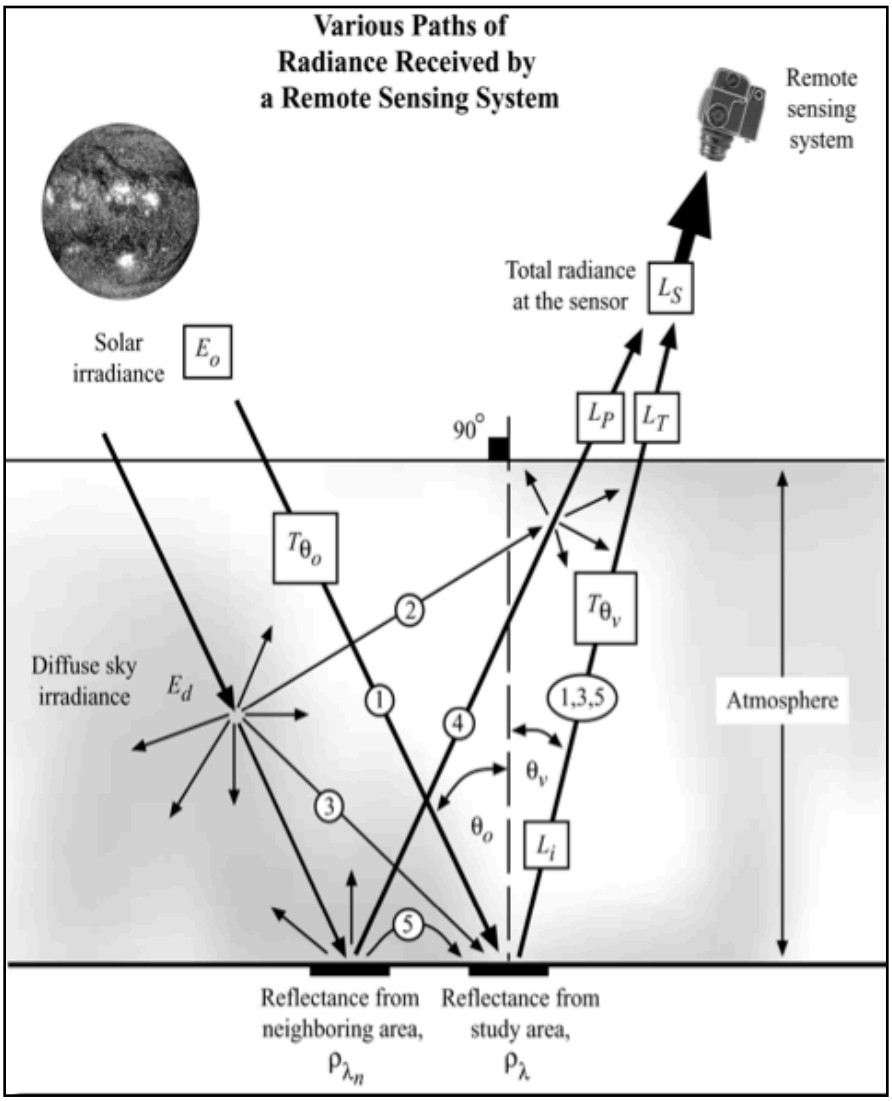

Figure 2.17. The various paths that solar radiance can take from the sun to the sensor. 6S corrects for atmospheric effects met by solar radiation along these paths. Jensen, 2000.

Within 6S the parameters entered were as follows:

1. Geometrical Conditions: The month, day and GMT time of acquisition for each scene along with the latitude and longitude of each mountain.

   Rainier: 46.85280N, -121.759W

   Hood: 45.37360N, -121.6925W

2. Atmospheric Model: “Midlatitude Summer” for the atmospheric profile with an optical depth of 0.1 at 550 nm and a Continental Aerosol Model.

3. Target & Sensor Altitude: A target altitude of -3 km (negative because it is 3000 m closer to the sensor) and satellite level for the sensor (The band and sensor were specified in step 4).

4. Spectral Conditions: Band 4 or band 5 for Landsat 5.

5. Ground Reflectance: Non-uniform with No Directional Effects. For target reflectance the glacier reflectance was chosen for the spectral band of interest. For band 4, a value of 0.8 was chosen and for band 5, a value of 0.6 was chosen. For Non-Target Reflectance the mean spectral value of green vegetation was chosen to discern the rock and ice from vegetation. A target radius around the Mt. Rainier and Mt. Hood locations was given to be 15 km.

6. Signal: Atmospheric Correction with Lambertian surface assumption.

These steps were repeated for band 4 and band 5 of each Landsat scene for both Mt. Rainier and Mt. Hood. This code produces atmospheric calibration

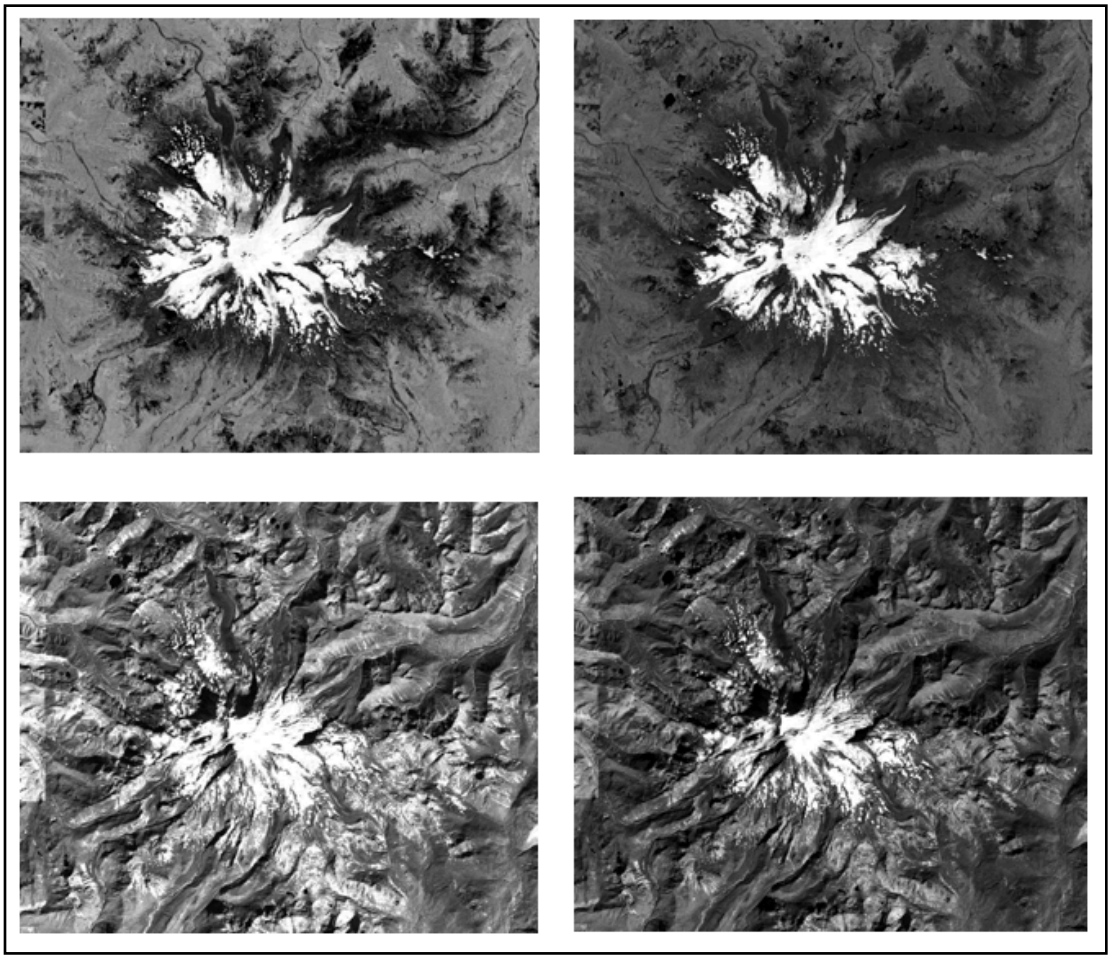

Figure 2.18. Top: Mt. Rainier 1990 rand ratio without atmosphere correction (left) and after atmospheric correction (right). Bottom: Mt. Rainier 1990 band 4 before atmosphere correction (left) and after atmospheric correction (right).

coefficients (Xa, Xb, and Xc). In the software package ENVI 4.5, band math and the 6S calibration values for each band in each scene were used to mathematically correct atmospheric effects for each pixel. The following equations were used: y=Xa*(Top or atmosphere radiance)-Xb and then y(1.+Xc*y) which gives the corrected surface

reflectance of the desired scene. The effects of correctly adjusting for atmospheric effects can be seen in Figure 2.8.

2.23 Computing Normalized Difference Glacier Index Images

After bands 4 and 5 of each scene were pre-processed and atmospherically corrected they needed to be cropped from an area of 185 km wide by 170 km long to a region of interest surrounding both peaks. The cropping parameters used within ENVI are listed in Table 2.4.

Table 2.4. Coordinates used to crop Landsat scenes to an appropriate area encompassing all the glaciers for both Mt. Hood and Mt. Rainier.

	Upper Left	Upper Right	Lower Left	Lower Right
Rainier	46° 59' 8.12"N 121° 57' 45.12"W	46° 58' 51.83" N 121° 32' 47.58" W	46° 43' 51.05" N 121° 58' 2.74" W	46° 43' 34.90" N 121° 33' 12.27" W
Hood	45° 25' 33.32" N 121° 47' 5.23" W	45° 25' 25.45" N 121° 35' 39.63" W	45° 17' 54.81" N 121° 47' 14.70" W	45° 17' 46.98" N 121° 35' 50.98" W

Regions of debris-free glacial ice show a large contrast between the two spectral bands, thus analyzing the magnitude of difference between them produces a clear delineation of debris-free ice extent. This is accomplished by creating a new normalized difference ratio image based on the magnitude of difference between the two bands:

$$NDGI = \frac{\rho_4 - \rho_5}{\rho_4 + \rho_5}$$

where ρ_4 is Landsat band 4 and ρ_5 is Landsat band 5. A normalized difference glacier index (NDGI) was used to produce a ratio of the two bands that clearly

delineated debris-free ice (Kargel, 2005). The large difference between radiometric brightness values between band 4 and band 5 (Figure 2.20) is what allows for a clear delineation of the debris-free ice on the glaciers. Illumination effects are reduced by

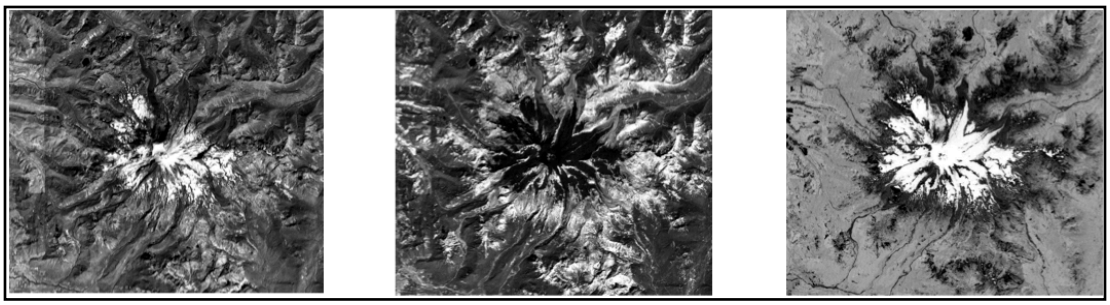

Figure 2.19. Landsat band combination (far right) composed of Band 4 (left) divided by band 5 (middle).

using a normalized difference rather than a simple ratio. The resulting scene with scaled values from -1 to +1 was then output as a floating point raster file for processing within ESRI ArcMap. These steps were repeated for each scene for all years from both Mt. Rainier and Mt. Hood.

2.24 NDGI Threshold Selection

The most important step of this study was to find a threshold value within the NDGI image that accurately represents the boundary of debris-free ice. Once this value was established it could be consistently used for every scene for both mountains. Because the sensors on both Landsat 5 and Landsat 7 measure the same spectrum for both bands and do not change over time once a threshold value is established it is thus applicable for every scene over both Mt. Rainier and Mt. Hood.

A 1956 USGS outline of the full Eliot Glacier on Mt. Hood, provided by Fountain, was modified in ArcMap to encompass just the area of visible debris-free ice in the orthorectified 2005 NAIP photos. The small 1.6 km^2 Eliot glacier on the northeast face of Mt. Hood has a well-defined headwall at 2900 m and lower limit of debris-free ice at 2120 m (Jackson, 2007). The lowest 27% of the glacier in the ablation zone is clearly covered with debris (Lundstrom, 1992). The 2005 NAIP photos for Mt. Hood were chosen for several reasons. First the NAIP photos were taken later in the summer at the end of the ablation season. Second, the year 2005 was one of the lowest snow years on record according to SNOTEL data. Third, the orthorectified NAIP photo with its 0.5 m resolution, served as an accurate image for hand-digitizing the visible debris-free ice. Therefore, 2005 represented the best possible scenario for producing an accurate glacier outline without incorporating remnant snow from the previous season. Using spatial analyst tools in ArcMap the projected area of the modified 1956 outline was determined. The Eliot Glacier was delineated from the 2005 Landsat NDGI image using the original full Eliot Glacier outline.

To determine the best threshold value a range of values were tested between -1 and +1 using the Elliot-cropped band 4/5 ratio image. The NDGI image was reclassified within spatial analyst using a defined interval method with the interval size set to 0.05. Although a smaller incremental change in the threshold could have been used with the floating point NDGI image, because of the inherent error in

digitizing the glacier outline on the NAIP photos, the 0.05 increment was deemed

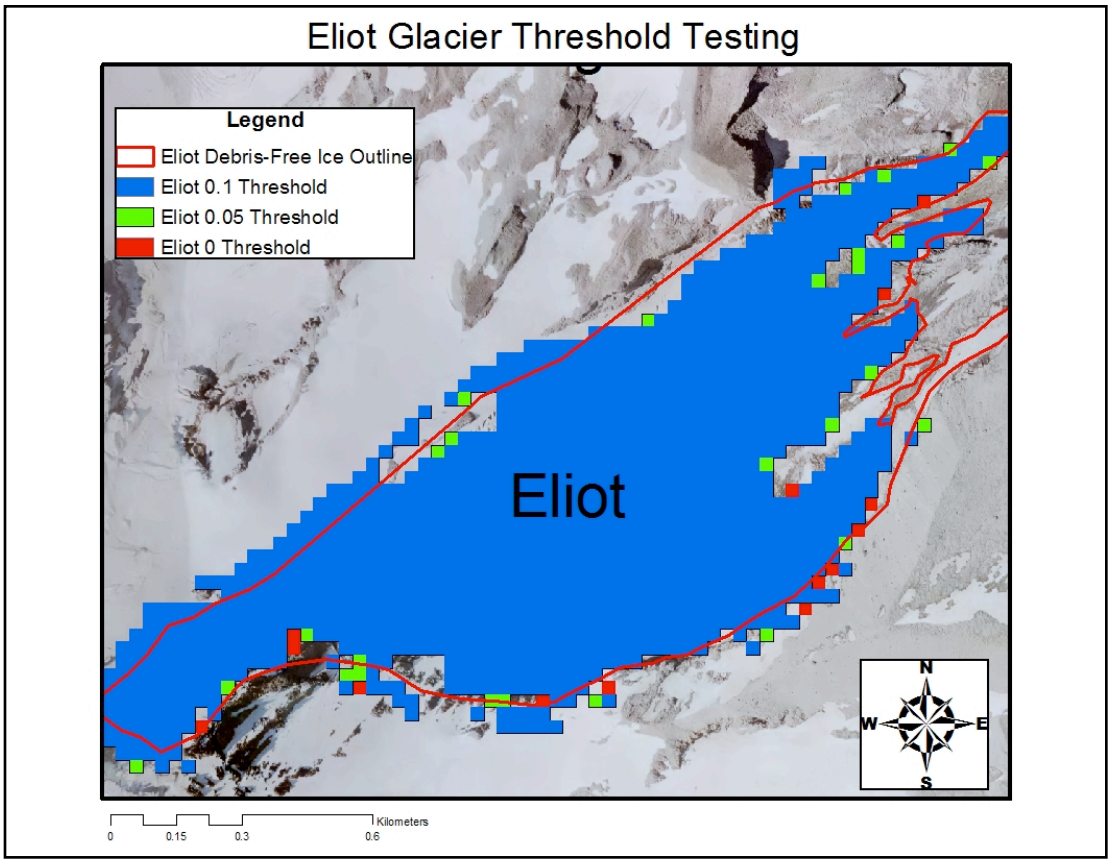

Figure 2.20. Determining the debris-free ice threshold with the Eliot Glacier.

sufficient. Two classes were used, one from -1 to the threshold and one from the threshold to +1 which effectively classified the NDGI image into debris-free ice and non-debris-free ice. From a visual inspection of the 2005 NDGI image it was evident that the best threshold value would be between values 0 and 0.1. The projected area of the Eliot glacier using values 0, 0.05 and 0.1 were then compared to the projected area of debris-free ice from the modified Eliot Glacier Outline. Results of the various threshold values can be seen in graphically in Figure 2.21 and numerically in Table 2.5.

Due to the importance of choosing an accurate threshold, the Reid glacier on the southwestern side of the volcano was also used to compare threshold values and act as a validation of the 0.05 threshold chosen using the Eliot Glacier. The Reid glacier does not have a debris-covered tongue so it provides a good comparison of how well the threshold will define the limit of debris-free ice (Jackson, 2007). Its elevation spans 1800 to 3000 m. The same steps were repeated using the well-defined debris-free Reid glacier and the 2005 NAIP photos with results of the various threshold tests again confirming the 0.05 threshold value to be the most accurate.

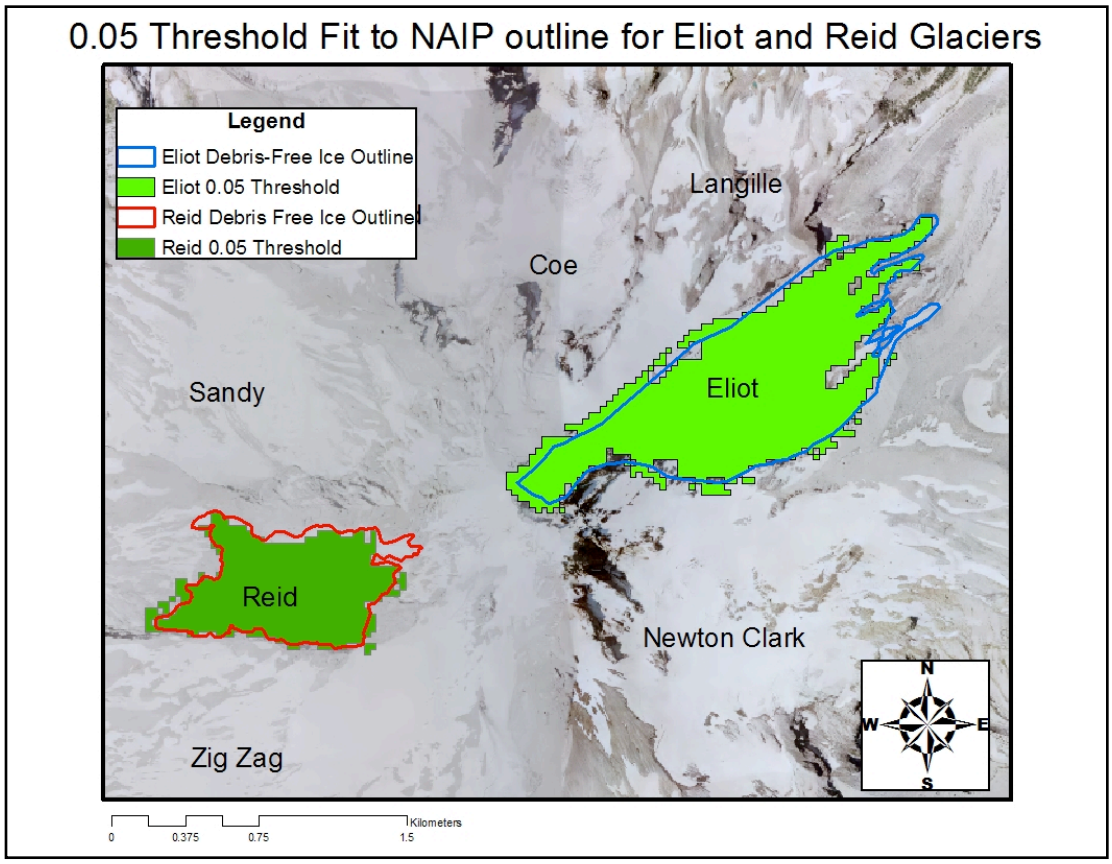

Figure 2.21. Comparison of estimated glacier areas using 0.05 threshold value for the Eliot and Reid glaciers.

Figure 2.21 shows the fit of the 0.05 threshold to the glacier outlines derived from the NAIP photos and tables 2.5 and 2.6 show results of the threshold tests.

For the Eliot Glacier, the glacier are derived from the NAIP photos was determined to be 1.14 km^2. All threshold values below 0.0 produced glacier areas far greater than this and all threshold values above 0.1 produced values far lower than this. The threshold 0.05 was slightly lower than the projected area calculated from the NAIP photo for both glaciers but it provided the closest result, being within 1% of the modified NAIP photo outlines for both the Elliot and the Reid (Tables 2.5 and 2.6). With less than a 1% margin of error it was not necessary to test threshold values at a smaller interval size. This is the same level of accuracy Paul (2000) obtained when comparing TM 4/5 derived ice cover with higher resolution SPOT imagery. A false color composite image using TM bands 5, 4, and 3, as RGB to was also used to qualitatively assess the accuracy of the chosen threshold (Khalsa, 2004; Hall, 2003).

Table 2.5. Threshold testing results for Eliot Glacier, Mt. Hood.

Debris-free Ice by Hand	1,144,410 m^2	Difference	Percent Deviation from NAIP Outline
0 Threshold value	1,167,300 m^2	22,890 m^2	2
0.05 Threshold value	1,154,700 m^2	-10,290 m^2	0.9
0.1 Threshold value	1,130,400 m^2	-14,010 m^2	1.22

Table 2.6. Threshold testing results for Reid Glacier, Mt. Hood.

Debris-free Ice by Hand	542,294 m^2	Difference	Percent Deviation from NAIP Outline
0 Threshold value	549,000 m^2	6,706 m^2	1.24
0.05 Threshold value	538,200 m^2	-4,094 m^2	0.75
0.1 Threshold value	528,300 m^2	-13,994 m^2	2.58

2.3 Area Change Analysis with LiDAR - Projected Area vs. Slope-Corrected

The area of the debris-free ice computed from the NDGI images is not representative of the actual glacial area on the steep slopes of both volcanoes. To find the slope-corrected area it was necessary to use the average slope of each glacier. The airborne LiDAR was used in ArcMap to create a detailed slope raster image. The average slope of each debris-free glacier extent was calculated using zonal statistics within ArcMap using a 3×3 cell moving window calculation. Average slope values were found for all glaciers for both the 1913 and 1994 outlines for Rainier and both the 1972 and 1984 outlines for Mt. Hood. To find slope-corrected glacial area the projected debris-free ice area was divided by the cosine of the average slope of the same area for each glacier:

$$A' = \frac{A}{\cos\theta}$$

where A' is the slope corrected area, A is the projected area and θ is the average slope of the glacier as computed from the LiDAR-derived DEM.

2.4 Analysis of Climate Data

To reduce the possibility of seasonal snow being mapped as glacier ice, SNOTEL data were used to identify years of minimum snowfall and early snowmelt for each decade within the 1982 to 2009 period. Peak snow water equivalent, air temperature and dates of snow disappearance were examined at the Mt. Hood and

Paradise SNOTEL sites. Climate data for both Mt. Rainier and Mt. Hood can be found in appendices A through E.

Based on the SNOTEL data analysis, three Landsat images were selected for the following dates: 30 Sept 1987, 26 Aug, 1992 and 24 Sept 2005. The scenes were also visually inspected to ensure no new snow at higher elevations. These three years were used to assess decadal changes of the glaciers on Mt. Hood and Mt. Rainier.

2.5 Comparison of Debris Flow Initiation Sites and Glacier Areas

Locations of debris flows for both Mt. Rainier and Mt. Hood were compared to the recession rates of nearby glaciers in an attempt to correlate glacial recession rates with debris flow initiation locations. This proved somewhat difficult and imprecise as the most accurate debris flow initiation points only existed for Mt. Rainier and Mt. Hood for the November, 2006 storm (Copeland, 2009; Pirot, 2010). Before these dates only the drainage was known that the debris flow travelled down for both volcanoes. Therefore, only a general relationship between drainages that experienced debris flows and glacier recession could be attained and any debris flow dates on both peaks prior to the first Landsat scene of 30 Sept 1987 are not relevant to this study but they are included as a reference to which drainages have been most historically active for debris flows. A list of all the known debris flows to date for both Mt. Rainier and Mt. Hood can be found in Tables 2.7 through 2.10.

2.6. Debris Flow Data

Table 2.7. Historical debris flows on Mt. Rainier by glacial drainage.

Year	S.Tahoma	Pyramid	Kautz	Van Trump	Nisqually	Winthrop	Inter	Sum	Source
1926					1			1	A
1932					1			1	A
1934					1			1	A
1947			1					1	A
1955					1			1	A
1961			1					1	A
1967	3							3	A
1968	1				1			2	A
1970	1				1			2	A
1971	1							1	A
1972					1			1	A
1979	1							1	A
1981	1							1	A
1985			1					1	B
1986	2		1		1			4	B
1987	4					1		5	B
1988	3							3	B
1989	2							2	B
1990	2							2	B
1991	1							1	B
1992	3							3	B
1993	1							1	B
2001				1				1	C
2003	NA			1				1	D
2004								0	D
2005	1	1	1	1				4	D
2006	1	1	1	1		1	1	6	D

Source of debris flow records: "A" Walder and Driedger (1993), "B" Walder and Driedger (1994), "C" Vallance et al. (2002), and "D" P. Kennard (personal communication, 2008)

Table from Copeland, 2009.

Table 2.8. Historical debris flows at Mt. Hood by glacial drainage.

Year	Month	Drainage	Initiation Elev.	Terminus Elev.	Volume (CY)
1907	August	White	?	?	?
1926	August	White	?	?	?
1926	October	White	?	?	?
1927	?	White	?	?	?
1930	October	White	?	?	?
1935?	?	White	?	?	?
1947	October	White	?	?	?
1949	?	White	?	?	?
1958	November 8	Coe	?	?	?
1959	September	White	?	?	?
1959	October	White	?	?	?
1961	September 1	Ladd	7000	2300	400000
1961	September	White	?		?
1966	January	White	?		?
1967	January	White	?		?
1968	September	White	?		?
1978	August	Newton	?		?
1980	December 25	Polallie	6400	2800	100000
1981	*September*	White	?		?
1991	November	Newton	?	4000	?
1995	?	Newton	?	4200	?

1996	?	Ladd	?	2400	?
1997	October	Polallie	6100	2900	40000
1997	?	Clark	?	4400	*30000*
1998	August 30	Newton	7600	6100	10000
1998	September 3	White	7000	4200	220000
1999	November 26	Eliot	6300	2600	130000
1999	November 26	Clark	7400	4200	*40000*
2000	*January*	Eliot	6300	2700	40000
2000	October 1	Newton	7200	3500	300,000+
2000	October 1	Clark	8000	5400	10000
2000	October 1	Eliot	6300	2700	40000
2000	October 1	Sandy	7000	2600	90000
2000	October 1	Muddy Fork	6000	2900	70000
2000	October 1	Coe	6000	3600	*60000*
2000	October 1	White	6800	4000	440000
2002	June 14	Muddy Fork	5600	2900	200,000+
2003	September 2	White	*6800*	4800	30000
2003	October 21	Newton	*6800*	?	*60000*
2003	October 28	White	*6800*	4200	*30000*
2003	October 28	Sandy	?	?	*20000*
2003	October 30	Clark	*7600*	5900	*10000*
2005	September 30	W. Compass	*6000+*	4100	*5000*
2005	September 30	Newton	7600	3800	*80000*

2005	September 30	Clark	?	4300	*30000*
2005	September 30	White	7200	4400	*100000*
2005	September 30	Sandy	?	3300-	*100000*
2005	October 31	White	*7200*	4300	?
2006	November 7	White	7200	3800	?
2006	November 7	Clark	?	?	?
2006	November 7	Newton	6600	3600	?
2006	November 7	Eliot	6300	960	?
2006	November 7	Ladd		?	?
2006	November 7	Sandy		?	?
2008	August 20	Eliot	?	3000	*5000*
2008	August 20	Newton	?	4200	*10000*
2008	November 12	Eliot	?	2800	*5000*
2008	November 12	White	?	4200	*10000*

Confidence level in data is depicted by text style, from high confidence to low: regular, italics, question mark. Blanks indicate the data is still to be determined. (DeRoo, Personal Communication).

As previously noted, a debris flow was observed in 1922 exiting and then re-entering crevasses on the Zigzag glacier, spurring eruption concerns. Also, the Coe event mentioned earlier that forced the "round-the-mountain" trail to be rerouted may be the same event as the one from 8 Nov 1958 (T. DeRoo, personal communication).

Detailed locations and elevations of debris flows on Mt. Rainier and Mt. Hood originating from the November 2006 storm event are detailed in Tables 2.9 and 2.10

(Copeland, 2009; Pirot, 2010). Locations can also be seen graphically in Figures 3.1 and 3.8. Mapped debris flows and inundation areas from the November 2006 for Mt. Hood can be seen in Figure 2.23.

Table 2.9. Debris flow initiation locations from the November 2006 storm for Mt. Rainier. Locations in WGS 84 UTM Zone 10 (Copeland, 2009).

Initiation	Elevation	Notes
597717E, 5192979N	2172 m	Inter Glacier. The magnitude of the event was large. Multiple meltwater channels from the Inter Glacier show evidence of debris transport
592871E, 5185046N	2037 m	Kautz Glacier Debris flow is estimated to have initiated at a location of stagnant terminus of the Kautz Glacier where a gully was seen cut into the debris-covered ice.
592284E, 5185477N	2250 m	Pyramid Glacier. Debris flow initiated from a gully below a fragment of the Pyramid Glacier
590478E, 5185532N	2000 m	South Tahoma Glacier. Assumed to have initiated at one of the many incised channels in the bedrock wall below the glacial terminus or from a old moraine slope failure from stream incision at a lower elevation.
594156E, 5184620N	2335 m	Van Trump Glacier. Debris flow initiated from several small glacier fragments.
595370E, 5193680N	2450 m	Winthrop Glacier. Debris flow initiated from a small lake at the bottom of a small remnant of the Winthrop Glacier to the west of the main glacier

Table 2.10. Debris flow initiation locations from the November 2006 storm for Mt.Hood. Locations in WGS 84 UTM Zone 10 (Pirot, 2010).

Initiation Location	Elevation	Description
5028150E, 604827N 5028133E, 604976N	1800-1850 m	Eliot Glacier. Debris flow initiated from two landslides of lateral moraines where Eliot Creek appeared to incise into.
5024282E, 598770N	1790-1860	Far below Zigzag Glacier. Debris flow initiated from an area where the Sandy River appeared to have undercut the toe of a scarp slope.
5022541E, 602168N	2140	White River Glacier. There was no clear debris flow initiation site. Debris flow deposits morphed into a single debris trail with no clear starting point.
5024158E, 605032N	Hill slope 1810-2170 m	Newton Clark Glacier. No clear debris flow initiation site but debris tracks seen upstream to just below the glacier.
5022881E, 604875N	1720-1760	Newton Clark Glacier. Debris flow initiation caused by landslide into Heather Creek.
5021833E, 601382N	2020-2200	Palmer Glacier. Debris flow initiation zone in snowfields below glacier.
5027916E, 600239N	1880-1930	Far below Ladd Glacier. Debris flow initiation from a landslide into Ladd Creek.

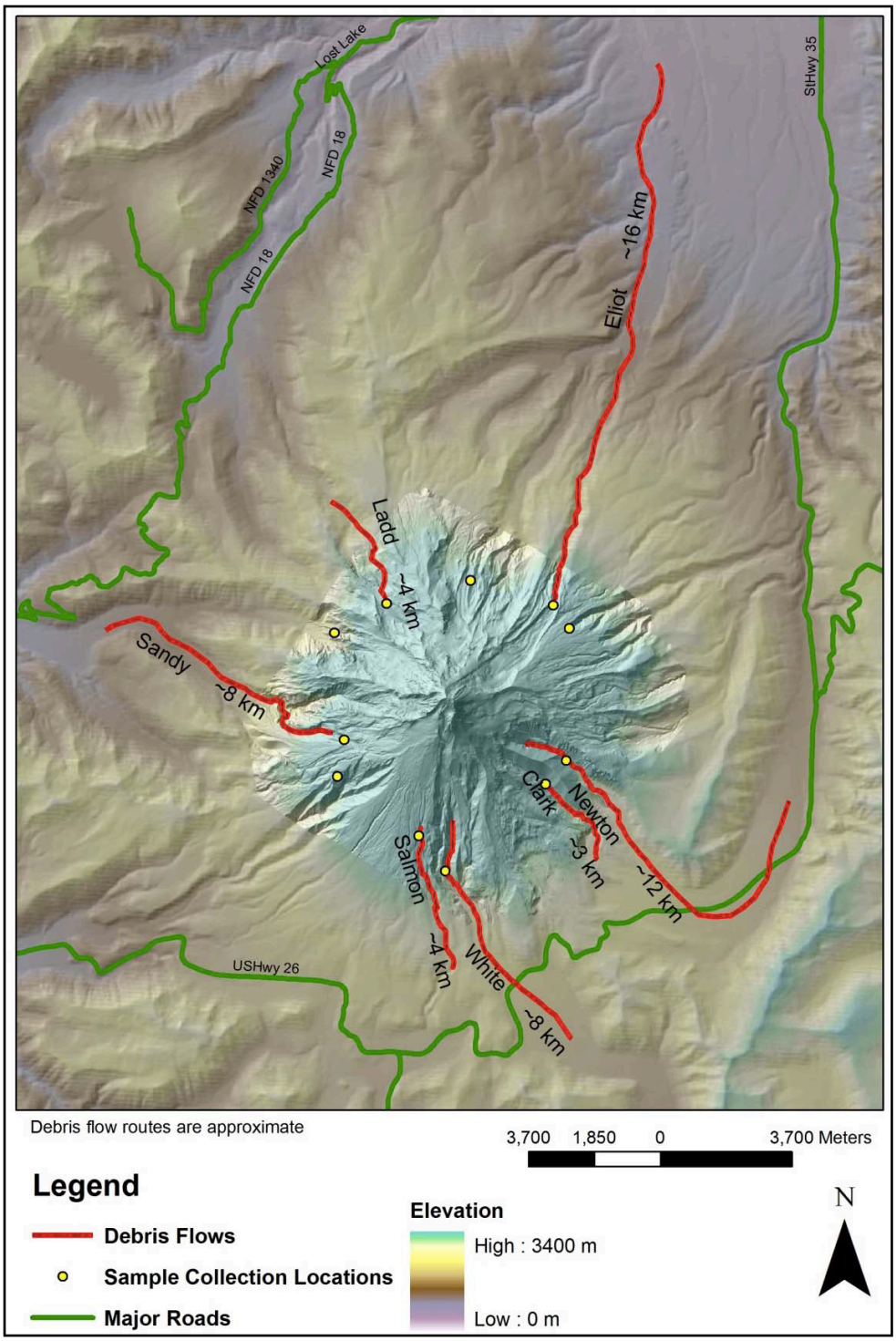

Figure 2.22. Debris flow paths from the November 2006 storm event occur on all sides of Mt. Hood. Courtesy Pirot (2010).

Chapter 3: Results

Recession of debris-free ice can be seen on both Mt. Hood and Mt. Rainier with both showing faster rates of glacier recession now than earlier in the 20th century (Nylen, 2004; Lillquist, 2006). Mt. Hood and Mt. Rainier saw a decrease in glacier area of 13.9% and 14.0%, respectively, between 1987 and 2005, an interpolated loss of about 5% per decade (Figures 3.1 and 3.8). These numbers are small in comparison to work done by Paul et. al (2007) in the Alps which showed a 14% loss in glacial area per decade. Paul also showed that mean glacier area loss accelerated for the same period as this study. In a study by Nylen (2004) Mt. Rainier lost 18.5% of its total glacial area from 1913 to 1972, a loss of about 3% per decade. Mt. Hood has seen even more dramatic glacial recession, with Lillquist (2006) finding glaciers to have retreated up to 61% of their former lengths during the last century. Medley (2008), using ASTER imagery, found Mt. Hood to have the fastest rate of glacier recession in the Northwest at 67% decrease in debris-free ice cover from 1956 to 2003, a loss of about 13% per decade. This rate is four times that of Mt. Rainier and the North Cascades.

For both Mt. Hood and Mt. Rainier the slope-corrected area of debris-free ice change was greater than the projected area change due to the steep slopes of both mountains (Figures 3.2 and 3.9). Projected debris-free ice area results from the Landsat NDGI images were in good agreement with previous glacier area estimates from Kennard (1984).

3.1 Mt. Rainier Glacier Changes

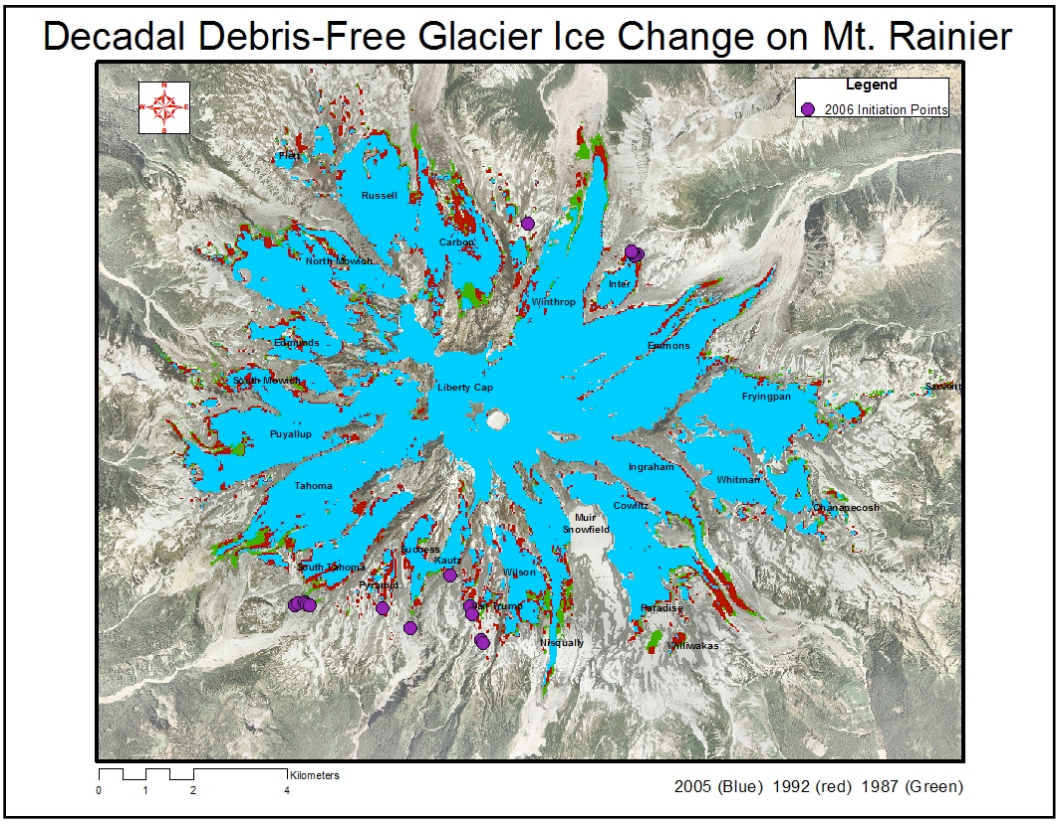

Figure 3.1. Decadal debris-free glacier ice change on Mt. Rainier. 2005 slope-corrected is blue, 1992 is red and 1987 is green. Purple dots are debris flows from the November 2006 storm event courtesy Copeland, 2009.

3.1.1 Projected & Slope-corrected Areas of Change on a Glacier-by-Glacier Basis

Because of the topographic relief of Mt. Rainier it was necessary to incorporate the slope into area calculations to get the slope-corrected area of the debris-free ice for each glacier. The significant difference between the two area calculations is also shown in Figure 3.2. The glaciers with the steepest slopes also have the largest difference between the slope-corrected and projected debris-free ice

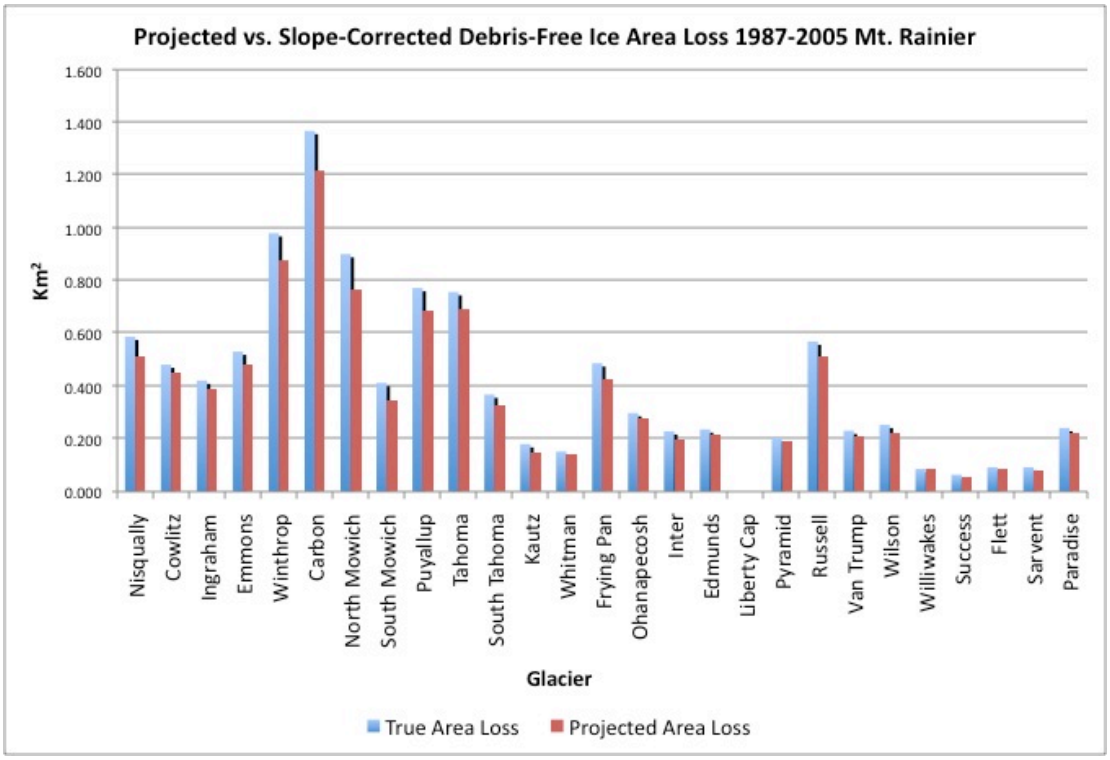

Figure 3.2. Projected vs. slope-corrected debris-free ice area loss 1987-2005, Mt. Rainier.

area results. For example, the Kautz and the South Mowich glaciers have the steepest slope for the area of debris-free ice found with the Landsat band ratio, thus they also have the largest percent difference between the projected and the slope-corrected area of debris-free ice. Nylen's 1994 outline, which was determined to be the most appropriate for this study, was used to crop out the debris-free ice regions of the glaciers. Figure 3.3 shows the total debris-free ice area change per decade for each glacier on Mt. Rainier. The percent of debris-free ice loss for each glacier can also be seen in Figure 3.4. The Williwakas Glacier on the southerly side of the mountain lost 90% of its debris-free ice area from 1987 to 2005 with the largest glacier, Emmons, losing just 5.3%. Liberty Cap retained its full debris-free ice area due to its elevation

(base at 4298 m) above the ELA as well as consistently cold temperatures for most of the year.

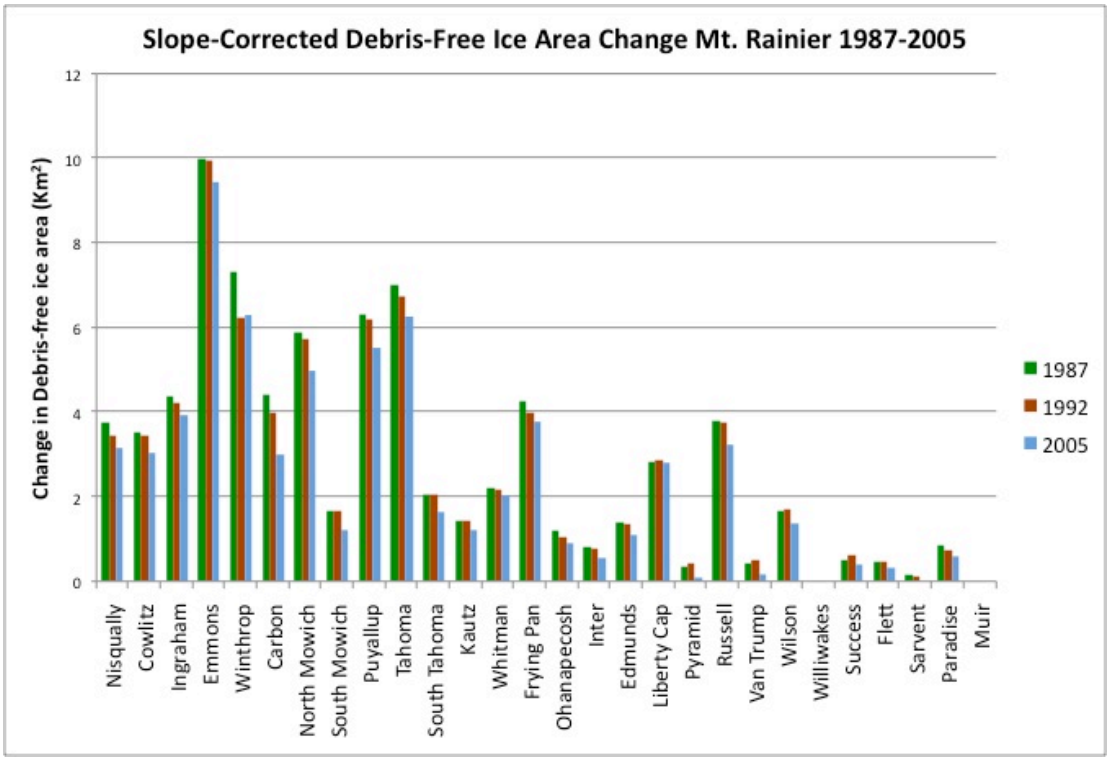

Figure 3.3. Decadal slope-corrected debris-free ice area change for Mt. Rainier 1987-2005.

Table 3.1 lists the 1987 Landsat-derived projected debris-free ice area in m^2 for Mt. Rainier. For all glaciers except Liberty Cap the projected areas from Landsat are in close agreement with previous area calculations completed in 1983 (Kennard, 1984). The projected areas are all slightly smaller than those of Kennard because they only represent the debris-free ice area instead of the whole glacial extent that Kennard accounted for.

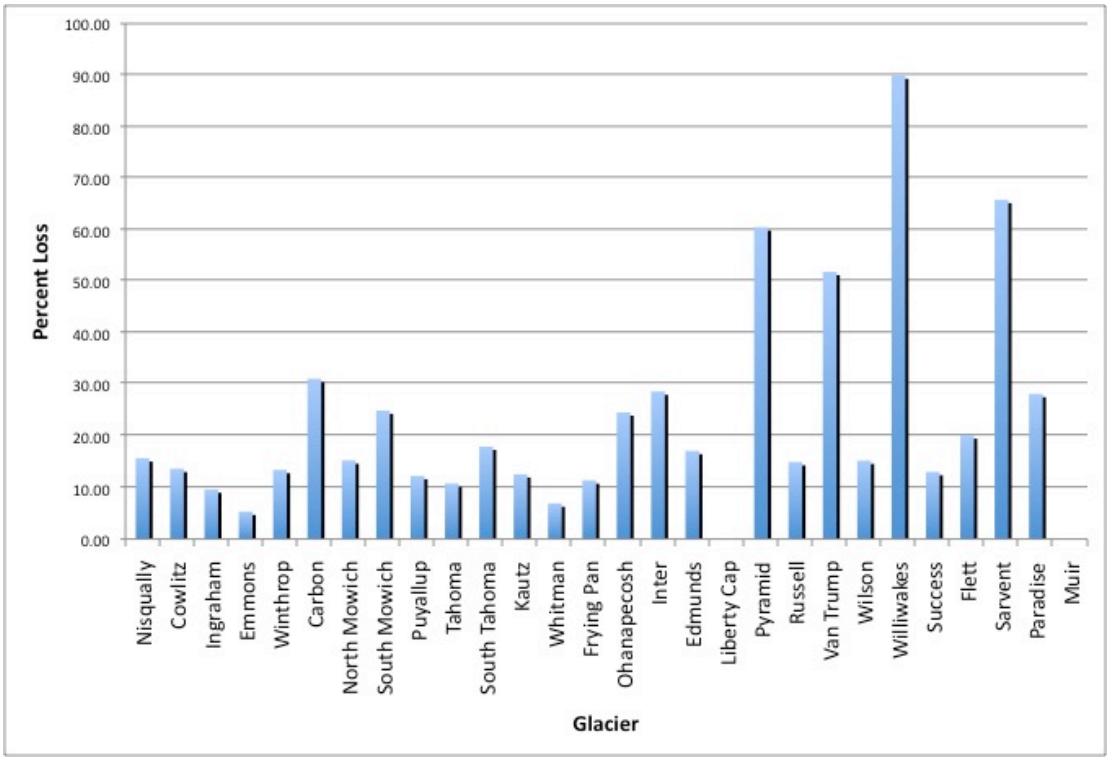

Figure 3.4. Percent debris-free ice loss 1987-2005, Mt. Rainier.

The manner in which the boundary is determined for two adjacent glaciers affects the computed areas of the glaciers. There is a large difference between the 1987 projected area for the South Mowich and that of Kennard's measured area for this glacier. For the Puyallup glacier, the 1987 projected area is larger than that of Kennard's. This is explained by my choice of splitting up Nylen's glacial outline for the two glaciers as explained in section 2.16. It is evident that Kennard used a different split line than was used for the area calculation here. The split line chosen by Nylen between the Whitman and Frying Pan glaciers may also account for the slightly higher 1987 Landsat-derived projected area of the Frying Pan Glacier or it could simply be due to a misclassification of one or several of the many snowfields

around the Frying Pan Glacier as debris-free glacial ice. The 1987 projected area for the Tahoma Glacier is also slightly higher than the area found by Kennard. This may be due to the high elevation split line Nylen chose between the Puyallup and the Tacoma being different than the one used by Kennard. Finally, the 1987 projected debris-free ice area of the Liberty Cap Glacier is far greater than the area determined by Kennard. This is due to the large glacier outline I used for the multi-lobed glacier and misclassification of the perennial snow at the high altitude where the glacier resides, around 4300 m. The debris-free ice area of the Liberty Cap Glacier does not appear to change from 1987 to 2005.

Table 3.1. Landsat-derived 1987 projected area compared to glacial area calculations of Kennard & Driedger in 1983 for Mt. Rainier.

Glacier Name	1987 Projected Landsat Area in km^2	Kennard & Driedger 1983 area in km^2	Kennard & Driedger Volume in km^3	Glacier Drainage
Nisqually	3.16	4.62	0.22	Nisqually River
Cowlitz	3.12	3.42	0.17	Cowlitz River
Ingraham	3.71	3.96	0.20	Cowlitz River
Emmons	8.45	11.17	0.67	White River
Winthrop	6.18	9.11	0.52	White River
Carbon	3.81	7.92	0.71	Carbon River
North Mowich	5.13	6.17	0.27	Puyallup River
South Mowich	1.39	3.57	0.13	Puyallup River
Puyallup	5.57	5.09	0.29	Puyallup River
Tahoma	6.05	5.65	0.33	Nisqually River
S. Tahoma	1.81	2.82	0.13	Nisqually River

Kautz	1.20	1.15	0.04	Nisqually River
Whitman	2.09	2.21	0.12	Cowlitz River
Frying Pan	3.87	3.27	0.08	White River
Ohanapecosh	1.12	1.61	0.04	Cowlitz River
Inter	0.71	0.78	0.02	White River
Edmunds	0.12	0.14	0.03	Puyallup River
Liberty Cap	2.48	0.16	0.003	Carbon River
Pyramid	0.31	0.54	0.01	Nisqually
Russell	3.48	3.30	0.09	Carbon River
Van Trump	0.39	0.62	0.01	Nisqually River
Wilson	1.49	1.44	0.05	Nisqually River
Williwakes	0.92	No Data	No Data	Cowlitz River
Success	0.42	0.69	0.01	Nisqually River
Flett	0.43	0.30	0.01	Puyallup River
Sarvent	0.12	0.58	0.01	White River
Paradise	0.78	1.03	0.02	Cowlitz River
Muir	0.96	0.94	0.02	Cowlitz River

The total projected area of debris-free ice for all glaciers on Mt. Rainier in 1987 was 68.4 km^2 while the total area for all glaciers, including areas of debris-covered ice found by Kennard and Driedger in 1983 was 82.2 km^2. Table 2.10 shows that the NDGI method of classifying debris-free glacier ice area compares well with the results of previous studies.

In addition, these results were compared with those from Medley (2008) who used 2003 ASTER imagery to calculate projected total debris-free ice area for Mt. Rainier. For Mt. Rainier Medley found a projected debris-free ice area of 66.0 ± 3.3

km^2 which closely matches the value from this study of 58.9 km^2 total for 2005 just two years later.

3.12 Calculating Rates of Glacier Change

According to USGS maps from 1956 Mt. Rainier had a total glacier area of 74.1 ± 1.3 km^2. The USGS maps account for the entire glacial area, but even with this considered the results of this study show a drastic glacial recession over the last

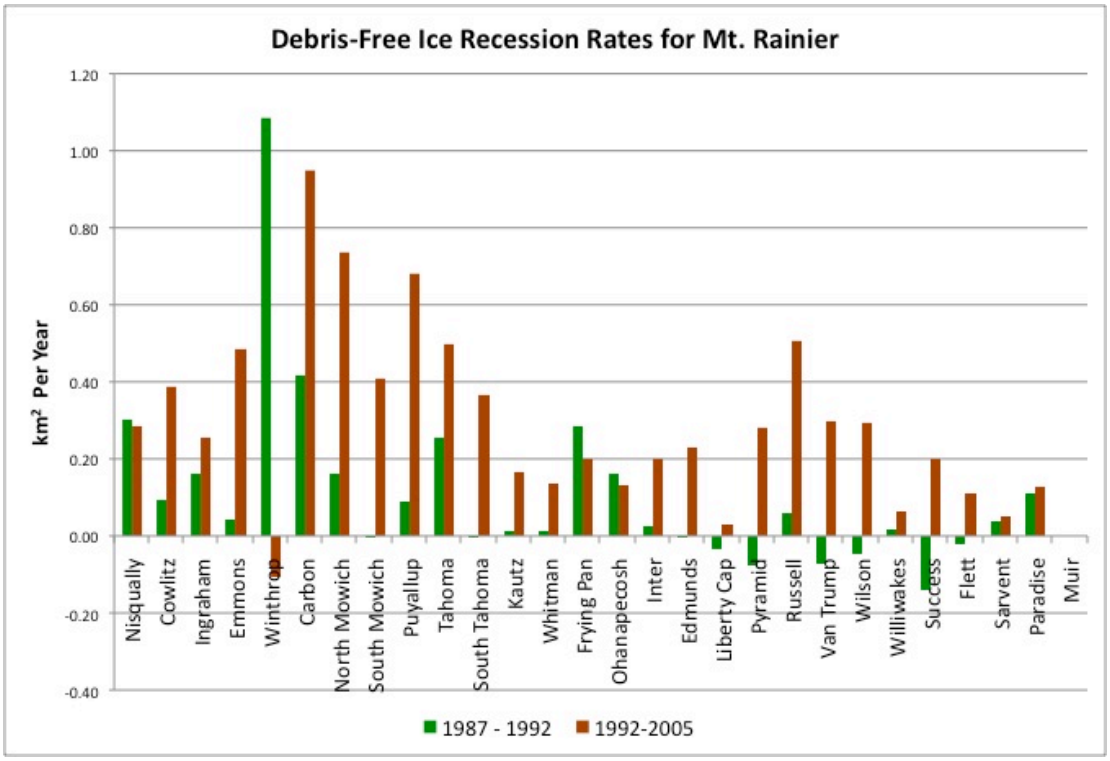

Figure 3.5. Debris-Free ice recession rates for Mt. Rainier. 1987-1992 in Green and 1992-2005 in red.

half century (Medley, 2008). Figure 3.5 shows the debris-free ice recession rates for Mt. Rainier. For most glaciers there is an increase in the rate of recession from 1992 to 2005 compared to 1987 to 1992 with the exception of the Winthrop Glacier. The

debris-free ice area for the Winthrop glacier in 1992 was lower than the debris-free ice area for 2005. This may be due to misclassification of snowfields as glacier ice in 2005. Without including Winthrop in the calculation, the average rate of debris-free ice recession for all the glaciers on Mt. Rainier from 1987 to 1992 was -378443 m^2y^{-1}, compared to -624853 m^2y^{-1} for the years 1992 to 2005, a 30% increase in the rate of glacier recession.

3.13 Analysis of Climate record and comparison of changes

Unfortunately, the Paradise SNOTEL site for Mt. Rainier was missing average daily temperature data from 1984 to 1989 so a comparison between 1989 to 1992 vs.

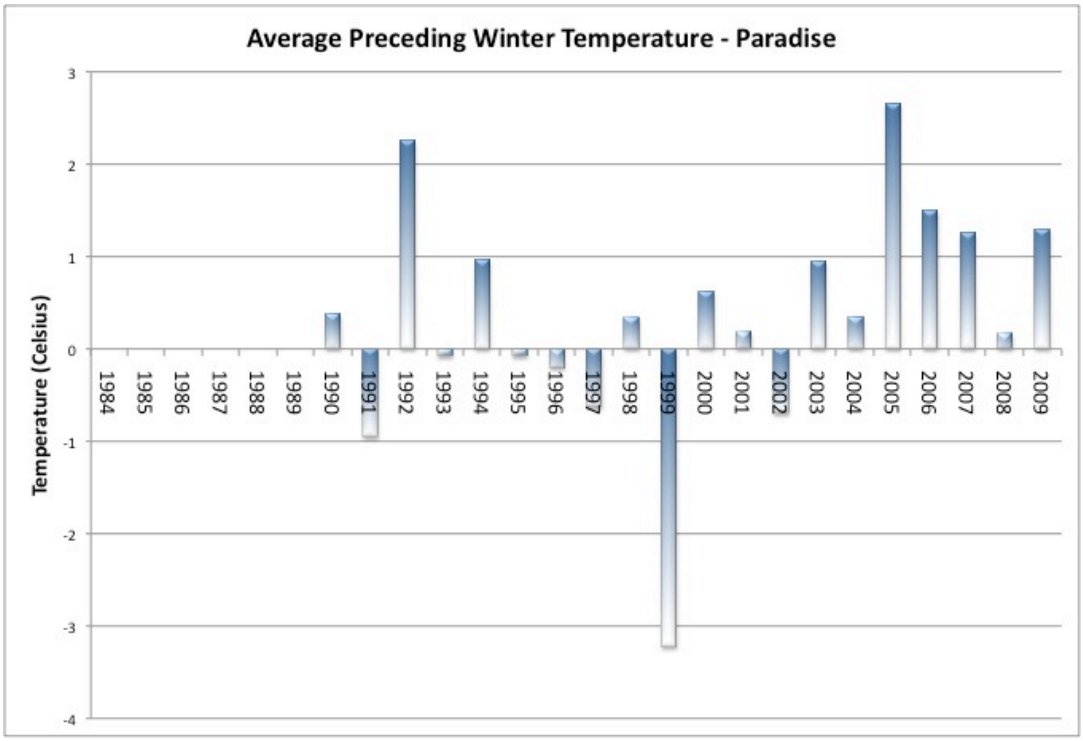

Figure 3.6. Average preceding winter temperature at the Paradise SNOTEL on Mt. Rainier, 1984-2009. Winter is defined as October 1 - May 30.

1992 to 2005 was used. For this analysis "summer" (the ablation season) was considered to be June 1st through September 30th of each year preceding the chosen Landsat scene. No trend is present in the temperature data. During the period 1989-1992 the average summer temperature was 10.5°C while during the period 1992-2005 the average summer temperature was 10.0°C, a decrease of 0.5°C. Figure 3.6 shows the average winter temperatures from 1990 to 2009 for the Paradise SNOTEL.

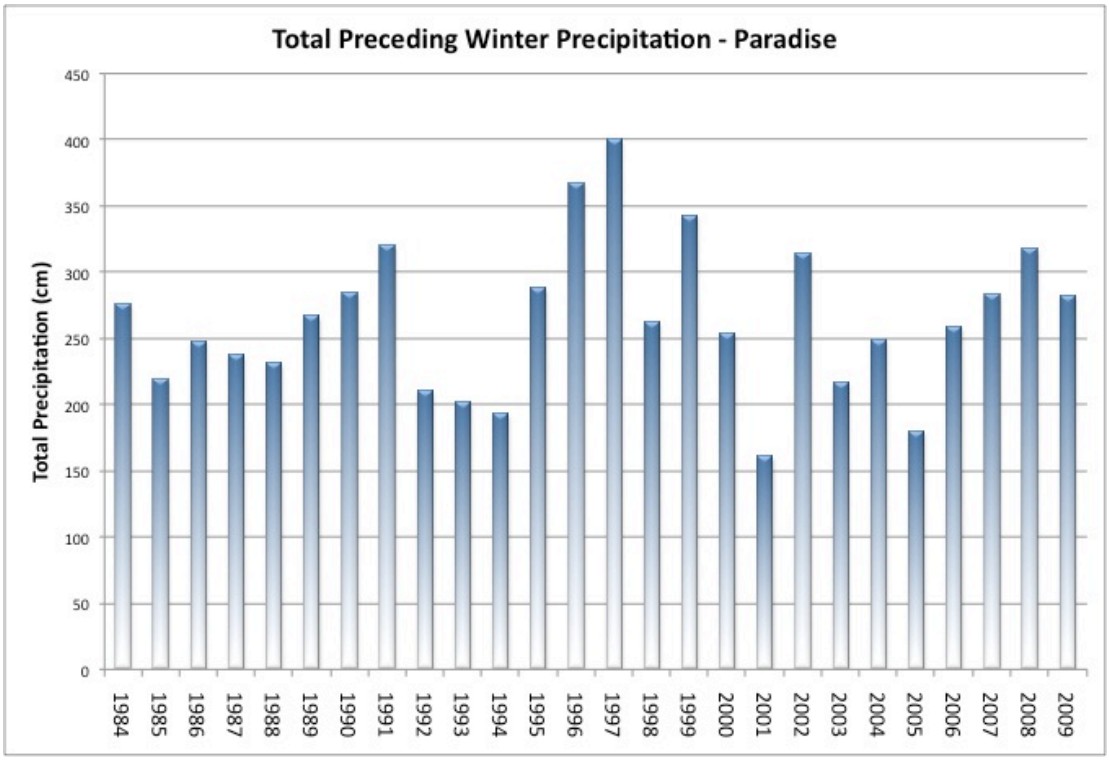

Figure 3.7. Total preceding winter precipitation at the Paradise SNOTEL station on Mt. Rainier 1984-2009. Winter is defined as October 1 - May 30.

A decrease in average winter temperature is observed from 1992 to 2009 compared to 1989 to 1992. This decrease may be attributable to the extremely cold winter of 1999. Without 1999 included in the calculation the general trend has been towards

warmer winter temperatures than in the past. The "winter" temperature analysis is composed of average daily temperatures between October 1st and May 31st for each year. The years 1992 and 2005 have the highest average daily winter temperature while the year 1999 was very cold in comparison to the overall average. Figure 3.7 shows the total winter precipitation for each year from 1987 to 2005. The years 1997 and 1999 have both colder temperatures and higher precipitation during the winter, while the years 1987 and especially 1992 and 2005 experienced warmer temperatures and less precipitation than the average during the winter months, possibly resulting in lower snow fall in the accumulation zone of the glaciers.

3.2 Mt. Hood Glacier Changes

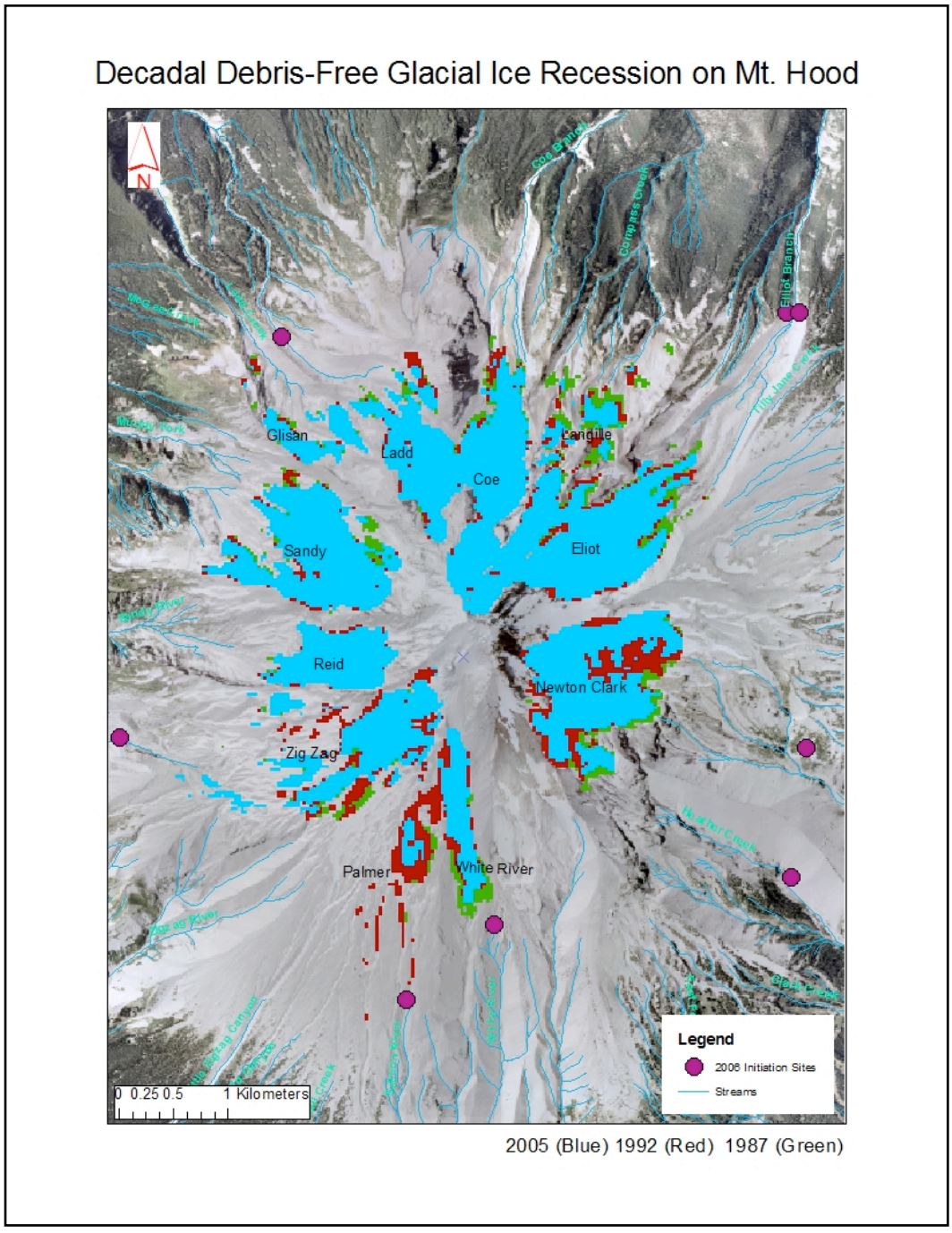

Figure 3.8. Decadal debris-free glacial ice change on Mt. Hood. 2005 slope-corrected is blue, 1992 is red, and 1987 is green. Purple dots are debris flow initiation locations from the November 2006 storm event (Pirot, 2010).

3.2.1 Projected & Slope-Corrected Area Change on a Glacier-by-Glacier Basis

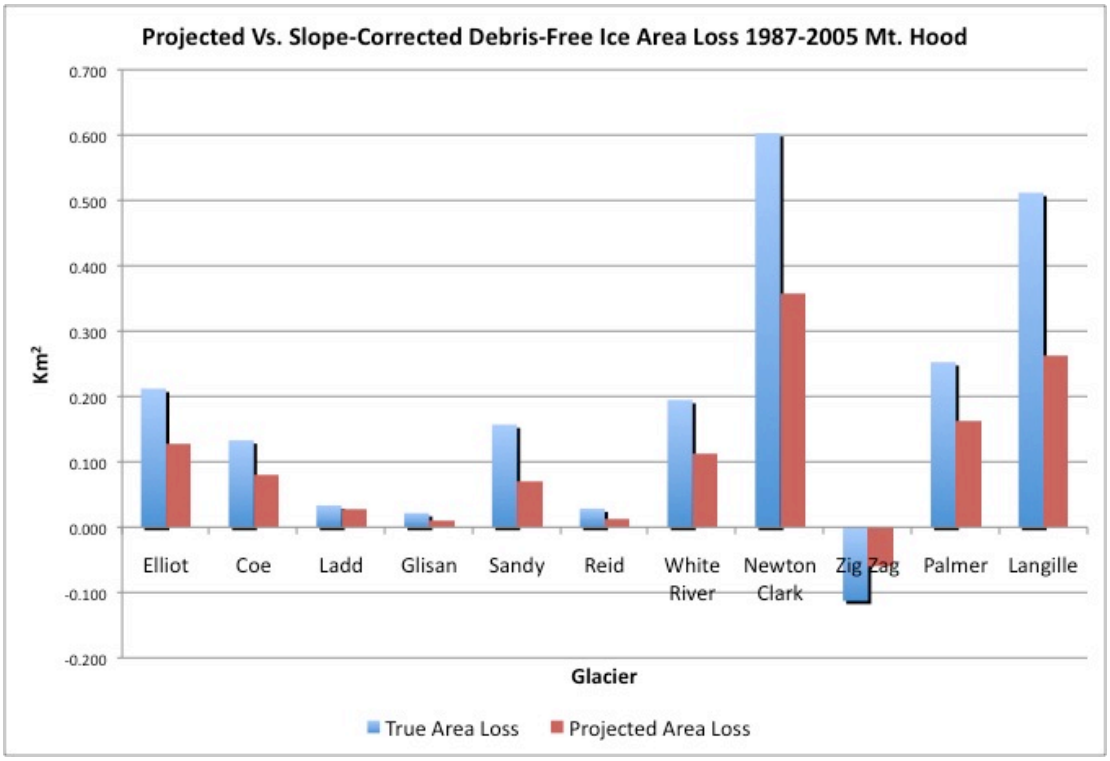

Figure 3.9. Projected vs. slope-corrected debris-free ice area loss from 1987-2005, Mt. Hood.

For all glaciers on Mt. Hood the slope-corrected area change of debris-free ice was greater than that of the projected change. Because of the topographic relief of Mt. Hood it was necessary to incorporate the slope into area calculations to get the slope-corrected area of the debris-free ice for each glacier. Figure 3.9 shows the projected and slope-corrected areas for each of the 11 glaciers on Mt. Hood. The Fountain 1984 outline, which was determined to be the most appropriate for this study, was used to crop out the debris-free ice regions of the glaciers. Figure 3.10 shows the total decadal debris-free ice area change for each glacier on Mt. Hood. The percent of debris-free ice loss for each glacier can also be seen in Figure 3.11. The

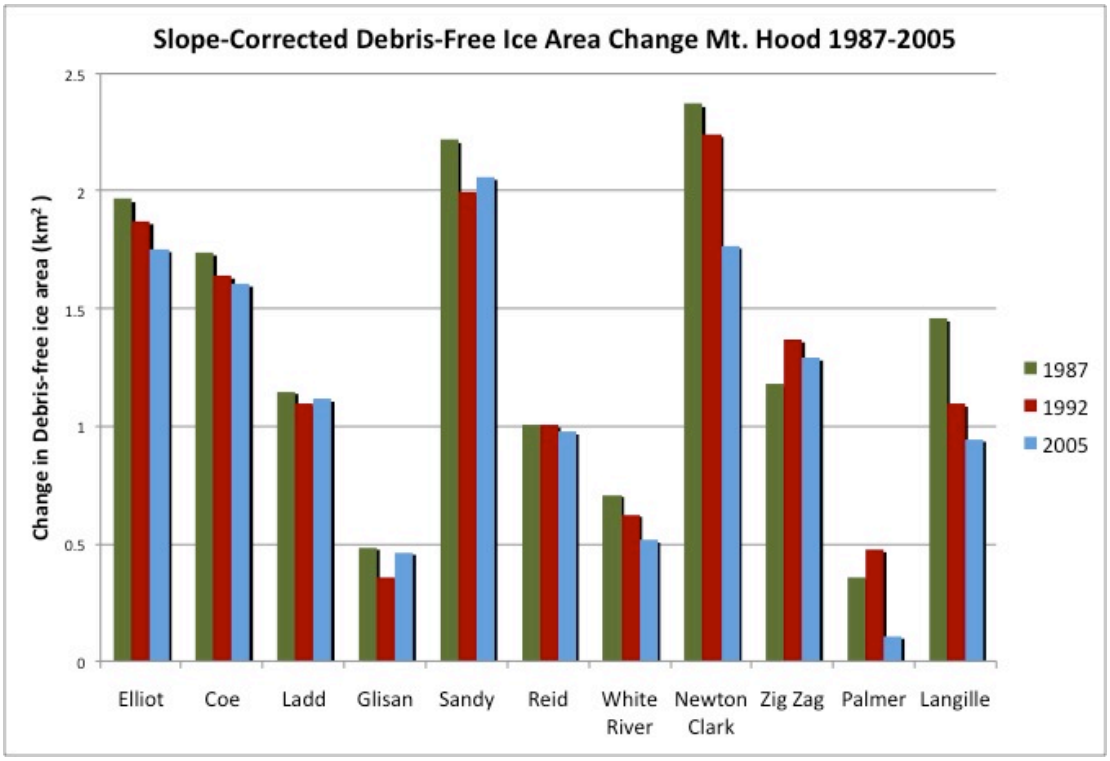

Figure 3.10. Decadal slope-corrected debris-free ice area change for glaciers on Mt. Hood, 1984-2009.

Palmer Glacier on the southern of the mountain lost 70% of its debris-free ice area from 1987 to 2005, while the Reid and the Ladd both lost less than 5%. The large recession of the Palmer can be seen in Figure 3.12, a 3D view of Mt. Hood from ArcGlobe. The Zigzag Glacier is shown to have grown in debris-free ice area. This may be due to a misclassification of the snowfields below the Zigzag Glacier as debris-free ice for 2005 (Figure 3.12)

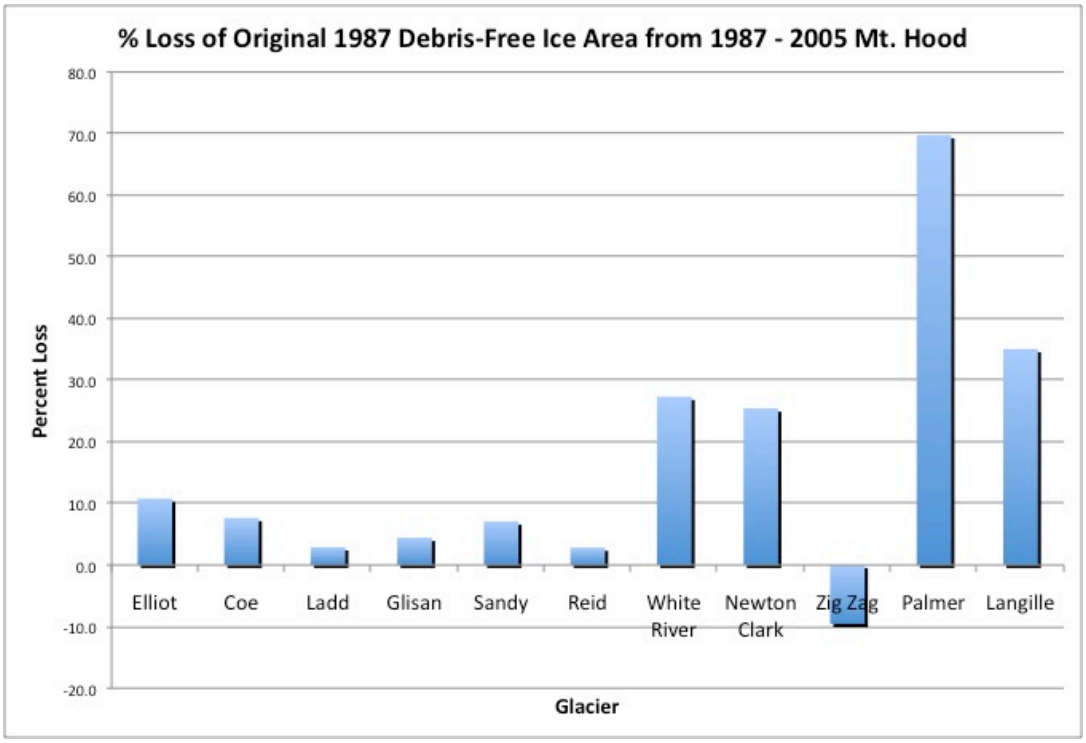

Figure 3.11. Percent debris-free ice loss from 1987-2005, Mt. Hood.

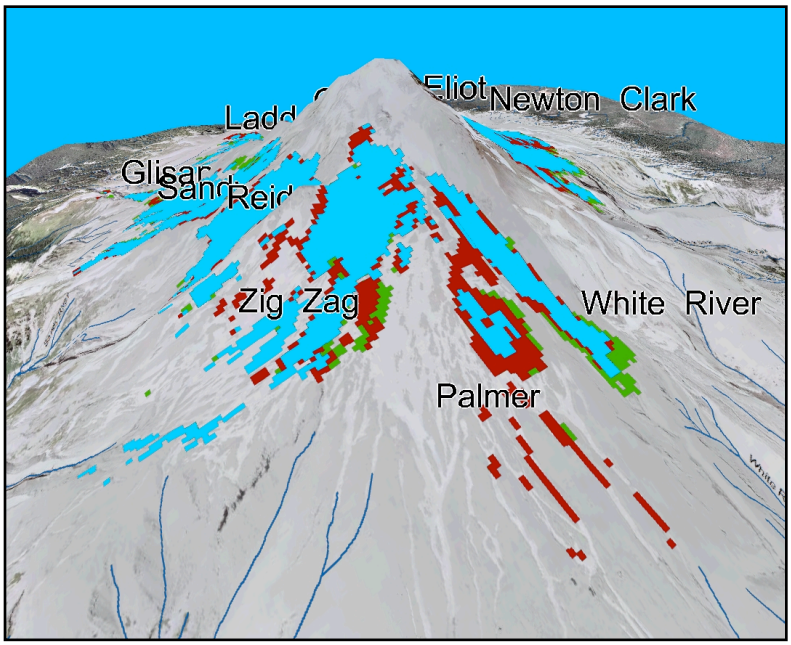

Figure 3.12 ArcGlobe image showing misclassification of lower elevation snowfields as glacier ice for the Zigzag and Palmer Glaciers of Mt. Hood.

Table 3.2 lists the 1987 Landsat-derived projected debris-free ice area for Mt. Hood. Projected areas from Landsat are in good agreement with previous area calculations completed in 1983, except for the Langille and Palmer Glaciers

Table 3.2. 1987 Landsat-derived projected debris-free ice area compared to area calculations of Kennard and Driedger in 1983 for Mt. Hood.

Glacier Name	Projected 1987 Landsat Area in km^2	Kennard & Driedger 1983 in km^2	Kennard & Driedger Volume in km^3	Drainage Glacier Feeds
Elliot	1.15	1.68	0.09	Eliot Creek, a tributary of Middle Fork Hood River
Coe	0.93	1.24	0.05	Coe, a tributary of Middle Fork Hood River
Ladd	0.64	0.90	0.03	Ladd & McGee Creek, a tributary of West Fork Hood River
Glisan	0.23	No Data	No Data	McGee Creek, a tributary of West Fork Hood River
Sandy	1.12	1.19	0.002	Muddy Fork, a tributary of the Sandy River
Reid	0.50	0.75	0.02	Sandy River
White River	0.39	0.54	0.01	White River
Newton Clark	1.39	1.99	0.04	Clark and Newton Clark Creek then East Fork Hood River
Zigzag	0.72	0.77	0.04	Zigzag River
Palmer	0.23	0.13	0.002	Salmon River
Langille	0.73	0.40	0.01	West Compass Creek

(Kennard, 1984). For these glaciers the projected areas are lower than those estimated by Kennard because the Landsat-derived areas only represent the debris-

free ice area rather than the full glacier extent. The large Landsat-derived projected area of the Palmer Glacier is most likely due to misclassification of the large snowfields below it as glacial ice. These snowfields are artificially maintained by the Timberline Ski Resort, so are not considered for analysis in this study. The large difference between the Landsat-derived projected area of the Langille and the area derived by Kennard and Driedger cannot easily be explained. It could be due to a difference in the glacial outline used to calculate glacial area between this study and that of Kennard.

The total projected area of debris-free ice for all glaciers on Mt. Hood in 1987 was 8.0 km^2 while the total area for all glaciers, including areas of debris-covered ice found by Kennard in 1983 was 9.6 km^2 but the calculation did not include the Glisan Glacier which this study found to have a debris-free ice area of just under 0.5 km^2. With Glisan included, Kennard's 1983 total glacier area for Hood can be assumed to be just over 10 km^2. Table 3.2 shows that the NDGI method of classifying debris-free glacier ice area stands up to the results of previous studies.

AS with Mt. Rainier, these glacier estimates were compared with results from Medley (2008) who used 2003 ASTER imagery to calculate projected total debris-free ice area for Mt. Hood. For Mt. Hood Medley found a projected debris-free ice area of 7.1 ±0.4 km^2 which matches well with this studies 6.9 km^2 total for 2005 just two years later. The Coe and Eliot projected debris-free ice areas also match well

with total areas calculated for those glaciers using ASTER imagery by Jeff Phillippe in 2008.

3.22 Calculating Rates of Glacier Change

According to USGS maps from 1956 Mt. Hood had a total glacier area of 19.7

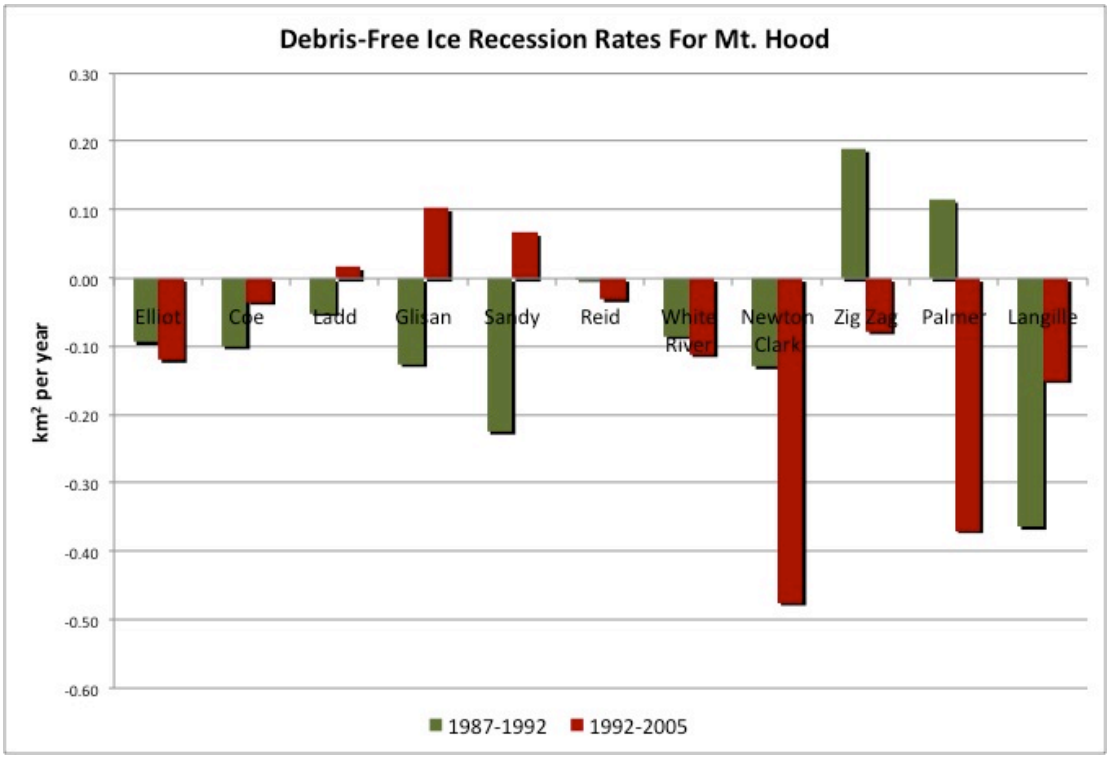

Figure 3.13. Slope-corrected debris-free ice recession rates for Mt. Hood.

±0.8 km^2. The USGS maps account for the entire glacial area but even with this considered the results of this study show a drastic glacial recession over the last half century. Figure 3.13 shows the rate of recession for each glacier on Mt. Hood from 1987 to 1992 and from 1992 to 2005 in m^2y^{-1}. The growth of the Zigzag and Palmer glaciers during the period 1987 to 1992 is attributable to the misclassification of

lower snowfields as glacial ice. The Newton Clark Glacier experienced the greatest increase in recession rate.

For Mt. Hood the recession rate has decreased from 1992 to 2005 when compared to 1987 to 1992. Lillquist (2006) notes that high precipitation in the late 90s caused measurable glacier length advances during 2000 to 2001 which may account for the slower rate of debris-free ice recession also found in this study. From 1987 to 1992 the rate of recession of debris-free ice area was -15617 m^2y^{-1} while from 1992 to 2005 this rate lowered to -8213 m^2y^{-1}.

3.24 Analysis of Climate Record and Comparison of Changes

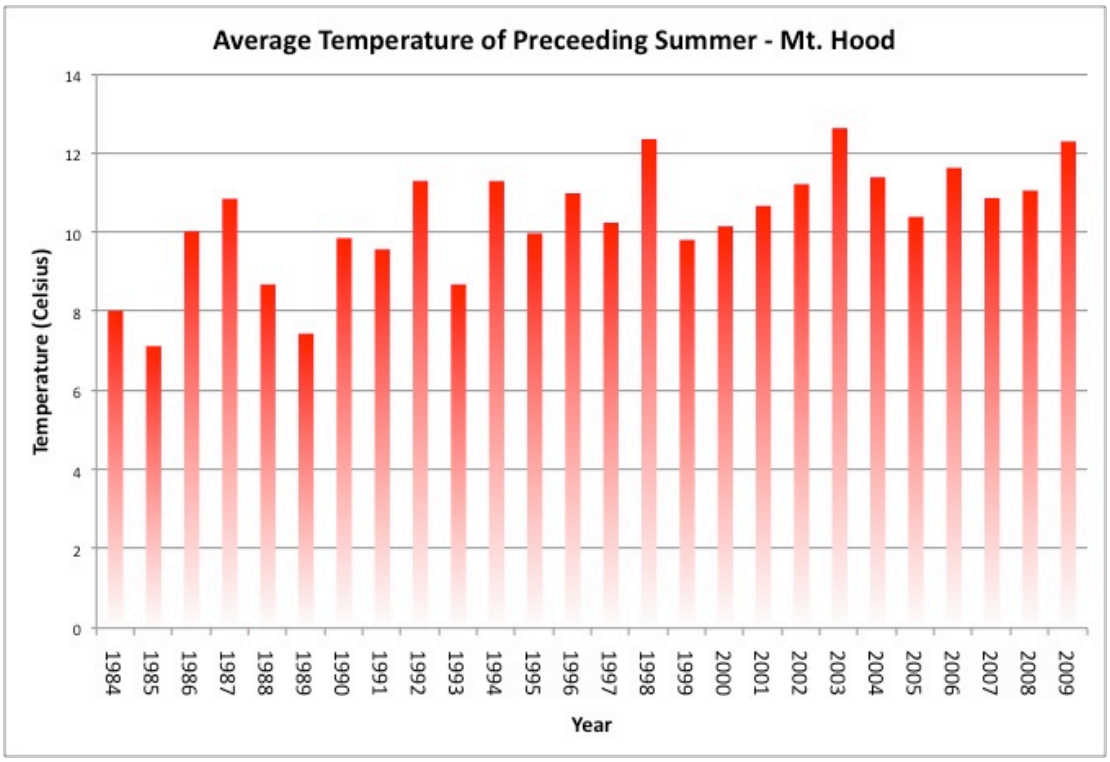

Figure 3.14. Average temperatures of preceding summers before Landsat scenes for Mt. Hood, 1984-2009. Summer is defined as June 1 - September 30.

The average summer daily temperatures for Mt. Hood show an upward trend since 1987 (Figure 3.14). During the period 1987 to 1992 the average summer temperature was 9.22°C while during the period 1992 to 2005 the average summer temperature rose to 10.77°C, an increase of 1.55°C. This daily summer temperature average is a dramatic increase from the average summer temperature of 5.6 °C in 1902 (Daly, 1997). Winter temperatures for Mt. Hood are also increasing over time (Figure 3.15). During the period 1987 to 1992 the average winter temperature was -0.40°C while during the period 1992 to 2005 the average winter temperature rose to

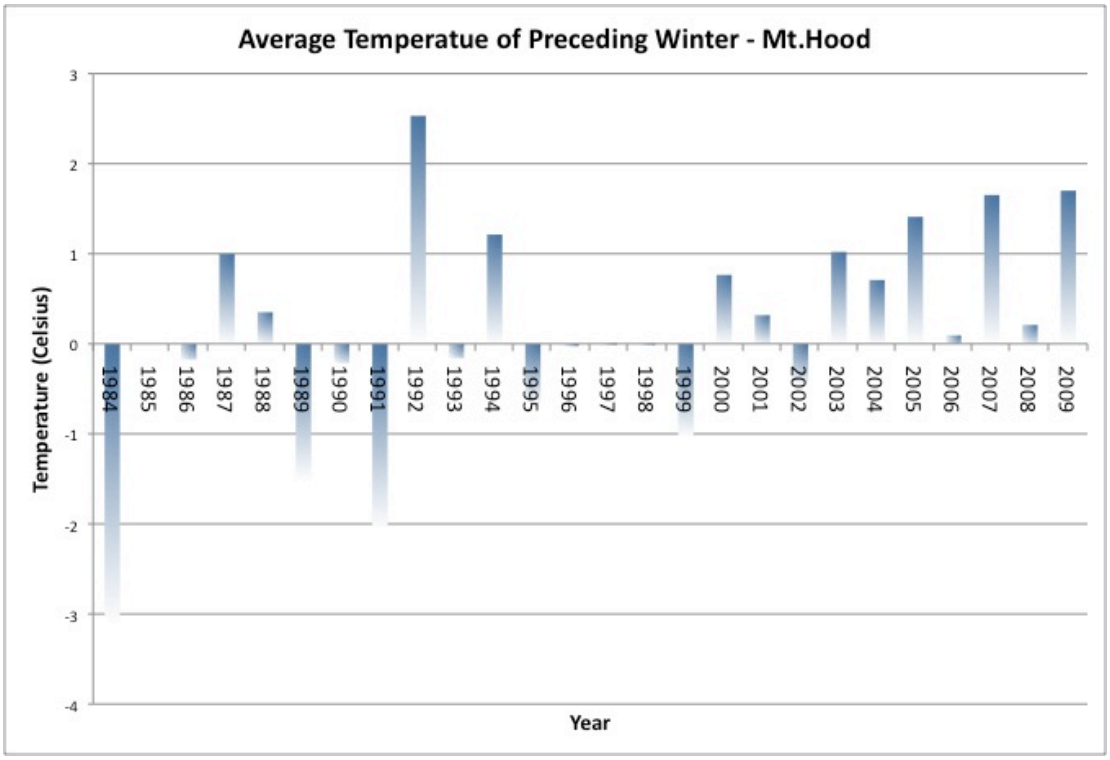

Figure 3.15. Average temperatures of preceding winters before Landsat scenes for Mt. Hood, 1984-2009. Winter is defined as October 1 - May 30.

0.24°C, an increase of 0.84°C. The average daily temperature for all days of the year during the period 1987 to 1992 was 2.91°C while during the period 1992 to 2005 the

average daily temperature was 3.80°C, an increase of 0.89°C. These figures show that summer temperatures for Mt. Hood may be increasing at a rate that is nearly double the winter and annual average temperature rates of increase.

An analysis of the total winter preceding precipitation for Mt. Hood does not

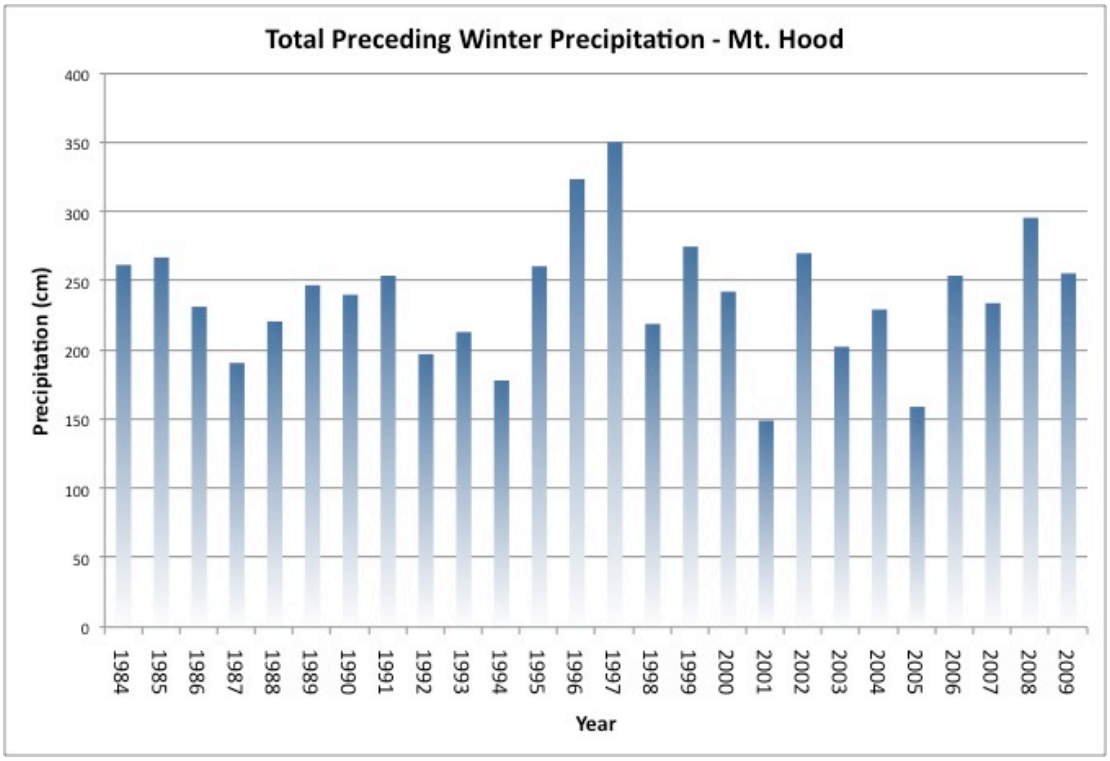

Figure 3.16. Total preceding winter precipitation preceding Landsat scene, Mt. Hood 1984-2009. Winter is defined as October 1 - May 30.

show a trend towards more or less precipitation in the future, although together with the increasing winter average daily temperatures it could mean that more of the precipitation will fall as rain rather than as snow as the equilibrium line altitude shifts to higher elevations (Figure 3.16).

3.3 Comparison of Glacier Retreat Rates and Debris Flow Dates/Locations

The debris flows with known locations in this study are all the result of the November 2006 rain event when a major storm deposited record amounts of rainfall at Mt. Hood and Mt. Rainier. Glaciers appear to play a role in the initiation of debris flows in their drainages but the likelihood of debris flow initiation is greatly enhanced by intense rain events such as the November 2006 storm (Pirot, 2010). This is particularly the case in the fall after the ablation season when rainfall may be rapidly accumulated into the englacial drainage network through cracks and crevasses in the glacier surface (Copeland, 2009). The build up of subglacial water pressure, and possibly the occurrence of a glacial outburst flood in combination with increased streamflow may increase toe slope erosion of glacial moraines and carrying capacity of debris deposited by glacial recession. These mechanisms of debris flow generation are seen in many of the documented initiation locations of the November 2006 storm debris flows (Table 2.9 & 2.10).

The glaciers that have produced the most debris flows historically, the White River, Eliot and Newton Clark, had some of the highest percentage losses of their original 1987 debris-free ice areas, 27.3%, 25.4%, and 10.77%, respectively. The Newton Clark glacier lost the most amount of debris-free ice area on Mt. Hood since 1987 and its two drainage basins, Clark Creek and Newton Clark Creek, have experienced 6 and 8 known debris flows, respectively, since 1980, the most associated with any single glacier on the peak. However, the Langille Glacier also

experienced a high total loss of slope-corrected debris-free ice area at 512000 m^2 but historically it is not known to have produced any debris flows. As mentioned previously, the Palmer Glacier has lost the greatest debris-free ice area at 70% but it is artificially maintained by the Timberline Ski Resort.

All drainages on Mt. Hood are capable of producing debris flows but those connected directly to a glacier with little vegetation to secure the soils are the most susceptible to debris flow initiation (Pirot, 2010). In 2006, the drainages that did not experience debris flows during the intense rain event were the Polallie, which is not associated directly with a glacier, the Coe below the Langille Glacier, the Muddy Fork and the Zigzag. Pirot (2010) suggests that, due to the very steep gradients of the Muddy Fork and Zigzag drainages, that material is constantly being transported downstream through typical fluvial processes, thereby resulting in a smaller reservoir for debris flow initiation (Pirot 2010). None of the 2006 debris flow initiation sites fell within the 1987 to 2005 debris-free ice recession area found in this study and none fell within the 1972 or 1984 glacier boundary outline produced by Nylen. The Eliot Creek initiation sites were very close to the boundary of the 1972 outline, suggesting loose debris within the last half century of recession may be responsible for the slope failures that initiated the debris flows. The Salmon Creek debris flow site is within the 1972 Palmer Glacier outline but I believe there was misclassification of snowfields as part of the glacier and that the debris flow did not initiate from glacier recession but possibly instead from melting perennial snowfields destabilizing

slopes. Figure 3.17 graphically shows the percentage loss of debris-free ice for each glacier on Mt. Hood from 1987 to 2005 along with the 2006 debris flow initiation points, in purple, from Pirot (2010).

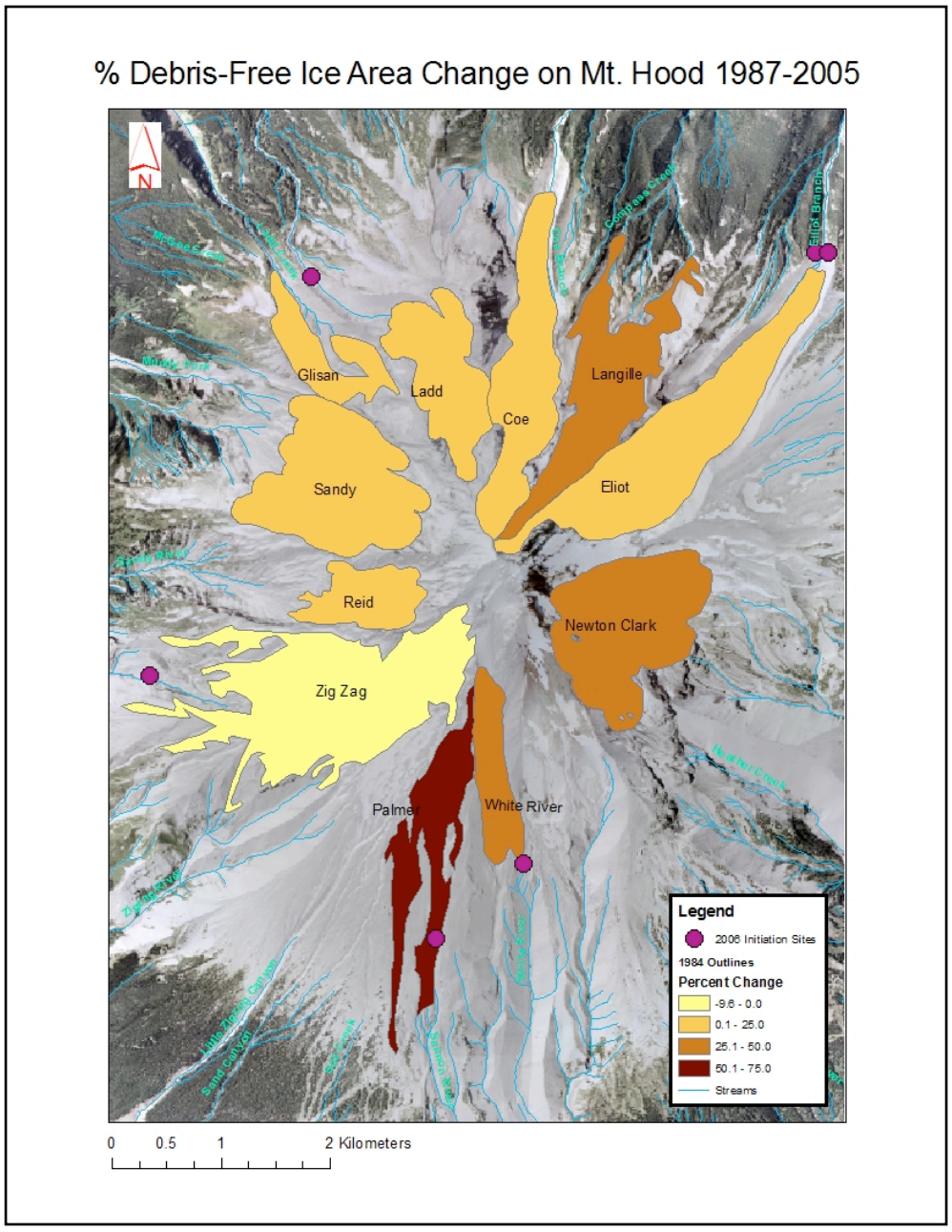

Figure 3.17. Percent debris-free ice area change for each glacier on Mt. Hood from 1987 to 2005 in relation to the November 2006 storm event debris flow locations (Pirot, 2010).

The glaciers on Mt. Rainier that have produced the most debris flows historically, the Nisqually and Winthrop, did not lose a higher percentage of their 1987 debris-free ice extent than glaciers that have not traditionally produced debris flows. Figure 3.18 shows the percentage loss of debris-free ice for each glacier on Mt. Rainier from 1987 to 2005 along with the 2006 debris flow initiation points, in purple (Copeland, 2009).

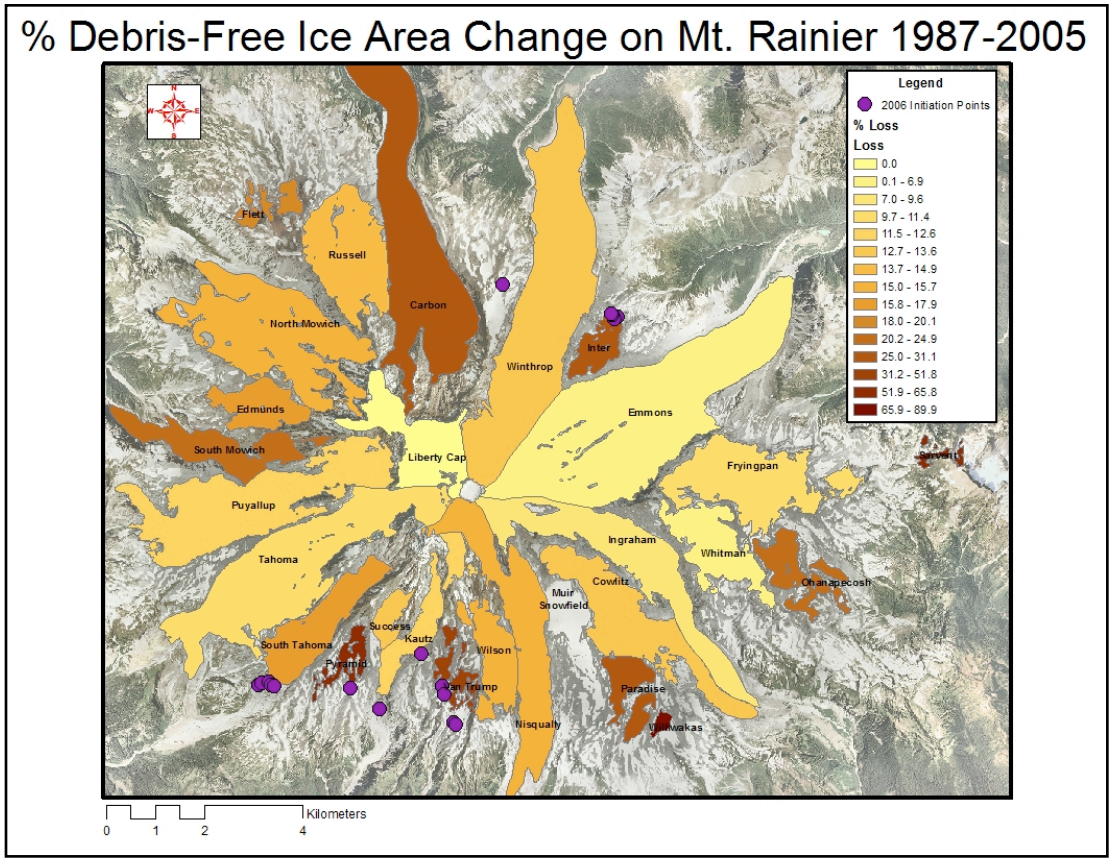

Figure 3.18. Percent debris-free ice area change for each glacier on Mt. Rainier from 1987 to 2005 in relation to the November 2006 storm event debris flow locations (Copeland, 2009).

According to Copeland (2009) twelve debris flows have occurred in six drainages since 2001 with three drainages experiencing debris flows for the first time.

The Inter Fork of the White River, Pyramid Creek and Van Trump Creek all experienced debris flows for during the November 2006 storm. When looking at the percent change of debris-free ice area for these three glaciers, all had lost a high percent of their original debris-free area size, 28.6%, 60.5%, and 51.8%, respectively (Figure 3.20). All three glaciers also experienced a significant increase in debris-free

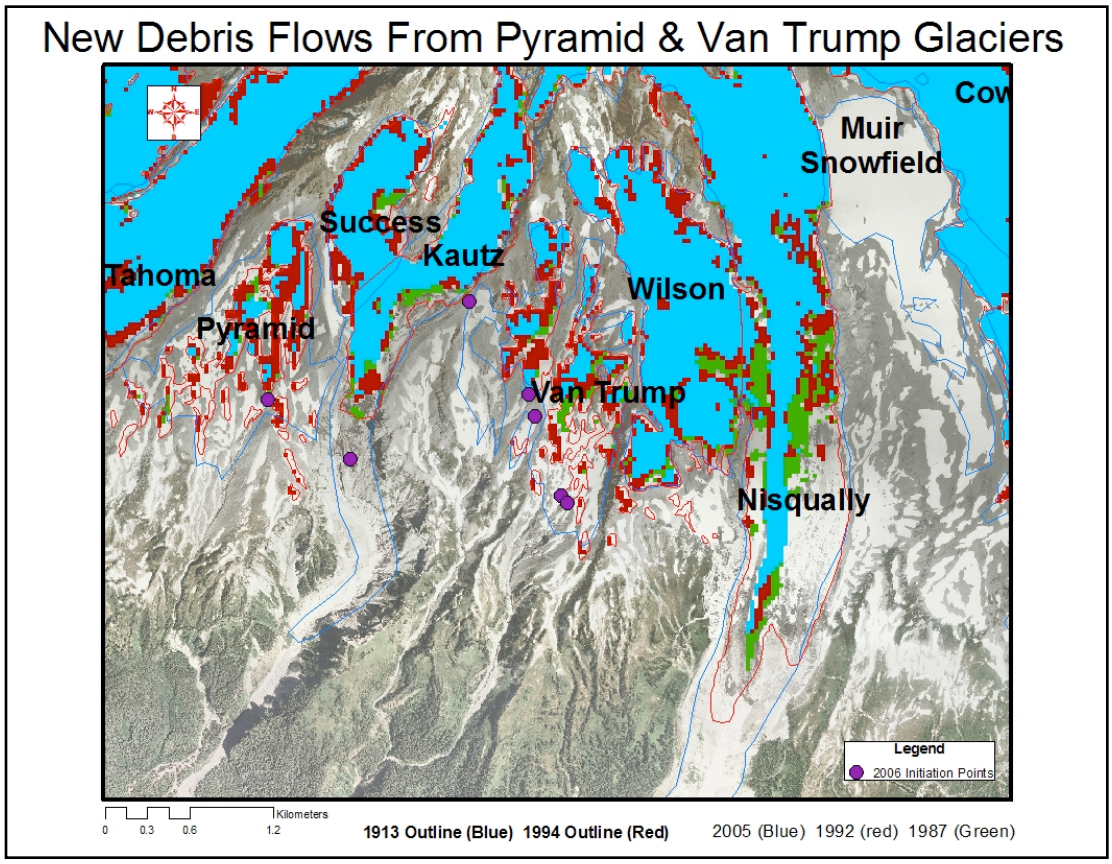

Figure 3.19. New debris flows locations from the Pyramid and Van Trump glaciers on Mt. Rainier after the November 2006 storm event.

ice recession rate from 1992 to 2005 compared to 1987 to 1992. The 2006 debris flow initiation sites for Mt. Rainier show that all the drainages experiencing debris flows for the first time had initiation locations within the glacier recession boundaries of 1987 to 2005 and most are within or very close to the glacier boundary for 1994

defined by Nylen (Copeland, 2009; Nylen, 2004; Figure 3.19). In particular, the

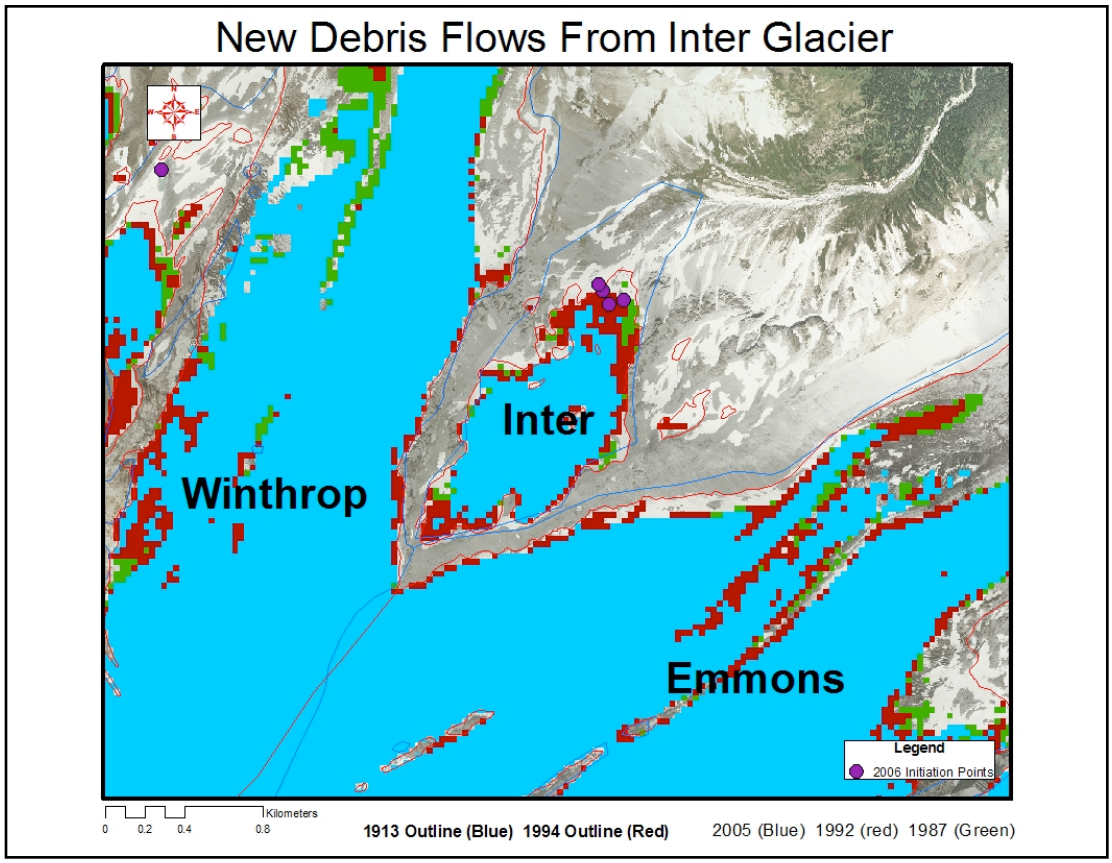

Figure 3.20. New debris flow locations in the 1987-2005 recession area of the Inter Glacier on Mt. Rainier after the November 2006 storm event.

recession rate for the Inter Glacier increased from a loss of 5400 m^2/y from 1987-1992 to a loss of 15500 m^2/y from 1992-2005. The Inter Glacier produced its first recorded debris flow in the November 2006 storm event. The initiation location of the debris flow is located within the 1987 to 2005 recession area (Copeland, 2009) (Figure 3.20).

3.4 Statistical Analysis

For Mt. Hood, the glacier debris-free ice area change from 1987 to 2005 for debris flow producing glacial basins from the November 2006 storm and the glacier debris-free ice area change for glacial basins not associated with debris flows during the same storm is not significantly different (Welch Two Sample T-test: t-statistic = 0.1069, df = 7, p-value = 0.9178). These statistics did not include the Palmer Glacier as it is artificially maintained by the Timberline Ski Area. For Mt. Rainier, glacier debris-free ice area change from 1987 to 2005 for debris flow producing glacial basins from the November 2006 storm and glacier debris-free ice area change for glacial basins not associated with debris flows during the same storm is not significantly different (Welch Two Sample t-test: t-statistic = 0.2612, df = 8, p-value = 0.6208). Statistically, there is not a significant relationship between glacial recession overall and the initiation locations of the November 2006 debris flows for either Mt. Hood or Mt. Rainier.

For both volcanoes more debris flows occurred on the south-facing aspects. For Mt. Hood five of the seven debris flows from November 2006 occurred on the south side of the mountain while on Rainier four south-facing glacial drainages experienced debris flows compared to two north-facing drainages. Nylen (2004) also found pronounced differences in glacier recession based on aspect.

Table 3.3. Statistical comparison of debris flow producing glaciers from non-debris flow producing glaciers from the 2006 storm for Mt. Hood.

Assessment	Avg Do	Avg Don't	t-statistic	df	p-value
Loss of debris-free ice area (km^2)	0.19	0.17	0.1069	7	0.9178
% Loss of debris-free ice area since 1987	11.4%	11.4%	-0.0039	7	0.997
Recession rate (m^2yr^{-1}) 87-92	6622	32370	-1.5282	7	0.1704
Recession rate (m^2yr^{-1}) 92-05	11754	648	1.5229	7	0.1786

Table 3.4. Statistical comparison of debris flow producing glaciers from non-debris flow producing glaciers from the 2006 storm for Mt. Rainier.

Assessment	Avg Do	Avg Don't	t-statistic	df	p-value
Loss of debris-free ice area (km^2)	0.37	0.44	0.2612	8	0.6208
% Loss of debris-free ice area since 1987	30.8%	22.3%	0.8883	8	0.4002
Recession rate (m^2yr^{-1}) 87-92	32705	20295	0.3304	5	0.7544
Recession rate (m^2yr^{-1}) 92-05	15523	26052	-1.5675	12	0.143

Table 3.5. Statistical comparison of debris-free ice recession rate between south- and north-facing glaciers on Mt. Hood, not including the Palmer Glacier.

Assessment	North-facing	South-facing
Loss of debris-free ice area (km)	1.10	0.68
% Loss of debris-free ice area since 1987	10.09%	14.38%
Recession Rate (m2/yr) 87-92	27213	1489
Recession Rate (m2/yr) 92-05	1583	16975

Table 3.6. Statistical comparison of debris-free ice recession rate between south- and north-facing glaciers on Mt. Rainier, not including the Liberty Cap Glacier.

Assessment	North-facing	South-facing
Loss of debris-free ice area (km)	6.67	4.33
% Loss of debris-free ice area since 1987	21.69*	26.46
Recession rate (m^2yr^{-1}) 87-92	36688	11562
Recession rate (m^2yr^{-1}) 92-05	28645	19318

* = including the very small Sarvent Glacier that lost 66% of it's original 1987 debris-free ice extent. Without Sarvent included the average percent loss for north-facing glaciers would be 17.68%.

Chapter 4: Discussion

4.1 Glacier Change in Relation to Debris Flow Initiation Sites

We speculate that there is a link between glacier recession and the supply of debris needed for initiation of debris flows on both Mt. Rainier and Mt. Hood.

For example, initiation zone elevations for the November 2006 storm debris flows all occurred in a narrow band representative of the distal extent of the most recent glacial moraine deposits (Pirot, 2010). However, because not all glacier drainages produced debris flows in the November 2006 event, other mechanisms of debris flow initiation must be considered. From the results of this study it is evident that recession alone does not determine whether or not a periglacial debris flow will occur in a glaciated basin.

The volume of debris available for debris flow generation in a glacial drainage is directly related to glacial recession. This study shows that the glaciers producing the most debris flows also have rapid debris-free ice area recession. Furthermore, glacier drainages on Mt. Rainier that generated the first recorded debris flows from the November 2006 storm event have some of the highest recession rates for 1992 to 2005. Yet, still there are other, often highly dissected glaciers, such as the Sarvent and the Williwakas on Mt. Rainier, that have experienced high debris-free ice glacier recession yet are unassociated with recorded debris flows. Therefore, we speculate that the supply of debris is not the only parameter needed for debris flow generation.

Studies have shown that the transport capacity of streams in glacierized basins is an important factor to consider when assessing debris flow generation mechanisms (Fountain, 1998). Only drainage basins that are directly connected to glaciers on both Mt. Rainier and Mt. Hood produced debris flows during the November 2006 rain event. This could indicate that the added contribution of water stored in the glacier from the summer melt season or runoff over the smooth glacial ice was critical to push the stream flow past the threshold needed to mobilize the loose debris of the glacial moraines below. The volume of water stored within each glacier is directly dependent on the rate of surface melt (Fountain, 1998). The pressure of water flow within englacial channels increases in times of high glacier melt such as the hot, dry ablation season of the Pacific Northwest Aleutian High, but most often it is increased through rainfall.

Glaciers have been shown to frequently release small discharges of their stored water but with the water pressure added to the system by strong rainstorms such as the one from November 2006 these small discharges may transform into a much larger glacial outburst flood (Fountain, 1998). Walder and Dreidger (1994) assert that even during wet weather, debris flows are often the result of glacier drainage pressures. The small discharges of water from a melting glacier to the drainage below may serve to continually erode away at the slope of glacial moraines left by recession. A glacial outburst flood of meltwater precipitated by an intense

rainfall event may supply the needed discharge force and carrying capacity of alpine streams to trigger a landslide above the incised toe slope of glacial moraines.

The combined supply rate of debris and meltwater from glacial recession has been shown to be directly tied to debris flow initiation during intense rain events. In a study of the French Alps, Jomelli (2007) showed that alpine debris flows on a decadal time scale are more dependent on the occurrence of intense rain events than the re-accumulation of debris at glacier tongues. The spatial and temporal overlap between intense rainfall events and areas of loose debris left behind by retreating glaciers is important. Therefore, if a flow is initiated from a heavy rainfall at year t, the probability of a flow being triggered at year $t + 1$ will be low because the stored reservoir of loose available debris is mobilized during the first flow (Jomelli, 2004). The combination of increased englacial meltwater pressure from long ablation seasons, together with large reservoirs of debris from high rates of glacial terminus recession over the last century, produce conditions favorable for debris flow generation when the intense rainstorms occur.

For Mt. Hood four of the seven recorded debris flows for the November 2006 storm event and at least one of the six recorded from Mt. Rainier were initiated by slope failure due to streams undercutting the toe of moraine slopes. The exact method of how this occurred is not known but it is possible that glacial outburst floods from the terminus of the associated glaciers were sufficient to trigger the slope failures. Therefore, we speculate that glaciers in the Pacific Northwest with higher recession

rates may also be associated with higher subglacial water pressures during rain events, which may help to initiate debris flows.

Topographic aspect is also important when looking at recession rates of alpine glaciers. On Mt. Rainier a majority of the known debris flow initiation sites are located on south-facing sites. For example, south-facing Van Trump, Williwakas and Pyramid glaciers are the only glaciers on the volcano to have lost over 50% of their initial debris-free ice area. Their recession rate is nearly double that of the north-facing Carbon Glacier, which lost 30% of its 1987 original debris-free ice area. Furthermore, the only north-facing glacier on Mt. Rainier to historically produce debris flows is the Winthrop. Nylen (2004) reports that south-facing glaciers have retreated 26.7% compared to the north-facing glaciers at 17.5% for the years 1913 to 1971. Copeland (2009) also notes that only three times in the recorded debris flow history of Mt. Rainier have debris flows been associated with north-facing glaciers, and since 1913 south-facing glaciers have retreated over three times the distance of their north-facing counterparts.

Differences in glacier recession rates based on aspect are also observed for Mt. Hood. The south-facing White River and the Southeast-facing Newton Clark have seen a large percentage of their original 1987 debris-free ice area disappear in 2005, compared to most of the north-facing glaciers with the exception of the Langille. Lillquist (2006) also notes that glacier termini for north-facing glaciers such as the Coe and Eliot fluctuated very differently than the south-facing glacier

termini of the White River and Newton Clark glaciers. However, with historical and recent debris flows occurring on all sides of Mt. Hood a clear correlation between rate of recession and debris flow initiation site cannot be found from looking at aspect alone (Figures 1.13 and 2.13).

4.2 Decadal Change vs. Annual Change using Landsat Imagery

Upon comparing several band-ratio reclassified scenes based on the 0.05 threshold it became apparent that the 30×30 m resolution of the Landsat TM sensor was too coarse to analyze glacier change on an annual basis. It is not likely that any of the glaciers on Mt. Hood or Mt. Rainier will show length changes of debris-free ice greater than the 30 m resolution of the Landsat sensor. Phillippe (2008) found the annual retreat of the Eliot Glacier terminus to be 15 myr^{-1}, half the distance that the Landsat TM sensor is able to resolve. Errors would thus be larger than the recession of the glaciers. Research has shown that using Landsat is most appropriate for looking at long term glacier change over several decades. Glacier recession analysis over just one decade becomes less accurate (Hall, 2003).

Figures 4.1 through 4.3 show the slope-corrected debris-free ice area change for the Pyramid Glacier on Mt. Rainier and the White River Glacier on Mt. Hood. Both glaciers lost a large percent of their original 1987 debris-free ice extent, 60.5% and 27.3% respectively. The graphs illustrate that annual shifts in debris-free ice area coverage due to misclassification of snowfields are often larger than long term trends. It was not possible to obtain a clear scene for Mt. Hood in 2004 (Figure 4.3).

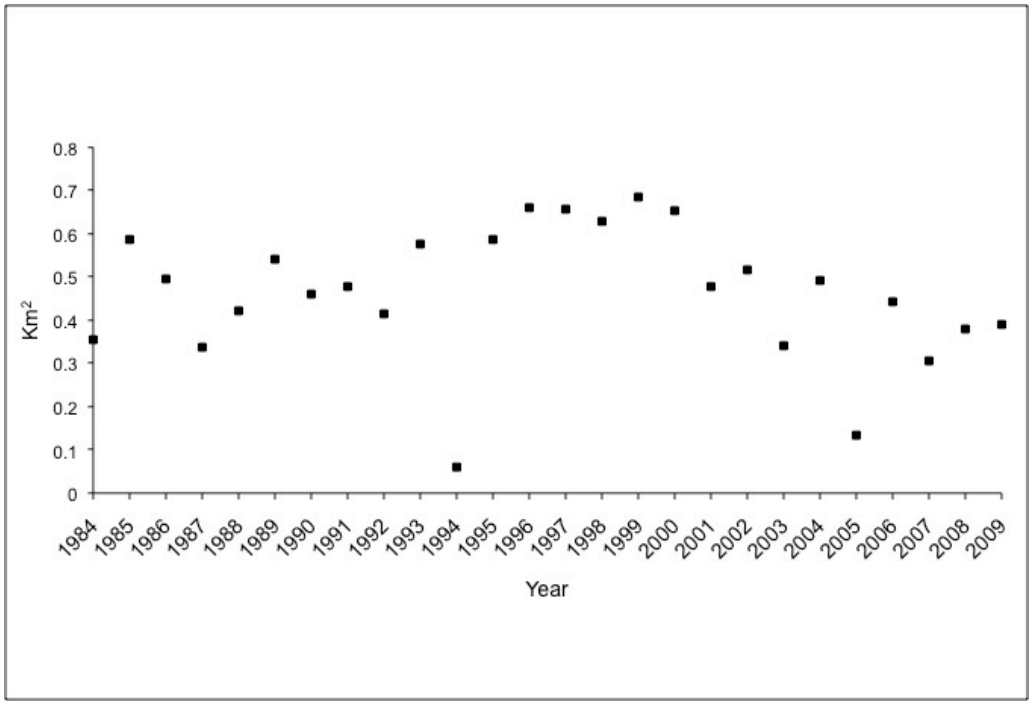

Figure 4.1. Slope-corrected debris-free ice area of the Pyramid Glacier, Mt. Rainier for each year 1984-2009.

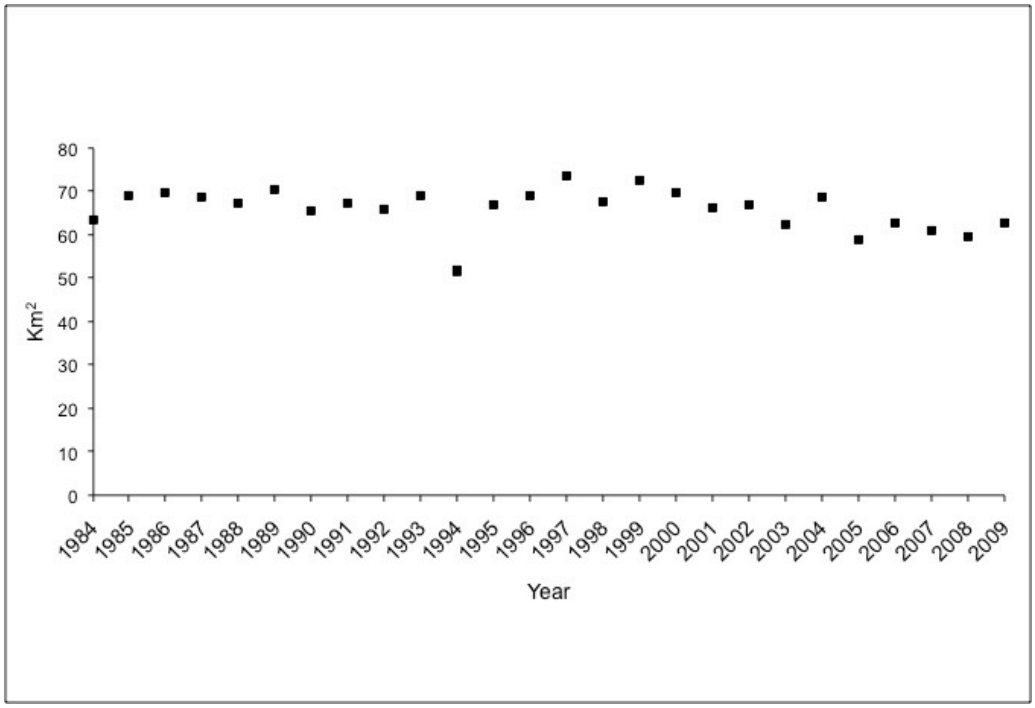

Figure 4.2. Total debris-free ice area of all glaciers on Mt. Rainier for each year 1984-2009.

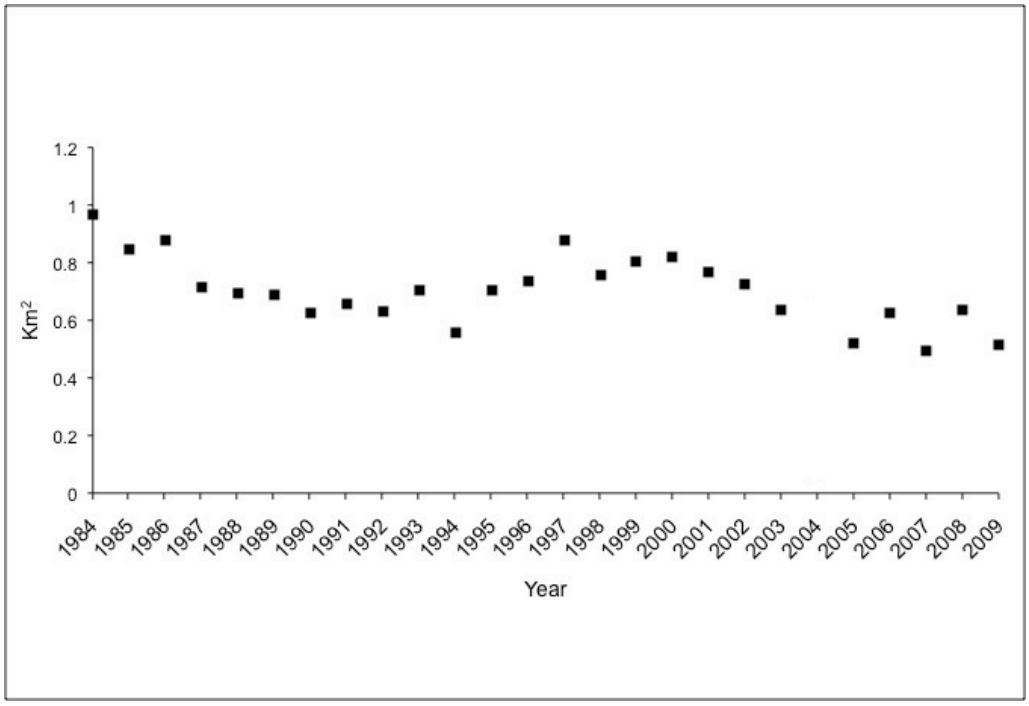

Figure 4.3. Slope-corrected debris-free ice area of the White River Glacier, Mt. Hood for each year 1984-2009.

Snowfields around the base of glaciers vary significantly year to year and because of their similar spectral reflectance to glacial ice they can misrepresent the actual debris-free ice extent (Figures 4.1 to 4.3). Therefore, to get the most accurate representation of debris-free ice it was necessary to compare Landsat scenes of years following accumulation seasons of minimal snowfall. SNOTEL data were analyzed to find the lowest snow year of each decade for glacial change analysis. Peak snow water equivalent, average temperatures and dates of melt-out were looked at for both Mt. Rainier and Mt. Hood. The selected years also show the highest summer temperatures. Based on this assessment, results from the thresholded NDGI images appear to accurately represent debris-free glacier ice rather than remnant snow from the previous winter.

New sensors like IKONOS with sub-meter spatial resolution provide better detail for studying changes on an annual basis and are also useful for detailed mapping of debris-covered glacier tongues through the use of color composite images but they are expensive and don't have the temporal span of the Landsat archive (Hall, 2003). Medley (2008) was able to successfully estimate both snow and ice cover over consecutive-year ASTER imagery to discern permanent features (glaciers) from the data but ASTER imagery is only available after February 2000. For the temporal scale of this study the ability to choose from multiple scenes from both Landsat 5 and Landsat 7 for all years from 1984 to 2009 proved crucial for identifying ideal dates for decadal scale glacier recession analysis.

4.3 Error Analysis

4.31 Debris Flow Locations

For both volcanoes there is an incomplete historic record of debris flows. As Copeland (2009) points out, many debris flows may also be misclassified or misinterpreted as floods. It is very likely that many smaller debris flows on both mountains have gone unnoticed especially due to their initiation at higher, often inaccessible, elevations and the fact that most debris flows occur during adverse weather.

Mt. Rainier has an incomplete record of debris flows from 1926 to 1985 and 1993 to 2001 (Copeland, 2009). There is also some uncertainty for the debris flow

locations found for the November 2006 event on Mt. Rainier, as several sites such as the Van Trump Creek and Kautz Creek initiation areas had several tributaries coalescing into a main channel. It was not certain which tributaries contributed most to mobilization of sediment (Copeland, 2009). Before 1985 only the year and drainage where the debris flow occurred was recorded.

Mt. Hood has a similar incomplete record of precise initiation locations and dates. For the historical debris flow occurrences obtained by T. DeRoo, often only the month of the year and drainage basin are known. The 2006 initiation points obtained from R. Pirot (2010, personal communication) were defined as the point at which there was evidence (scouring, lack of vegetation, boulder levees, rilling, etc.) of debris flow downstream but not upstream. As in the case of Mt. Rainier, several of the initiation sites, what Pirot labeled "headless", were a series of fluvial channels with no clear sign of debris mobilization. Only the initiation sites believed to have started from a slope failure were considered highly accurate in the study.

4.32 Spatial Resolution of Data Sources

The spatial resolution of Landsat bands 4 and 5 seems to ultimately be too coarse to track changes in small alpine glaciers on an annual basis, but at a decadal scale glaciers can be measured with a high degree of confidence (Bishop, 2004). With recent advances in satellite technology such as the French SPOT satellite and IKONOS it is now possible, yet expensive, to overcome the problems of spatial

resolution, but the limited spectral and temporal resolutions pose new problems (Bishop, 2004).

Aerial and remote sensing imagery such as the half-meter orthorectified NAIP photos and the LiDAR data used in this study remain the best choices for glacier change analysis, but again, their limited temporal span and acquisition costs often prohibit their use for long term glacial recession studies such as this one. Slopes were calculated from LiDAR obtained in 2007 and 2008 but over the 25-year span of this study the average slopes of glaciers on Mt. Rainier and Mt. Hood have likely changed as the glaciers have downwasted through melting. Unfortunately, prior DEMs were more coarse with spatial resolutions of 10 m or greater. Thus, to keep the measurements consistent, the average slope values derived from the recent LiDAR surveys were used for slope-corrected areas of all years in question thereby introducing additional error. These errors (average slope change over the years) were considered small compared to the errors that would have been introduced using DEMs with resolutions much coarser than expected natural slope change from downwasting.

Currently a detailed glacier inventory of the Pacific Northwest is being compiled by A. Fountain (Portland State University). The inventory is being created primarily through the use of USGS maps and historical oblique aerial photography (Fountain, 2010). Using NAIP photos to look at recent glacier change is best but the accuracy of USGS 1:24,000 scale maps from the 1950s may be questionable as

seasonal snow was often included as part of the glacier (Fountain, 2010). Oblique aerial photos also suffer from not having the same orthorectification of NAIP photos. Hall (2003) points out that it is not possible to assess uncertainty in glacier change analysis when comparing changes between digitized versions of old topographic maps and data from satellite images. The utility of this study lies in the consistent usage of a single format, the Landsat Thematic Mapper sensor which remains constant over time, to study glacial change over long times

4.33 Incomplete Climate/Snow Data for Highest Elevations

With the SNOTEL locations at just over 1500 m, the climate and snow observations recorded by the sensors are not representative of the climate as a whole for the mountain. With storm tracks hitting the mountains from the southwest, different aspects of the mountain may receive more rain than others. As air masses hit the western sides of the Cascade volcanic chain, adiabatic cooling results in increased precipitation at higher altitudes. This is due to moisture being cooled past its condensation point as clouds pass over the high elevation volcanic range. This also results in a "rain shadow" effect on the eastern side of the range as the clouds and air masses warm as they descend the mountain, having released most of their moisture content on the western side of the range.

The tall Cascade volcanos also have a large range of temperatures from their lower reaches to their summits. The temperature lapse rate of temperature change

with elevation is estimated at about 0.5 to 1°C per 100 m. Therefore, what may be falling as rain on the SNOTEL sensor may be falling as snow higher on the mountain. For example, the average daily temperature for the Mt. Hood SNOTEL test site for 1992 to 2005 was 3.8°C but with adiabatic cooling this could represent an average daily temperature of -16°C at the summit. With occurrences of temperature inversions in the Northwest and highly variable precipitation patterns, a complete analysis of the climate variability around Mt. Hood is difficult.

For future studies it may be advantageous to also look at the Northwest Avalanche Center rain gauges at both Timberline and Mount Hood Meadows ski areas which are at slightly higher elevations than the SNOTEL site. For higher elevations the use of technologies such as NEXRAD (Next Generation Radar) may provide rough estimates of precipitation at higher elevations (Pirot, 2010). For example, the NEXRAD data for the November 2006 rain event on Mt. Hood showed that there were variable intensities of rain on different aspects and at varying elevations (Pirot, 2010).

4.34 Threshold Value Choice

The threshold value choice may be the most important decision in satellite remote sensing of glacial ice. Studies often pick this value without properly documenting why a particular value was chosen. Here, an effort was made to compare various threshold values for two different glaciers on opposite aspects of Mt.

Hood, with both showing the 0.05 threshold value to be most accurate (within 1%). By using the 0.5 m 2005 NAIP photos with the 2005 Landsat scene, both following a low snow accumulation season, the probability of misclassifying snow as glacial ice was minimized. However, this value may not be as accurate for glaciers of different dimensions or glaciers with abnormally high numbers of snowfields surrounding them such as the nearby Zigzag glacier. This value is also not applicable to other parts of the world where cast shadows and other solar lighting effects may have different effects on the reflectivity of ice and snow in bands 4 and 5.

For this study the distance separating Mt. Hood and Mt. Rainier is not far enough to have a significant impact on the threshold value chosen between the two mountains. It should be noted that the date of 26 Aug 1992 is almost a full month before the 1987 and 2005 dates chosen for analysis but the lighting differences between that time and late September are not enough to warrant choosing another threshold value for that year.

4.35 Debris covered Glacier Tongues

The delineation of debris-covered glaciers is the crux of automated satellite data assessment of glacier change. Multispectral data analysis has not proven accurate enough to discern debris-covered ice from ice-free moraines (Nakawo, 1992; Williams, 1997) although attempts at using multispectral classifications with DEM derivatives, neighborhood analysis, and multiple band ratio combinations have been

attempted (Paul, 2004; Bolch, 2006; Keshri, 2009). In the case of mapping complete glacial extent, traditional methods such as ground surveys and aerial photographs remain best. This is especially important in this study since changes in debris-free ice area may not correlate with changes in debris accumulation or recession of the terminus of the glacier.

Debris-covered glaciers behave differently as it is believed the debris on top of them insulates them from solar radiation and precipitation. This may account for why several of the highly debris-covered glaciers on Mt. Rainier, such as the Emmons, Winthrop, and Cowlitz glaciers, experience slower terminus retreat rates (Nylen, 2004). In a study of the Eliot Glacier, of which 41.6% is covered by debris, Lundstrom (1992) found that glaciers with a higher average amount of supraglacial debris may extend to lower elevations and have lower rates of recession than glaciers with little debris cover. However, it was found that in just 18 years the terminus of the debris-covered Eliot Glacier receded 284 m (Lundstrom, 1992) and since 1901 it had the second fastest terminus retreat rate on the mountain (Lillquist, 2006). It was also discovered that, hydrologically, the debris-covered Eliot is equivalent to a clean glacier that is just 79% of its size (Phillippe, 2008). Therefore, to have a complete understanding of the complexity of glacial retreat in the Pacific Northwest the change in area of debris-covered glacial ice must also be accounted for.

4.4 Remote Sensing as a tool for looking at glacier change

Remote sensing is a valuable tool for assessing glacial change but it should not be the only one used for detailed studies. Satellite images can provide the basis for which study areas to focus on but they should not replace traditional methods such as ground surveys, rock glacier coring, and mass balance calculations, which are all essential for understanding the dynamic nature of glaciers. Generally, glacier length and area changes alone under-represent the magnitude of glacier ablation, because morphometric thinning (mass wasting) is also important and can't be seen directly from satellite measurements (Kargel, 2005). Detailed ground-based surveys in the Alps have revealed that many of the glaciers seem to be transitioning from active retreat up the mountain to downwasting, which was not previously seen in remote sensing studies of the region (Paul, 2005). In the Pacific Northwest Lillquist (2006) also notes that significant downwasting of extensively debris-covered glaciers such as the Eliot often obscures the extent of glacier tongues, which become identifiable only by drilling into ice-cored moraines.

However, much progress has been made towards automated methods of glacier recession analysis (Raup, 2007). The advantage of using satellite imagery to assess glacier change is that sensor capabilities remain static throughout time. This provides a consistency (relative accuracy) that is not achievable through traditional methods of glacier change analysis, which introduce human error such as inaccurately digitizing outlines from aerial photographs or misinterpreting historical maps.

Ultimately, the automated use of algorithms, band ratios, filters, and classification techniques using satellite data alone will not provide high-quality results without the tandem use of traditional methods such as ground surveys and mass balance measurements, especially in the case of rock glaciers, permafrost studies and debris-covered glacial tongues.

Chapter 5: Conclusions

5.1 Applicability of Landsat and Methods for Other Regions of the World

Just as the introduction of Google Earth allowed people to search the world spatially as never before, Landsat now allows people to do the same temporally. With a free archive spanning over 30 years, Landsat data provide an invaluable resource for assessing long-term glacier change and related hazards on a global scale. The methods used in this research along with similar methods using ASTER data have been verified and well documented in other studies throughout the world (Hall, 1987; Dozier, 1989; Paul, 2004; Andreassen, 2008; Silverio, 2005; Paul, 2000; Hall 2003; Kääb, 2003; Khalsa, 2004; Keshri, 2009; Bolch, 2008).

The choice of method used must be determined from the geomorphology and climate of the study area. For this study in the Pacific Northwest during the fall, the best method was the use of the Landsat TM band 4/5 ratio but as Bishop (2004) points out this method may not be best for consistently cloudier locations in the world such as the Peruvian Andes. For locations such as these the ratio does not work as

well as a Normalized Difference Snow Index (Silverio, 2005). Bishop (2004) also notes that at high latitudes with lower sun elevations, glaciers in the late fall cast large shadows and may benefit from an analysis using a TM band 3/5 combination. Still other studies have found that the best method is a combination of band ratios building upon one another to fine tune glacial ice delineation (Keshri, 2009). Creating an animated sequence of sequential years using false color composites from Landsat or higher resolution satellites such as SPOT or ASTER has also proven to be useful (Paul, 2007; Racoviteanu, 2008).

Ultimately, the most successful strategy for assessing glacial change and glacial hazards worldwide is combining remotely sensed data with the tools available for spatial analysis within Geographic Information Systems (GIS) such as this study has done. This study had the advantage of using highly accurate LiDAR data for both mountains. For studies where LiDAR data are unavailable or local DEMs are too coarse or nonexistent, detailed geophysical field surveys must be undertaken (Huggel, 2004).

Utilizing satellite data to assess glacial change is especially useful in parts of the world that are largely inaccessible. Glacier inventories in war torn countries such as Afghanistan are often limited due to the dangers of accessing study areas, but automated methods of glacier change analysis such as the ones used in this study may serve to fill the gaps in the records (Haritashya, 2009). In the coming decades, the focus should be on the often inaccessible arid regions of the world that depend on

glaciated mountains for freshwater such as Western China, Uzbekistan, Afghanistan, Kyrgyzstan and Pakistan (Kargel, 2005). The ice mass in the Hindu-Kush region is the third-largest on earth and current meltwater from the glaciers provides 70% of the summer flow in the Ganges and 50-60% of the flow in the other major rivers that feed the region (Barnett, 2005). Understanding the rate of glacier recession in these parts of the world is essential as it will determine their economic and political futures. With the world's population expected to increase by about 3 billion people by 2050 and all Global Climate Models pointing to higher temperatures, future wars in these areas may be fought over water instead of religious beliefs or fossil fuel (Watson, 2004; Kargel, 2005).

5.2 Implications for Natural Hazards in the Pacific Northwest

Although eruption events such as the one that occurred on Mt. St. Helens in 1980 are very unlikely in the Pacific Northwest, most cascade volcanoes are still active and thus are subject to natural hazards such as ice and snow avalanches, landslides, and what are considered by most scientists to be the most damaging recently, debris flows. It is important to have a detailed understanding of the physical processes that occur on volcanoes in the Pacific Northwest and how those processes may be changing with changing climate. In the Swiss Alps, a series of observation stations have been created to gather real-time data on the physical processes involved in debris flow creation (Hurlimann, 2003). There is enough data on debris flow locations on Mt. Rainier and Mt. Hood to establish similar stations

near glaciers that are historically known to regularly produce debris flows such as the South Tahoma on Mt. Rainier and the White River on Mt. Hood.

With the most recent regional climate models pointing to annual temperature increases of, on average, 3°C by the 2080s with little precipitation change, the Pacific Northwest will experience higher rates of glacier recession and thereby greater risks of potential natural hazards (Mote, 2010). Downwasting is already apparent on most of the glaciers in both Mt. Rainier and Mt. Hood. This is particularly for glaciers at lower elevations such as the Williwakas, Sarvent, Pyramid, Flett and Ohanapecosh on Mt. Rainier (Figure 3.18). The growing rock outcrops on these glaciers have a lower albedo (solar reflectance) which allow them to heat up during hot summer days and emit heat at night. This process creates gaps between the rocks and ice that grow through turbulent heat fluxes (Paul, 2005, 2007). As more surface area is exposed through cracks more of the remaining ice melts further fragmenting the glacier. It was fragmented glaciers such as these that produced new debris flows on the south side of Mt. Rainier during the 2006 storm event.

With temperatures increasing and more precipitation expected to fall as rain in the Pacific Northwest there may be a lowering of the glacial albedo with age as rockfall and dust accumulate on the glacial ice (Paul, 2007). This has been documented in the Alps were visual analysis of dark firn bands show they are darkening every year with more precipitation falling as rain rather than snow at high elevations (Paul, 2007). With less fresh white snow falling to reflect incoming solar

radiation and earlier spring melt-out dates, downwasting in the future will be rapidly enhanced. Furthermore, with the typical response time of alpine glaciers to climate change taking 10-20 years, the consequences of warmer annual temperatures on glacial coverage in the Pacific Northwest is yet to come (Paul, 2004).

The predicted warmer temperatures and longer ablation seasons could also potentially lead to more frequent debris flows in the Pacific Northwest. In a historical study of the Swiss Alps dating back to 1570 it was found that during long periods of warm weather debris flow activity was enhanced (Stoffel, 2006). Indeed, in 2001 a debris flow was witnessed by CVO scientists on a flyover of Mt. Rainier after a long period of hot, dry weather had settled upon the mountain. With seismographs failing to record any activity prior to the debris flow initiation, the mechanism of initiation was speculated to be an outburst flood resulting from rapid glacial melt during the hot weather (Vallance, 2002).

Although the possibility of damaging debris flows occurring more frequently in the future is worrisome, a far more threatening concern may be the disappearance of meltwater from glaciers. The Hood River Valley is one of the top producing fruit regions of Oregon. Its dark, nutrient rich volcanic soils are highly productive and summer melt from the glaciers on Mt. Hood provide water for irrigating crops (Phillippe, 2008; Scott, 2003; Figure 5.1). During the very dry summer months in the Northwest, Hood River receives as much as 75% of its streamflow as meltwater from the glaciers on Mt. Hood (Phillippe, 2008; Figure 5.2). Late summer stream flow in

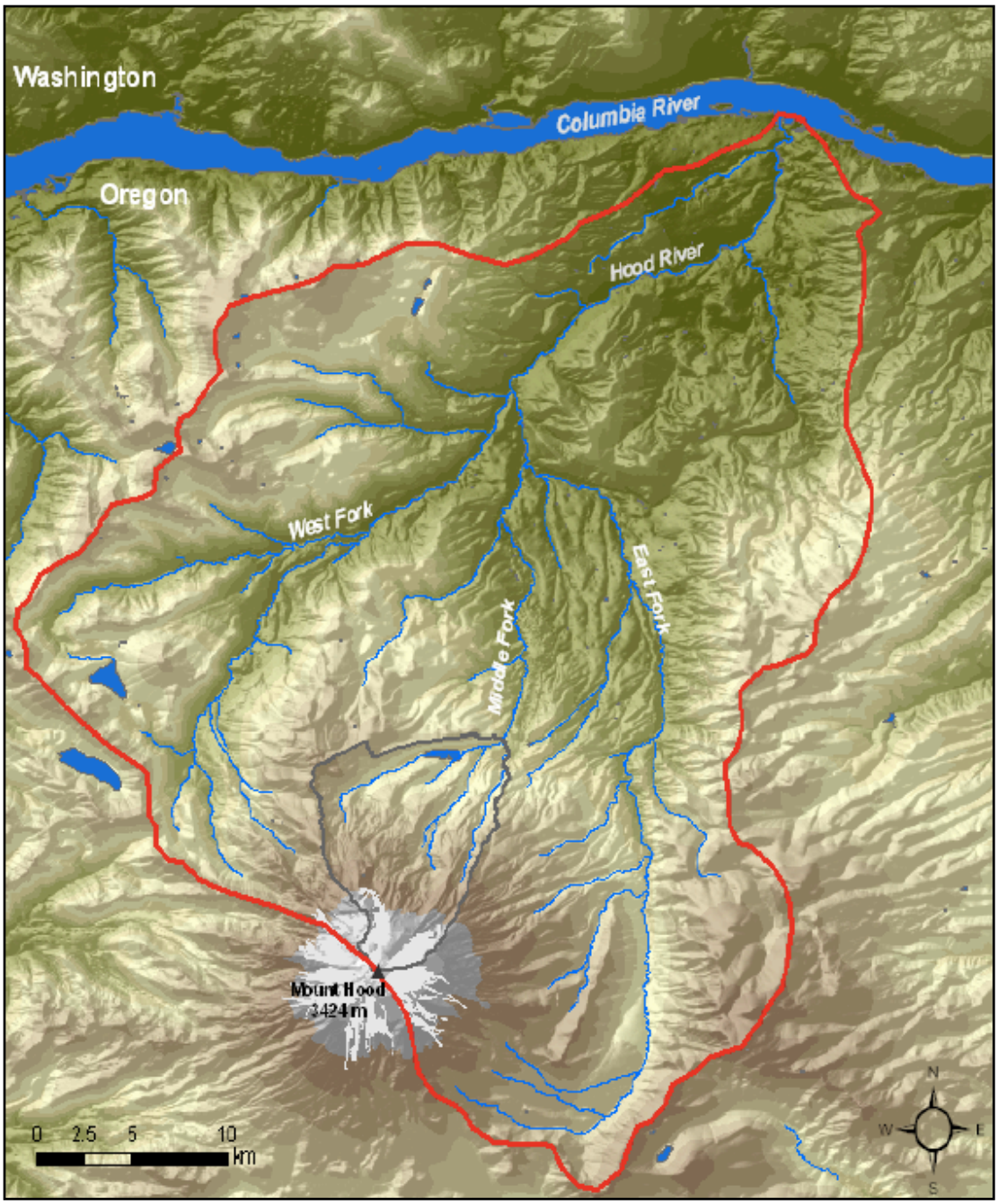

Figure 5.1. The Hood River Basin that depends on meltwater from Mt. Hood glaciers for irrigation. Figure Courtesy Jeff Phillippe (2008).

the North Cascades, an area dependent on hydropower for electricity, is predicted to

decrease by over 30% over the next century due to ice loss (Chennault, 2004; Granshaw, 2006). With glacier retreat occurring at about 5% each decade the security of future water supply for agriculture is in question (Figure 5.3). Mote (2003) found that SWE has been substantially declining with the biggest decreases at lower

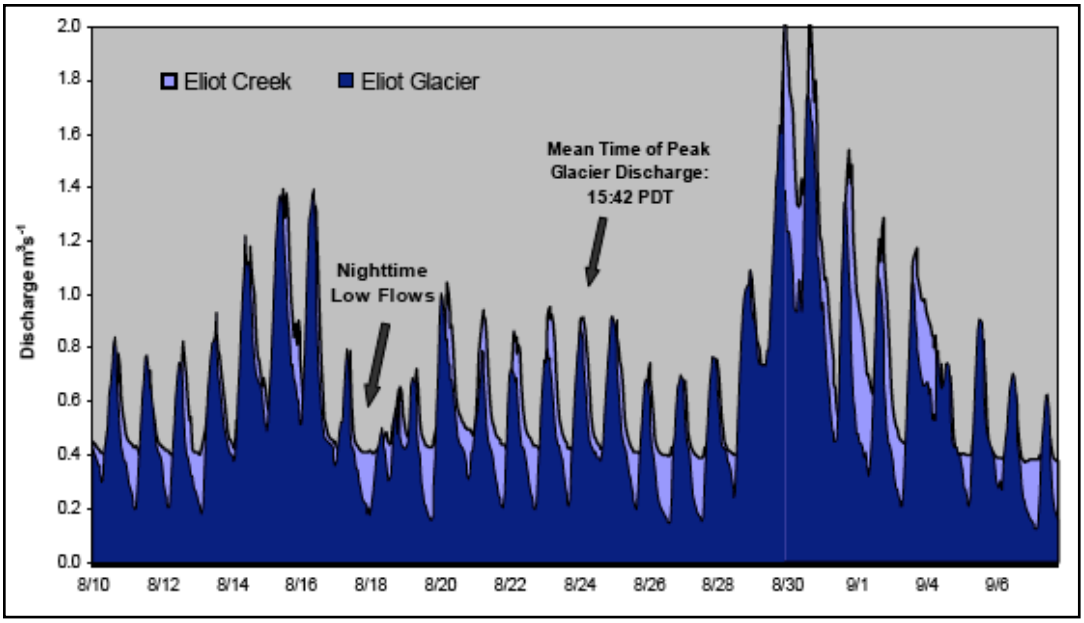

Figure 5.2. Glacier (dark blue) and total runoff (light blue) of Eliot Creek on Mt. Hood showing how dependent stream flow is on glacier meltwater. Taken from Phillippe (2008).

elevations. Thus, glaciers at lower altitudes will be most affected most by warmer temperatures rather than those that exist only at the highest elevations. This decline in SWE is expected to be greatest at elevations below about 1800 m (Mote, 2003). This projection corresponds with the very high debris-free ice area recession of the Williwakas, Sarvant, Van Trump Flett, and Pyramid which all reach down to the 2000-m level on Mt. Rainier.

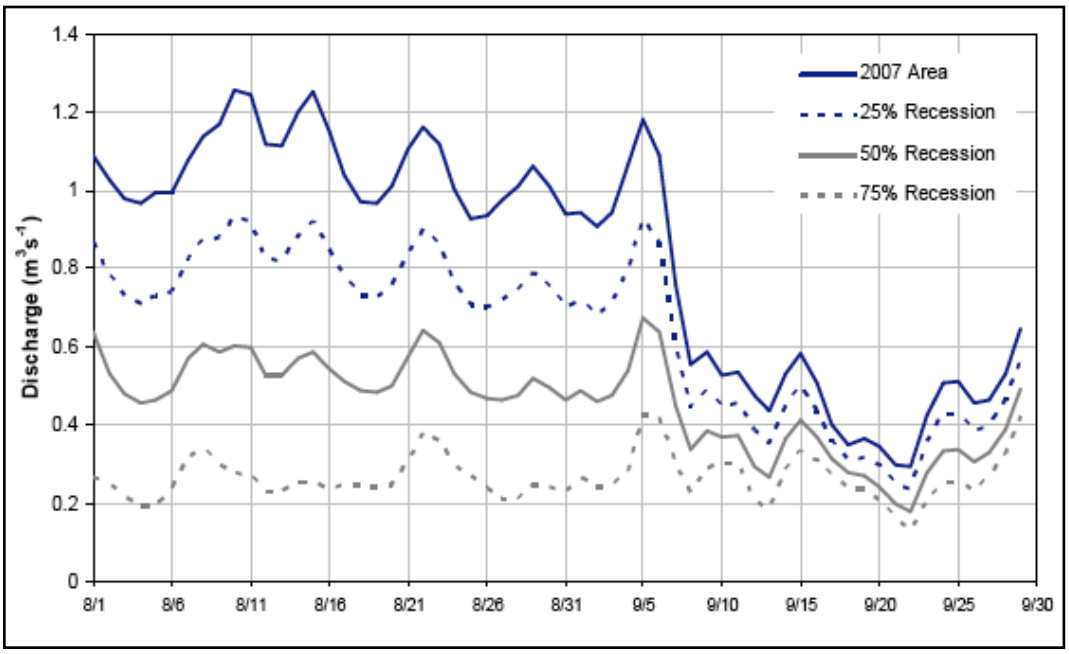

Figure 5.3. Stream flow sensitivity to simulated glacier recession of the Eliot Glacier on the Hood River Basin. Courtesy Phillippe (2008).

5.3 Potential for Identifying Locations of Possible Future Periglacial Debris Flows

The potential for identifying areas at risk for future periglacial debris flows depends on a thorough understanding of climate interactions in the Pacific Northwest, debris supply rates from glacial recession, and transport capacity of glacial drainage streams which can be greatly enhanced by contributions of glacial meltwater and intense rain events. This study has shown that drainages that generate debris flows on both Mt. Rainier and Mt. Hood are directly linked to the glaciers that feed them and although glacier recession is involved in debris flow generation it is not the sole determinant.

Results from this study also show that small, fragmented glaciers at lower elevations have undergone the fastest rates of recession and may be at higher risk for periglacial debris flows. Stream channels below glaciers should also be monitored for incision into potentially unstable moraines left by glacial recession. With sub-meter satellite imagery available today, it may be possible to monitor stream channel geomorphology beneath receding glaciers at regular intervals without the need for labor-intensive field studies.

Climate data such as precipitation and temperature trends must continue to be monitored in the Pacific Northwest, especially during landfall events of moisture-rich Atmospheric Rivers. Parker (2009) found that debris-flow producing storms in the Pacific Northwest were characterized by heavy rain and above average high tropospheric free air freezing altitudes. Other studies have shown that there may be a rainfall rate threshold associated with the initiation of debris flows (Bacchini, 2003; Steijn, 1996; Rebetez, 1997). Advanced stationary orbital weather satellites over the northern hemisphere such as the Advanced Very High Resolution Radiometer (AVHRR) administered by NOAA are now capable of accurately tracking Atmospheric Rivers days before they make landfall (NOAA). This technology may aid in the prediction of possible debris flow generating storms in the future.

The periglacial debris flows generated from the November 2006 storm destroyed popular hiking networks throughout the Pacific Northwest, forcing several large sections of the famous Pacific Crest trail to be re-routed. Multiple bridges were

torn from their foundations and major highways were ripped apart (Figure 5.4). Better knowledge of which glacial drainages have the potential to produce debris flows will allow planners to build roadways and other infrastructure in safe areas rather than go through the costly processes of rebuilding after each debris flow (Figure 5.5).

Figure 5.4 Highway 35 damage on the east side of Mt. Hood from the Newton Creek debris flow and flood after the November 2006 storm event.

The combination of GIS and remote sensing serves as an effective tool for mitigating potential periglacial debris flow hazards by integrating spatial and temporal information together into monitoring projects. One such project is the GIS-based model "LAHARZ" which is able to plot inundation limits of debris flows based

on knowledge of historical debris flow paths (Iverson, 1998). Historical debris flow records for such monitoring programs have been found through dendrogeomorphological tree-ring analysis in such places as the Swiss Alps (Stoffel, 2005; Gartner, 2003). Current satellite data can also be integrated into GIS to continually monitor potential glacial hazard features. Remote sensing technologies such as the combination of ASTER imagery along with NASA's Airborne Visible/ Infrared Imaging Spectrometer have been used to assess hydrothermally altered rocks

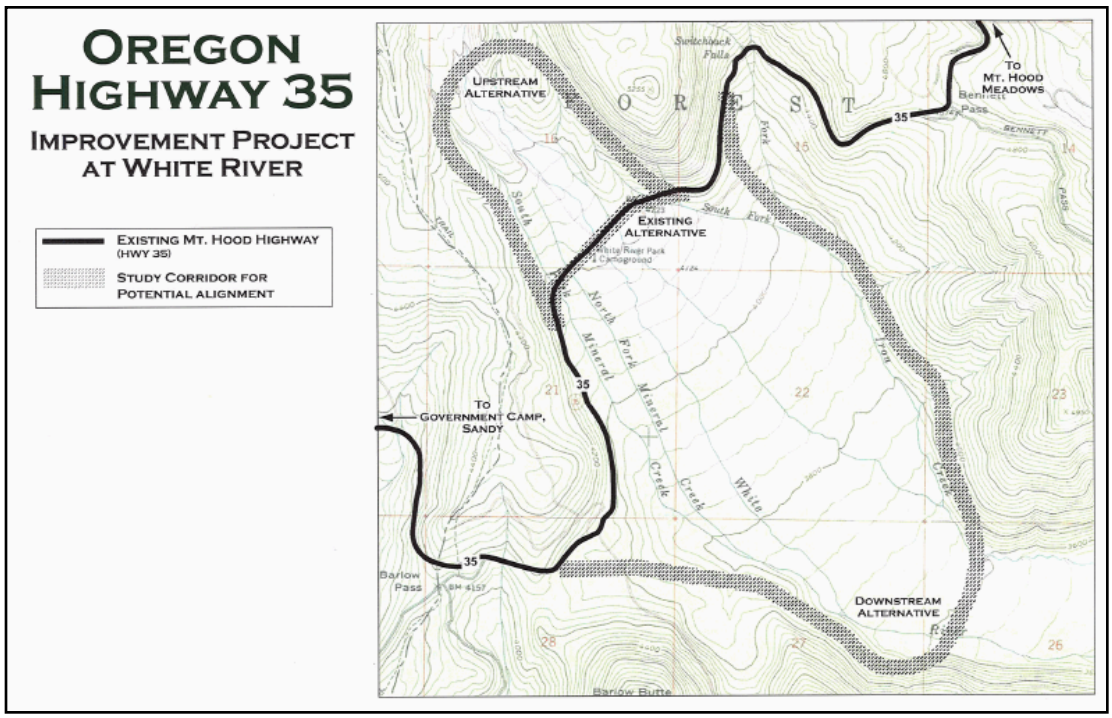

Figure 5.5. Proposed re-routing of Highway 35 based off historical debris flow channels and hazard mapping. Courtesy ODOT.

in relation to possible debris flow sites on Mt. Shasta, California (Crowley, 2003). Another glacial hazard that should be monitored in the Cascade Range and elsewhere like the Himalaya is the growth of proglacial lakes at the base of receding glaciers.

One such lake in this study, the pool below the western fragment of the Winthrop Glacier was found to be the source of a debris flow from the November 2006 storm event (Copeland, 2009). With monitoring projects like these planners can predict where glacial hazards may occur and can avoid the costly task of having to re-route existing infrastructure (Figure 5.5).

With remote sensing technologies continuously advancing, and satellite data archives such as the Landsat program becoming more readily available to the public, the future potential for assessing glacier change and related hazards looks strong.

BIBLIOGRAPHY

6SV1 - Second Simulation of a Satellite Signal in the Solar Spectrum Vector Code 1. 2010. [online] (Updated 25 Jun 2010) http://6S.ltdri.org/ (Accessed 25 June 2010).

Albert, T.H. 2002. Evaluation of remote sensing techniques for ice-area classification applied to tropical Quelccaya ice cap, Peru. Polar Geography, 26: 210-226.

Andreassen, L.M., Paul, F., Kääb, A., and Hansberg, J.E. 2008. Landsat-derived glacier inventory for Jotunheimen, Norway, and deduced glacier changes since the 1930's. The Cryosphere, 2: 131-145.

Armstrong, A., Browning, M.C., Veneroso, M.A., and Lofgren, D.C. Hydrologic and Geomorphic Assessment of Debris Flow Events for Mount Hood Highway Federal Highway Administration [online] (Updated 21 Jan 2010) Available at: http://www.fhwa.dot.gov/engineering/hydraulics/pubs/mthod/mthood.cfm (Accessed 25 Jun 2010).

Bacchini, M. and A. Zannoni, 2003. Relations between rainfall and triggering of debris flow: case study of cancia (Dolomites, Northeastern Italy). Natural Hazards and Earth System Sciences, 3: 71-79.

Barnett, T.P., Adam, J.C., and Lettenmaier, D.P. 2005. Potential impacts of a warming climate on water availability in snow-dominated regions. Nature, 438: 303-309.

Bayr, K.J., Hall, D.K., and Kovalick, W.M. 1994. Observations on glaciers in the eastern Austrian Alps using Satellite data. International Journal of Remote Sensing, 15(9): 1733-1742.

Beniston, M. 2003. Climate Change in Mountain Regions: A Review of Possible Impacts. Climate Change, 59: 5-31.

Berlepsch, H. U., 1861. Die Alpen in Natur - und Lebensbildern. Leipzig: Hermann Constenoble, 511 p.

Berthier, E., Arnaud, Y., Baratoux, D., Vincent, C., and Remy, F. 2004. Recent rapid thinning of the "Mer de Glace" glacier derived from satellite optical images. Geophysical Research Letters, 31: 1-4.

Bishop, M.P., Oslenholler, J.A., Shroder, J.F., Barry, R.G., Raup, B.H., Bush, A.B.G., Copland, L., Dwyer, J.L., Fountain., A.G., Haeberli, W., Kääb, A., Paul, F., Hall, D.K., Kargel, J.S., Molnia, B.F., Trabant, D.C., and Wessels, R. 2004. Global Land Ice Measurements from Space (GLIMS): Remote Sensing and GIS Investigations of the Earth's Cryosphere. Geocarto International, 19(2): 57-84.

Bolch, T., and Kamp, U. 2006. Glacier Mapping in High Mountains Using DEM's, Landsat and ASTER Data. Grazer Schriften der Geographie und Raumforschung, 41: 37-48.

Bolch, T. 2007. Climate change and glacier retreat in northern Tien Shan (Kazakhstan/Kyrgyzstan) using remote sensing data. Global and Planetary Change, 56: 1-12.

Burbank, D.W. 1981. A Chronology of Late Holocene Glacier Fluctuations on Mount Rainier, Washington. Arctic and Alpine Research, 13(4):369:386.

Cameron, K.A., and Pringle, P.T. A detailed chronology of the most recent major eruptive period at Mount Hood, Oregon. Geological Society of America Bulletin, 99 (6): 845-851.

Cascades Volcano Observatory (CVO) 2010. *Mt. Rainier, Washington* and *Mt. Hood, Oregon* [online] (Updated 25 Mar 2010) Available at: http://vulcan.wr.usgs.gov/Volcanoes/Rainier/framework.html and http://vulcan.wr.usgs.gov/Volcanoes/Hood/framework.html[Accessed 10 June 2010].

Chairle, M., Iannotti, S., Mortara, G., and Deline, P. 2007. Recent debris flow occurrences associated with glaciers in the Alps. Global and Planetary Change, 56: 123-136.

Chennault, J.W. 2004. Modeling the contributions of glacial meltwater to streamflow in Thunder Creek, North Cascades National Park, Washington. M.S. Thesis, Western Washington University, 78 p.

Chen, J., and Ohmura, A. 1990. Estimation of Alpine glacier water resources and their change since the 1870's. Hydrology in Mountain Regions. I - Hydrological Measurements; the Water Cycle (Proceedings of two Lausanne Symposia, August, 1990). IAHS Publication No. 193.

Christensen, J.H., B. Hewitson, A. Busuioc, A. Chen, X. Gao, I. Held, R. Jones, R.K. Kolli, W.-T. Kwon, R. Laprise, V. Magaña Rueda, L. Mearns, C.G. Menéndez, J.

Räisänen, A. Rinke, A. Sarr and P. Whetton, 2007: Regional Climate Projections. In: Climate Change 2007: The Physical Science Basis. Contribution of Working Group I to the Fourth Assessment Report of the Intergovernmental Panel on Climate Change [Solomon, S., D. Qin, M. Manning, Z. Chen, M. Marquis, K.B. Averyt, M. Tignor and H.L. Miller (eds.)]. Cambridge University Press, Cambridge, United Kingdom and New York, NY, USA.

Copeland, E.A. 2009. Recent Periglacial Debris Flows from Mount Rainier, Washington. M.S. Thesis, Oregon State University, 125 p.

Coudrain, A., Francou, B., and Kundzewicz, Z.W. 2005. Glacier shrinkage in the Andes and consequences for water resources. Hydrological Sciences, 50(6): 925-932.

Crandall, D.R. 1969. Geologic Story of Mt. Rainier Geological Survey Bulletin, 1292, 43 p.

Crandall, D.R. 1971. Postglacial Lahars from Mount Rainier Volcano, Washington. USGS Professional Paper 677.

Crandall, D.R. 1980. Recent eruptive history of Mount Hood, Oregon, and potential hazards from future eruptions. US Geological Survey Bulletin, 1492.

Daly, C., Taylor, G., and Gibson, W. 1997. The PRISM approach to mapping precipitation and temperature. 10th conference on Applied Climatology, Reno, Nevada. Boston, MA, American Meteorological Society. 208-209.

Deroo, T.G. 2010. Personal Communication. Mount Hood National Forest Headquarters, 16400 Champion Way, Sandy, OR 97055.

Dozier, J. (1984). "Snow reflectance from Landsat 4 thematic mapper." IEEE Transactions on Geoscience and Remote Sensing, 22: 323-328.

Driedger, C.L. 1986. A Visitors Guide to Mount Rainier Glaciers. Pacific Northwest Parks and Forest Association, 80 p.

Driedger, C.L., and Kennard, P.M. 1984. Ice Volumes on Cascade Volcanoes: Mount Rainier, Mount Hood, Three Sisters, and Mount Shasta. USGS Professional Paper 1365.

Driedger, C.L. 1993. Glaciers on Mount Rainier. USGS Open-File Report, 92-474.

Dyurgerov, M.B., and Meier, M. 2000. Twentieth century climate change: Evidence from small glaciers. PNAS, 97(4): 1406-1411.

Fagre, DB. 1997 Watershed Responses to climate change at Glacier National Park. Journal of American Water Resources Association, 33:755-765.

Farm Service Agency (FSA). The National Agriculture Imagery Program (NAIP). 2010. [online] (Updated 10 Mar 2010) Available at: http://www.fsa.usda.gov/FSA/apfoapp?area=home&subject=prog&topic=nai (Accessed 25 June 2010).

Fischer, L., Kääb, A., Huggel, C., and Noetzli, J. 2006. Geology, glacier retreat and permafrost degradation as controlling factors of slope instabilities in high-mountain rock wall: the Monte Rosa east face. Natural Hazards and Earth System Sciences, 6: 761-772.

Fountain, A. Glacier Research at Portland University. Professor Andrew Fountain & Kristina Thorneycroft. 2010. [online] (Updated 14 June 2010). Available at: http://www.glaciers.pdx.edu/ (Accessed 25 June 2010).

Fountain, A.G., and Walder, J.S. 1998. Water flow through temperate glaciers. Reviews of Geophysics, 36(3): 299-328

Gartner, H., Stoffel, I., Lievre, D., Grichting, M., and Monbaron, M. 2003. Debris-flow frequency derived from tree-ring analyses and geomorphic mapping, Valais, Switzerland. Debris Flow Hazards Mitigation: Mechanics, Prediction, and Assessment, 1: 207-217.

Gallino, G.L., and Pierson, T.C. 1985. Polallie Creek Debris Flow and Subsequent Dam Break Flood of 1980, East Fork Hood River Basin, Oregon. USGS Water Supply Paper 2273, 22 p.

Giles, P.T., 2001. Remote Sensing and Cast Shadows in Mountainous Terrain. Photogrammetric Engineering & Remote Sensing, 67(7): 833-839.

Granshaw, F.D., and Fountain, A.G., 2006. Glacier Change (1958-1998) in the North Cascades National Park Complex. Washington, USA. Journal of Glaciology, 52 (177): 251-256.

Hall, D.K., J.P. Ormsby, R.A. Bindschadler, and H. Siddaligaiah. 1987. Characterization of Snow and Ice Reflectance Zones On Glaciers Using Landsat Thematic Mapper Data. Annals of Glaciology, 9:1-5.

Hall, M., and Fagre, D.B. 2003. Modeled Climate-Induced Glacier Change in Glacier National Park, 1850-2100. Bioscience, 53(2): 131-140.

Hague, A. 1871. Mount Hood. In King, C. (ed.), On the discovery of actual glaciers on the mountains of the Pacific Slope. American Journal of Science, (3rd Series), 1: 165-167.

Haeberli, W., and Beniston, M. 1998. Climate Change and its impacts on glaciers and permafrost in the Alps. Ambio, 27(4) 258-265.

Haeberli, W., Rickenmann, D., and Zimmermann, M. 1990. Investigation of 1987 debris flows in the Swiss Alps: general concept and geophysical soundings. Hydrology in Mountain Regions. II - Artificial Reservoirs; Water and Slopes (Proceedings of two Lausanne Symposia, August, 1990). IAHS Publication, No. 194.

Hall, D., Bayr, K., Schoner, W., Bindschadler, R.A., and Chien, J.Y.L. 2003. Consideration of the errors inherent in mapping historical glacier positions in Austria from the ground and space (1893-2001). Remote Sensing of the Environment, 86: 566-577.

Hamlet, A.F., Mote, P.W., Clark, M.P., and Lettenmaier, D.P. 2005. Effects of Temperature and Precipitation Variability on Snowpack Trends in the Western United States. Journal of Climate, 18: 4545-4561.

Haritashya, U.K., Bishop, M.P., Shroder, J.F., Bush, A.B.G., and Bulley, H. N.N. 2009. Space-based assessment of glacier fluctuations in the Wakhan Pamir, Afghanistan. Climate Change, 94: 5-18.

Huggel, C., Haeberli, W., Kääb, A., Bieri, D., and Richardson, S. 2004. An assessment procedure for glacial hazards in the Swiss Alps. Canadian Geotechnical Journal, 41: 1068-1083.

IPCC (Intergovernmental Panel on Climate Change): A report of Working Group 1. 2007. [online] (Updated 20 Mar 2010) Available at: http://www.ipcc.ch/ipccreports/assessments-reports.htm (Accessed 3 Dec 2008).

Iverson, R. 2000. Landslide triggering by rain infiltration. Water Resources Research, 36(7): 1897-1910.

Jackson, K.M., and Fountain, A.G. 2007. Spatial and morphological change on Eliot Glacier, Mount Hood, Oregon, USA. Annals of Glaciology, 46: 222-226.

Jensen, J.R. 2000. Remote Sensing of the Environment: An Earth Resource Perspective. Prentice Hall. Upper Saddle River, NJ. 544 p.

Jomelli, V., Brunstein, D., Grancher, D., and Pech, P. 2007. Is the response of hill slope debris flows to recent climate change univocal? A case study in the Massif des Ecrins (French Alps). Climate Change, 85: 119-137.

Johnson, A. 1954. Observations on the Nisqually Glacier and other Glaciers in the Northwestern United States. International Union of Geodesy and Geophysics 39:511-516.

Johnson, S.L., and Jones, J.A. 2000. Stream temperature responses to forest harvest and debris flows in western Cascades, Oregon. Canadian Journal of Fish and Aquatic Sciences, 57(Suppl. 2): 30-39.

Jorsberger, E.G., Bidlake, W.R., March, R.S. and Kennedy, B.W. 2007. Glacier mass-balance fluctuations int he Pacific Northwest and Alaska, USA. Annals of Glaciology, 46: 291-296.

Kääb, A., Paul, F., Maisch, M., Hoelzle, M., and Haeberli, W. 2002. The new remote sensing derived Swiss glacier inventory: II. Final Results. Annals of Glaciology, 34: 362-366.

Kääb, A., Wessels, R., Haeberli, W., Huggel, C., Kargel, J., and Khalsa, S.J. 2003. Rapid ASTER Imaging Facilitates Timely Assessment of Glacier Hazards and Disasters, EOS 84:13: 117-124.

Kargel, J.S., Abrams, M.J., Bishop, M.P., Bush, A., Hamilton, G., Jiskoot, H., Kääb, A., Kieffer, H.H., Lee, E.M., Paul, F., Rau, F., Raup, B., Shroder, J.F., Soltesz, D., Stainforth, D. Stearns, L., and Wessels, R. 2005. Multispectral imaging contributions to global land ice measurements from space. Remote Sensing of the Environment, 99: 187-219.

Kennard, P. 2010. USGS (glacial outlines obtained through Beth Copeland)

Keshri, A.K., Shukla, A., and Gupta, R.P. ASTER ratio indices for supraglacial terrain mapping. International Journal of Remote Sensing, 30(2): 519:524

Khalsa, S.J.S., Dyurgerov, M.B., Khromova, T., Raup, B.H., and Barry, R.G., 2004. Space-based mapping of glacier changes using ASTER and GIS tools. IEEE Trans Geosci Rem Sens, 42(10): 2177-2183.

Knowles, N., Dettinger, M.D., and Cayan, D.R. 2006. Trends in Snowfall versus Rainfall in the Western United States. Journal of Climate, 19: 4545-4559.

Lambrecht, A., and Kuhn, M. 2007. Glacier changes in the Austrian Alps during the last three decades derived from the new Austrian glacier inventory. Annals of Glaciology, 46: 177-184.

The Landsat Program. 2008. NASA. [online] (Updated 25 June 2010) Available at: http://landsat.gsfc.nasa.gov/ (Accessed 25 June 2010).

Latif, M., and Barnett, T.P. 1994 Causes of decadal climate variability over the North Pacific. Science, 266(5): 634-637.

Lillquist, K., and Walker, K. 2006. Historical Glacier and Climate Fluctuations at Mount Hood, Oregon. Arctic, Antarctic, and Alpine Research, 38(3): 399-412.

Lundstrom, S.C, 1992. The budget and effect of superglacial debris on Eliot Glacier, Mount Hood, Oregon. Thesis for Doctor of Philosophy. University of Colorado. 183p.

Mantua, N.J., and Hare, S.R. 2002. The Pacific Decadal Oscillation. Journal of Oceanography, 58: 35-44.

McCabe, G.J., Clark, M.P., and Hay, L.E. 2007. Rain-on-snow events in the western United States. Bulletin of the American Meteorological Society, 88(3) 319-328.

Medley, B. 2008. A method for remotely monitoring glaciers with regional application to the Pacific Northwest. M.S. Thesis. Oregon State University 73 p.

Mennis, J.L. and Fountain, A.G. 2001. A spatio-temporal GIS database for monitoring Alpine glacier change. Photogrammetric Engineering and Remote Sensing, 67(8): 967-975.

Mote, P.W. 2003. Trends in snow water equivalent in the Pacific Northwest and their climatic causes. Geophysical Research Letters, 30(12): 4 p.

Mote, PW., and Salathe, E.P. 2010. Future Climate Change in the Pacific Northwest. Climate Change, Published online 18 May 2010.

Nakawo, M. Morohoshi, T., and Uehara, S. 1993. Satellite Data Utilization for Estimating Ablation of Debris-covered Glaciers. Snow and Glacier Hydrology, 218: 75-83.

Neiman, P.J., Ralph, F.M., Wick, G.A., Kuo, Y.H., Kwon, T.K., Ma, Z., Taylor, G.H., and Dettinger, M.D. 2008. Diagnosis of an Intense Atmospheric River Impacting the Pacific Northwest: Storm Summary and Offshore Vertical Structure Observed with COSMIC Satellite Retrievals. American Meteorological Society, 136: 4398-4420.

NOAA. 2010. National Oceanic and Atmospheric Administration. [online] (Updated 25 June 2010) Available at: www.noaa.gov. (Accessed 25 June 2010).

Nolin, A.W. 2010. Personal Communication. Oregon State University Department of Geosciences. Corvallis, OR 97331.

NRCS. United States Department of Agriculture: Natural Resources Conservation Service. SNOTEL Data for the Paradise and Mt. Hood Test Sites [online] (Updated 25 June 2010) Available at: http://www.or.nrcs.usda.gov/snow/ (Accessed 25 June 2010).

Nylen, T.N. 2004. Spatial and Temporal Variations of Glaciers (1913-1994) on Mt. Rainier and the Relation with Climate. M.S. Thesis, Portland State University, 111p.

Oerlemans, J. and Fortuin, J.P.F. 1992. Sensitivity of Glaciers and Small Ice Caps to Greenhouse Warming. Science, 258: 115-117.

Oerlemans, J. 2005. Extracting a climate signal from 169 glacier records. Science, 308: 675-677.

Ohmura, A. 2006. Changes in mountain glacier and ice caps during the 20th Century. Annals of Glaciology, 43: 361-368.

Parker, L. 2009. Meteorological conditions associated with rain-related periglacial debris flows on Mount Hood, Oregon and Mount Rainier, Washington. M.S. Thesis, Oregon State University, 88p.

Paul, F. 2001. Evaluation of different methods for glacier mapping using Landsat TM. Proceedings of EARSeL-SIG Workshop Land Ice and Snow, 1: 239-245

Paul, F., Huggel, C., Kääb, A., Kellenberger, T., and Maisch, M. 2002. Comparison of TM-derived glacier areas with higher resolution data sets. Proceedings of EARSeL-LISSIG-Workshop Observing our Cryosphere from Space, Bern, March 11-13 2002. 15-21.

Paul, F., Kääb, A., Maisch, M., Kellenberger, T., and Haeberli, W. 2004. Rapid disintegration of Alpine glaciers observed with satellite data. Geophysical Research Letters, 31: 1-4

Paul, F., Machguth, H., Kääb, A. 2005. On the impact of glacier albedo under conditions of extreme glacier melt: The summer of 2003 in the Alps. EARSeL eProceedings, 4: 139-149.

Paul, F., Kääb, A., Haeberli, W. 2007. Recent glacier changes in the Alps observed by satellite: Consequences for future monitoring strategies. Global and Planetary Change, 56: 111-122.

Phillippe, J. 2008. Present-day and future contributions of glacier melt to the Upper Middle Fork Hood River: Implications for water management. M.S. Thesis, Oregon State University, 90 p.

Pirot, R. 2010. Initiation Zone Characterization of Debris Flows in November, 2006, Mount Hood, Oregon. M.S. Thesis Portland State University.

ThorneyCroft, K. 2010. Personal Communication. M.S. Graduate Student at Portland State University working with Professor Andrew Fountain.

Quincy, D.J., Lucas, R.M., Richardson, S.D., Glasser, N.F., Hambrey, M.J., and Reynolds, J.M. 2005. Progress in Physical Geography, 29: 475-505.

Racoviteanu, A.E., Williams, M.W., and Barry, R.G. 2008. Optical Remote Sensing of Glacier Characteristics: A Review with Focus on the Himalaya. Sensors, 8: 3355-3383.

Racoviteanu, A.E., Arnaud, Y., Williams, M.W. and Ordonez, J. 2008. Decadal changes in glacier parameters in the Cordillera Blanca, Peru, derived from remote sensing. Journal of Glaciology, 54(186): 499-510.

Raup, B., Racoviteanu, A., Khalsa, S.J.S., Helm, C., Armstrong, R., and Arnaud, Y. 2007 The GLIMS geospatial glacier database: A new tool for studying glacier change. Global and Planetary Change, 56: 101-110.

Rebetez, M., Lugon, R., and Baeriswyl, P.A. 1997. Climatic change and debris flows in high mountain regions: The Case study of the Ritigraben Torrent (Swiss Alps). Climate Change, 36: 371-389.

Reid, H.F, 1906. The Glaciers of Mt. Hood and Mt. Adams. Mazama, p. 113-132.

Richardson, D. 1968. Glacier Outburst Floods in the Pacific Northwest. U.S. Geological Survey Professional Paper 600-D.

Roberts, M. 2005. Jokulhlaups: A reassessment of floodwater flow through glaciers. Review of Geophysics, 43:1-21.

Russell, I.C., and Smith, G.O. 1898. Glaciers of Mount Rainier. Government Printing Office, Washington, D.C.

Schilling, S.P., Carrara, P.E., Thompson, R.A., and Iwatsubo, E.Y. 2004. Posteruption glacier development within the crater of Mount St. Helens, Washington, USA. Quaternary Research, 61: 325-329.

Scott, W.E., Gardner, C.A., Tilling, R.I., and Lanphere, M.A. 2003. Geologic History of Mount Hood Volcano, Oregon - A Field Trip Guidebook. USGS Cascade Volcano Observatory, 39p.

Sharp, C.F.S. 1938. Landslides and related phenomena: New York, Columbia University Press. 137 p.

Sigafoos, R.S., and Hendricks, E.L. 1972. Recent Activity of Glaciers of Mount Rainier Washington. Geological Survey Professional Paper 387-B.

Silverio, W. and Jaquet, J.M., Glacial cover mapping (1987-1996) of the Cordillera Blanca (Peru) using satellite imagery. Remote Sensing of the Environment, 95: 324-350.

Sisson, T.W. 1995. History and Hazards of Mount Rainier, Washington. USGS Open-File Report 95-642.

Steijn, H.V. 1996. Debris-flow magnitude-frequency relationships for mountainous regions of Central and Northwest Europe. Geomorphology, 15: 250-273.

Stoffel, M., Lievre, I., Conus, D., Grichting, M.A., Raetzo, H., Gartner, H.W., and Monbaron, M. 2005. 400 Years of Debris-Flow Activity and Triggering Weather

Conditions: Ritigraben, Valais, Switzerland. Arctic, Antarctic, and Alpine Research, 37(3): 387-395.

Swanson, D.A., and Vance, J.A. 1989. Cenozoic volcanism in the Cascade Range and Columbia Plateau, southern Washington and northernmost Oregon: Seattle, Washington to Portland, Oregon. American Geophysical Union. Part of the Field Trip Guidebook Series T106.

U.S. National Park Service. Mount Rainier National Park [online] (Updated 25 June 2010) Available at: http://www.nps.gov/mora/ (Accessed 25 June 2010).

Vallance, J.W., Cunico, M.L., and Schilling, S.P. 2003. Debris-flow hazards caused by hydrologic events at Mount Rainer, Washington. USGS Open-File Report 03-368.

Varnes, D.J. 1978. Slope Movement Types and Processes. Landslides: Analysis and control. Edited by R.L. Schuster. National Academy of Sciences, Special Report 176, Washington, D.C. 11-33.

Vermote, E.F., Tanre, D., Deuze, J.L., Herman, M. and Morcrette, J.J. 1997. Second Simulation of the Satellite Signal in the Solar Spectrum, 6S: An Overview. IEEE Transactions on Geoscience and Remote Sensing, 35(3): 675-686.

Walder, J.S. and Driedger, C.L. 1993. Glacier-generated debris flows at Mount Rainier. U.S. Geological Survey Open-File Report, 93-124.

Walder, J.S. and Driedger, C.L. 1994. Rapid geomorphic change caused by glacial outburst floods and debris flows along Tahoma Creek, Mount Rainier, Washington, U.S.A. Arctic and Alpine Research, 26(4): 319-327.

Walder, J. D. and C.L., Driedger. 1995. "Frequent Outburst Floods from South Tahoma Glacier, Mount Rainier, U.S.A.: Relation to debris flows, meteorological origin and implications for subglacial hydrology." Journal of Glaciology, 41(137): 1-20.

Watershed Sciences. 2010. Corvallis, Oregon. 97330.

Watson, R.T., and Haeberli, W. 2004. Environmental threats, mitigation strategies and high-mountain areas. Royal Swedish Academy of Science Ambio, 33(7): 1-10.

Williams, R.S., Hall, D.K., Sigurdsson, O., and Chien, J.Y.L. 1997. Comparison of satellite-derived with ground-based measurements of the fluctuations of the margins of Vatnajökull, Iceland, 1973-92. Annals of Glaciology, 24: 72-80

Wise, W. 1969. Geology and petrology of the Mt. Hood area: a study of High Cascade volcanism. Bulletin from the Geological Society of America 80: 42p.

WWF 2005. An Overview of Glaciers, Glacier Retreat and its Subsequent Impacts in Nepal, India and China. Kathmandu: WWF-Nepal.

Wood, C.A., and Kienle, J. 1990. Volcanoes of North America: United States and Canada. Cambridge University Press.

Zimmermann, M. and Haeberli, W. 1992. Climate Change and Debris Flow Activity in High-Mountain Areas - A Case Study in the Swiss Alps. Catena Suppl, 22: 59-72.

APPENDICES

Appendix A. Previous year snow water equivalent SNOTEL data for the years of each decade for both Mt. Hood and Mt. Rainier

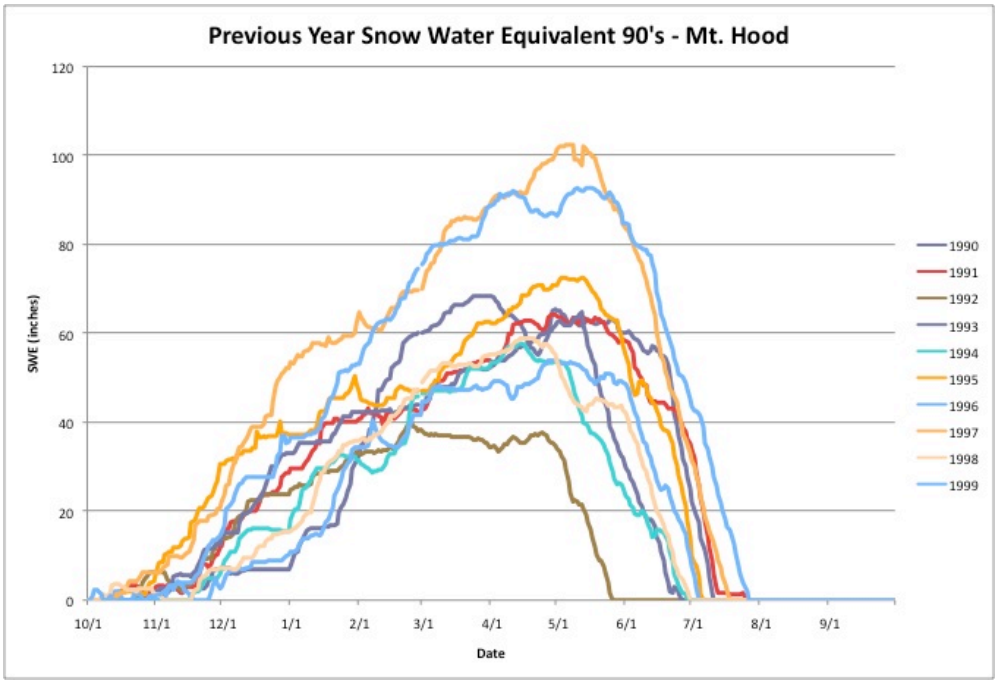

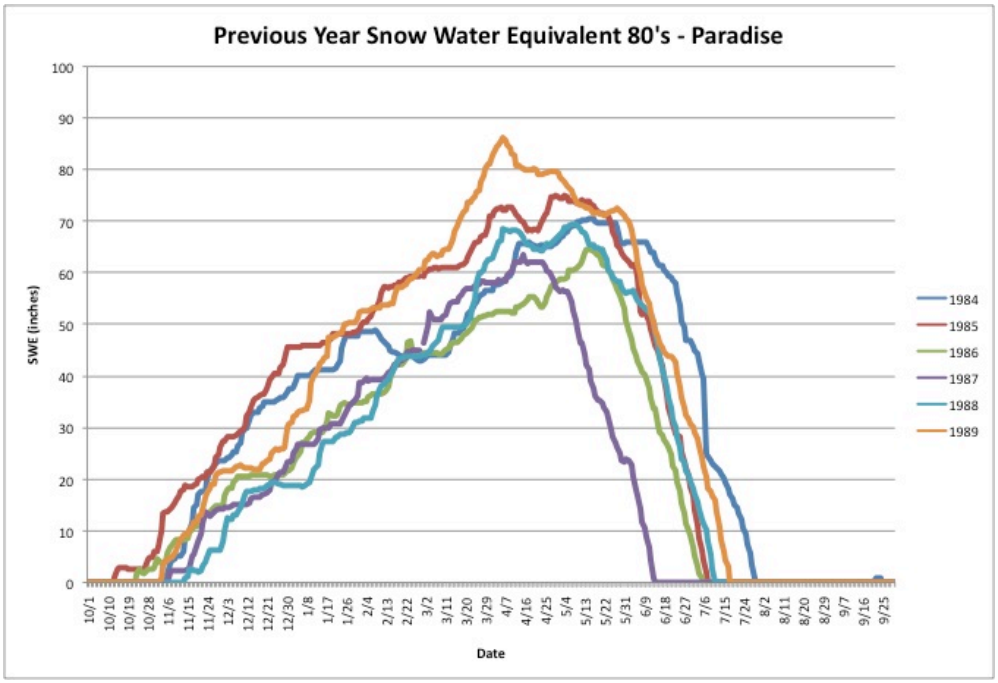

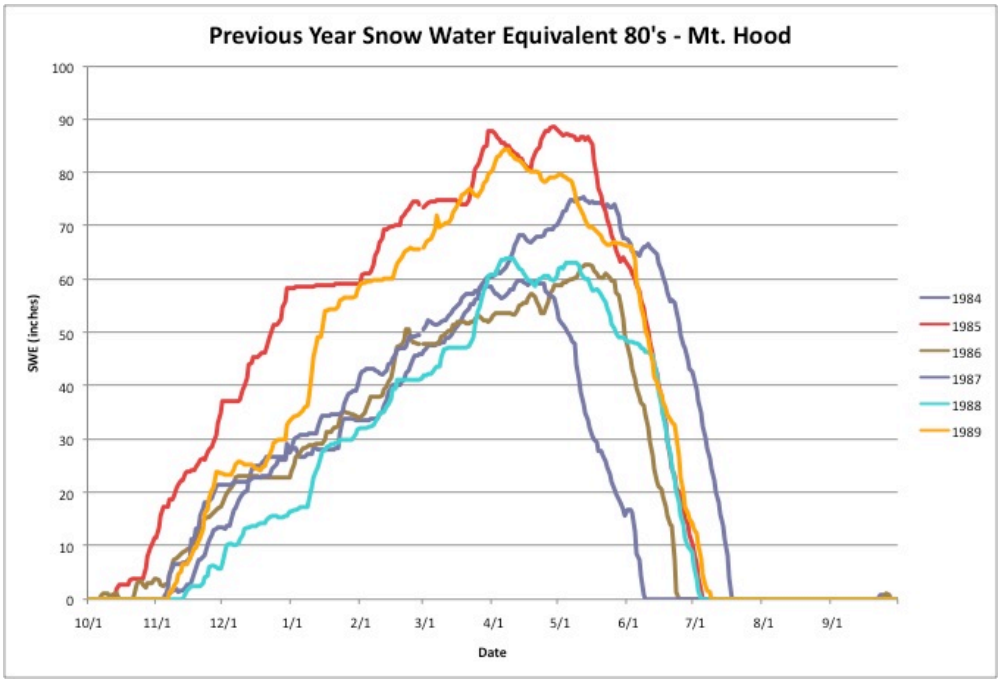
Previous Year Snow Water Equivalent 80's - Mt. Hood
SWE (inches)
100
90
80
70
60
50
40
30
20
10
0
10/1
11/1
12/1
1/1
2/1
3/1
4/1
5/1
6/1
7/1
8/1
9/1
Date
1984
1985
1986
1987
1988
1989

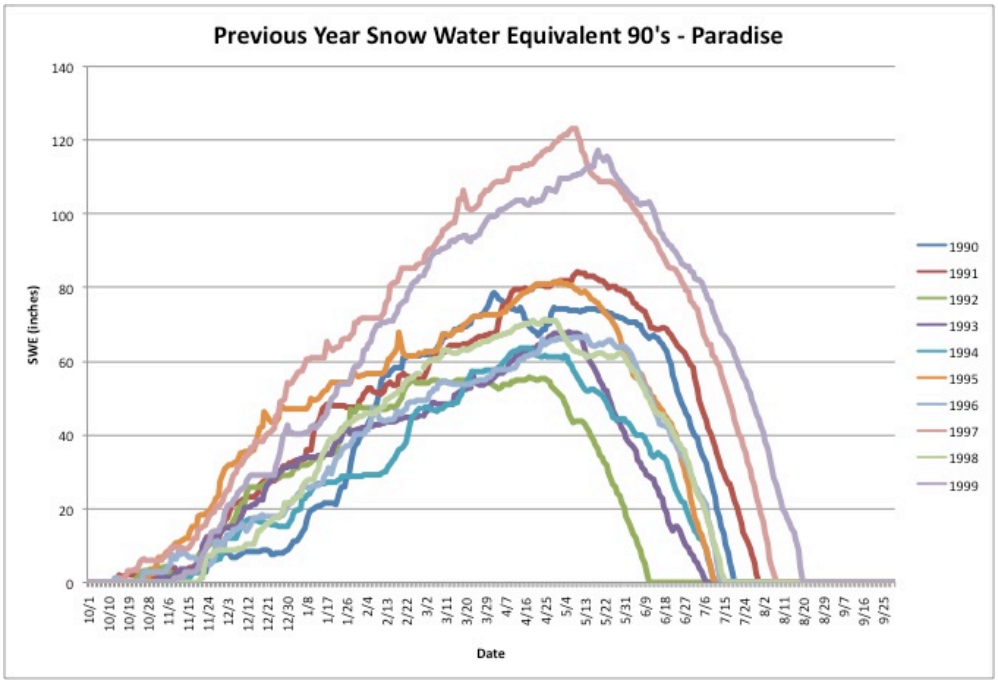
Previous Year Snow Water Equivalent 90's - Paradise
SWE (inches)
140
120
100
80
60
40
20
0
Date
1990
1991
1992
1993
1994
1995
1996
1997
1998
1999

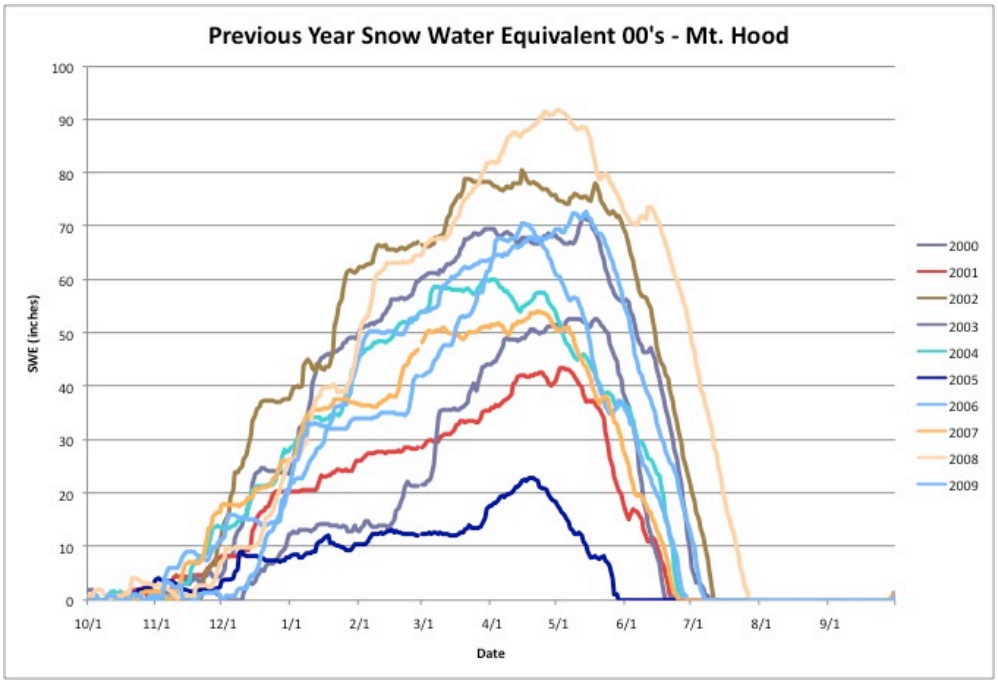
Previous Year Snow Water Equivalent 00's - Mt. Hood
SWE (inches)
100
90
80
70
60
50
40
30
20
10
0
10/1
11/1
12/1
1/1
2/1
3/1
4/1
5/1
6/1
7/1
8/1
9/1
Date
2000
2001
2002
2003
2004
2005
2006
2007
2008
2009

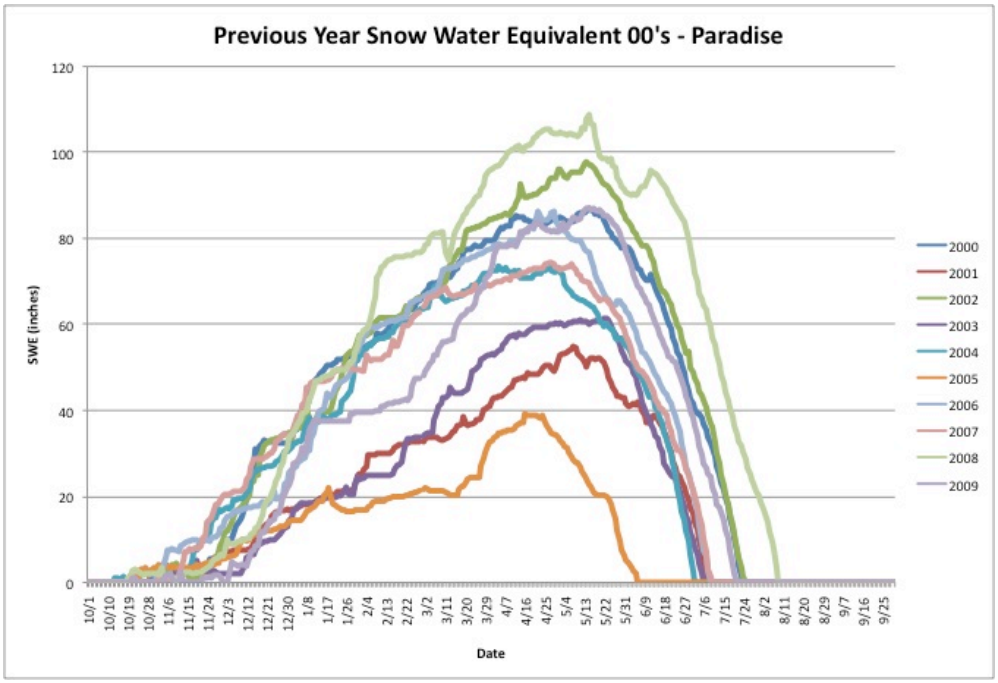
Previous Year Snow Water Equivalent 00's - Paradise
SWE (inches)
120
100
80
60
40
20
0
Date
2000
2001
2002
2003
2004
2005
2006
2007
2008
2009

Appendix B. Maximum snow water equivalent for 1984-2009 for both Mt. Rainier and Mt. Hood.

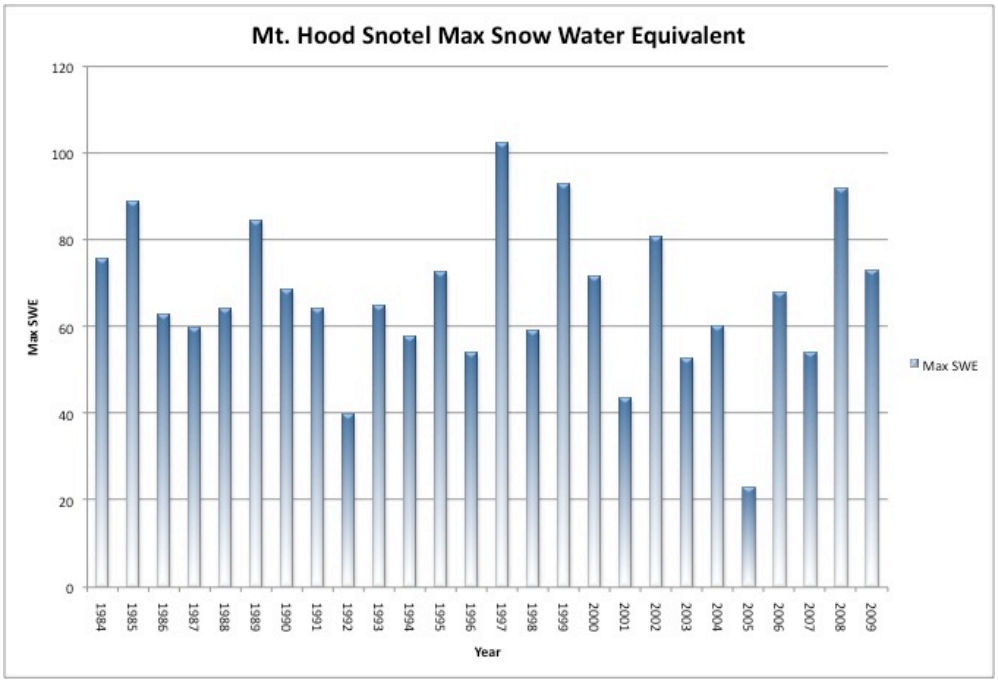

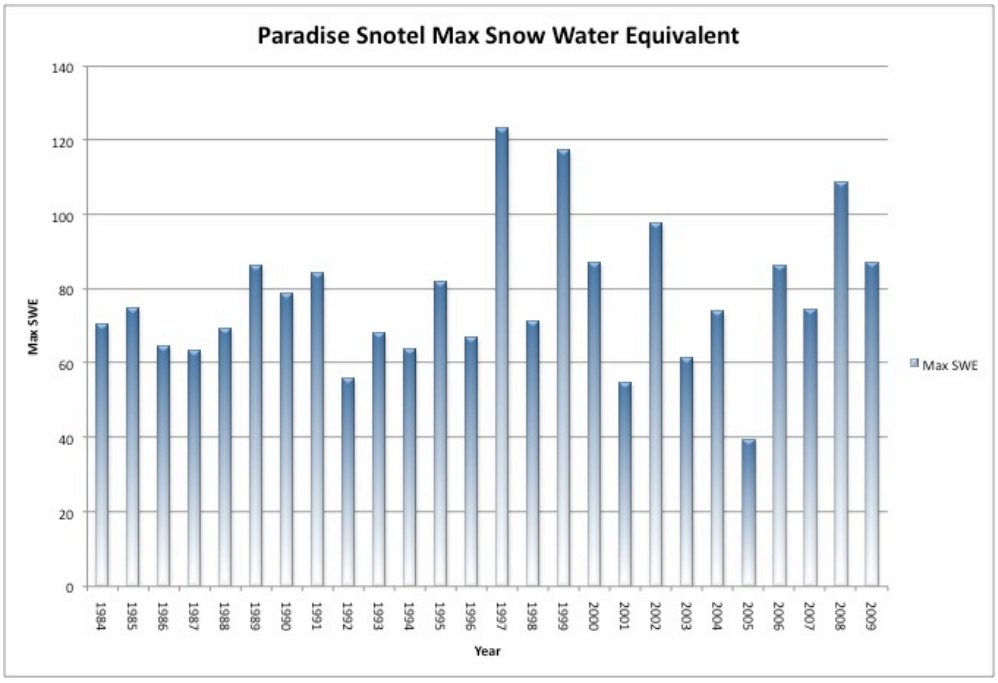

Appendix C. Average annual temperature for years 1984-2009 for both Mt. Rainier and Mt. Hood

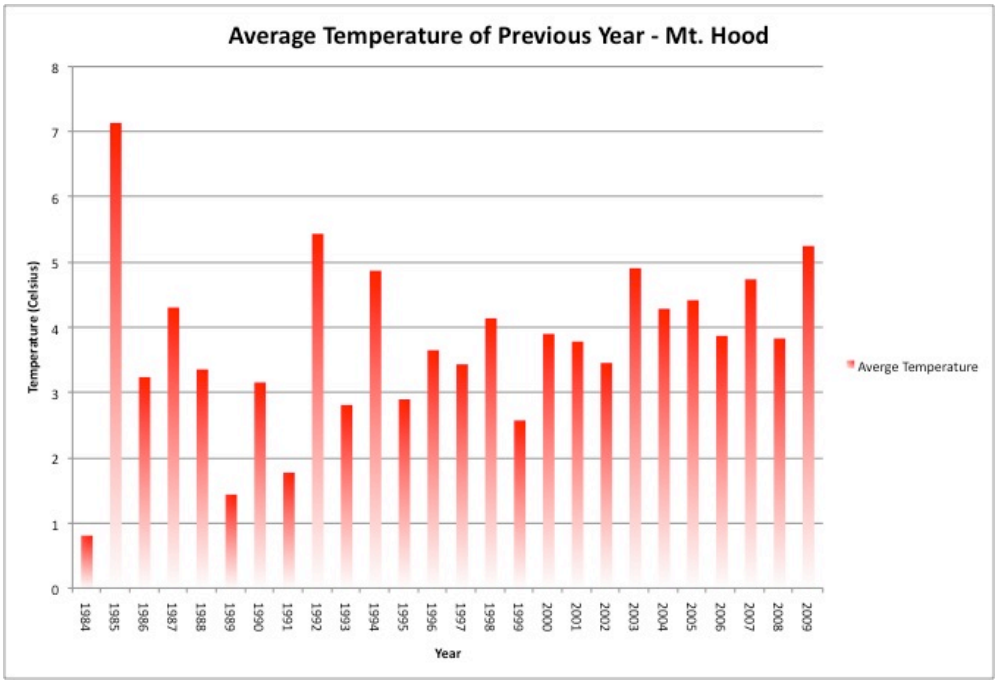

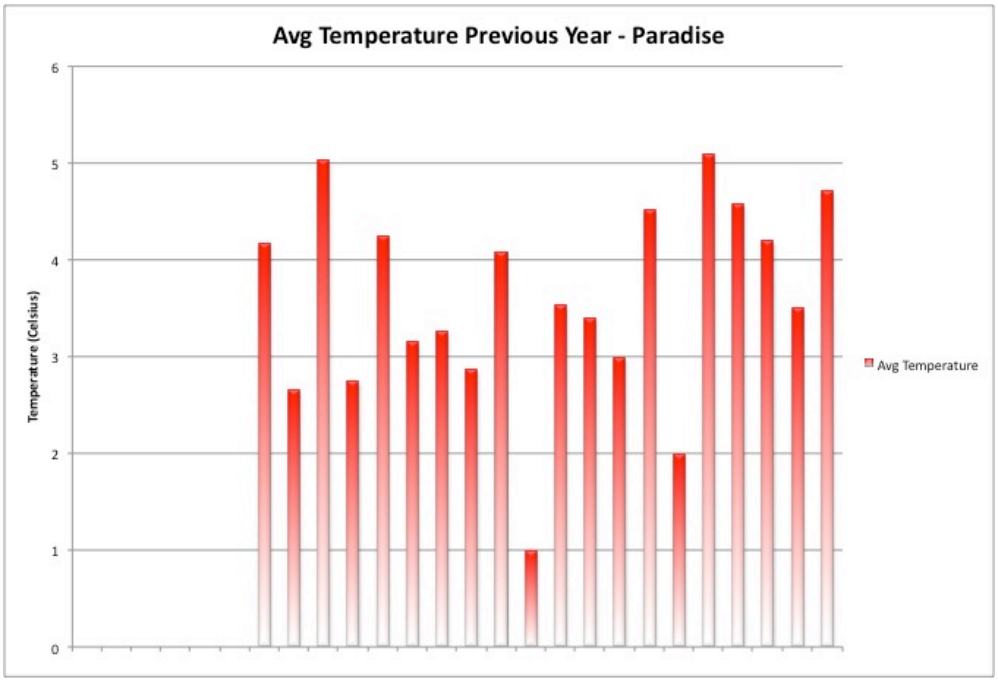

Appendix D. Total annual precipitation for years 1984-2009 for both Mt. Rainier and Mt. Hood

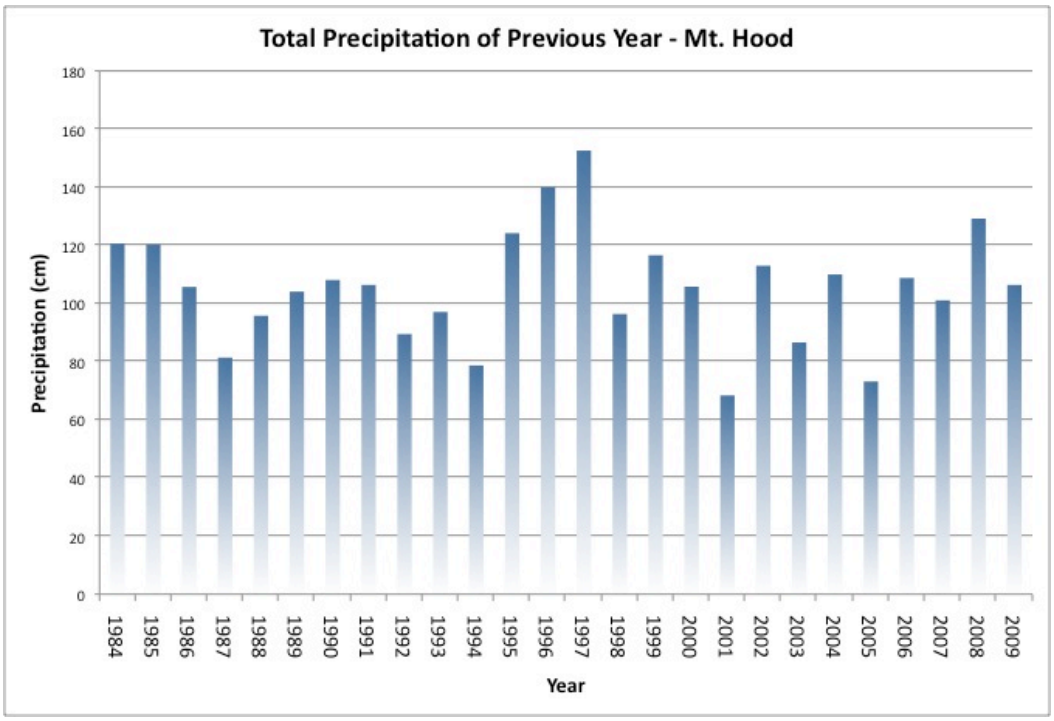

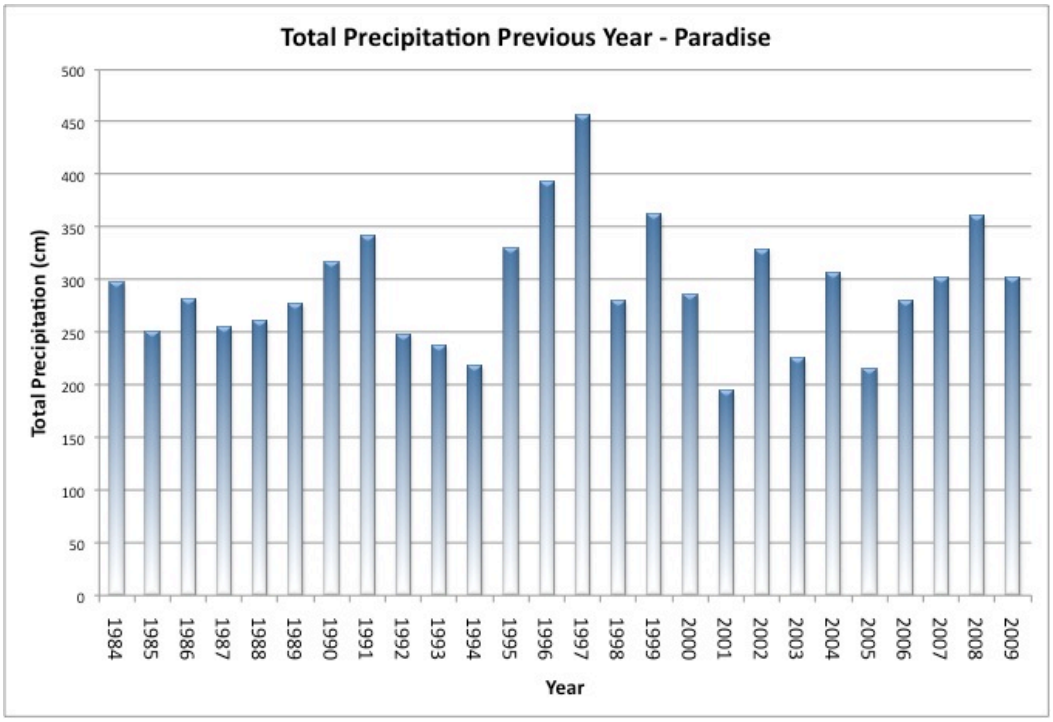

Appendix E. First Day of zero snow water equivalent for years 1984-2009 for both Mt. Rainier and Mt. Hood